Using neuroimaging and histology to understand hyperexcitability and atypical connectivity in Autism Spectrum Disorder

Mathura Ravishankar
Neuroanatomy and Cognition Group
Department of Neuropathology
St. Cross College, University of Oxford
Trinity 2015

A thesis submitted in fulfillment of the requirements for the degree of Master of Science to the University of Oxford.

Acknowledgements

This work would not have been possible without a large team of people. I would first like to say thank you to my supervisors, Dr. Steven Chance and Dr. Charles Newton, as well as my mentors, Dr. Sven Braeutigam, Dr. Anna Remington, and Dr. Uzay Emir, who have all played a pivotal role in different parts of this work. Thank you for your expertise, patience, and encouragement these last two years.

I would like to thank past and present members of the lab, including Rebecca McKavanagh, David Menassa, and Istvan Adjoran, who were each a great source of knowledge and motivation in different aspects of the work. I would like to thank David and Brianna Doherty, who helped plan and pilot the multimodal project in Chapter 3 two years ago, as well as Marwa Mathlouthi, who manually masked the regions of interest in Chapter 3 and assisted me with lab work in Chapter 4.

I would like to acknowledge Dr. Elizabeth Rapa, Michael Sanders, and Jon Campbell who helped with data collection in Chapter 3, Dr. Stamatios Sotiropoulos and Dr. Mark Jenkinson for their expertise on diffusion imaging, and Carolyn Sloan, Connor Scott, and Marie Hamard for their assistance with post-mortem tissue work. Additionally, I would like to acknowledge the Simons Foundation, Autism Speaks, the Shirley Foundation, and St. Cross College for financial support in different parts of this project. A special thank you to all the tissue donors and their families, Dr. Stefan Sunaert, the participants in Chapter 2, as well as the participants in the multimodal imaging study, who were each a pleasure to get to know.

Lastly, I am indebted to my family for their unwavering support. Thank you Mom and Dad for eagerly willing to read over this thesis despite not having taken a science class for over 30 years.

Abstract

The aim of this thesis was to better understand hyperexcitability and atypical connectivity in Autism Spectrum Disorder (ASD) by using a combination of neuroimaging and histology techniques. Three regions of interest were of particular interest: primary visual cortex, the fusiform gyrus, and dorsolateral prefrontal cortex. These functionally diverse regions have previously been implicated in ASD, and one of the goals was to determine whether the disorder is better characterized by primary sensory deficits or dysfunction in higher-order processing areas.

Diffusion Tensor Imaging results across two different datasets suggested that mean diffusivity in the cortex may be sensitive to detect microstructural differences in ASD. Gender and hemisphere were factors that significantly affected diagnostic differences in the first dataset. In the second dataset, ASD individuals (n = 14) compared to Typically Developing (TD) individuals (n = 25) showed reduced mean diffusivity across regions, which may be linked to increased neuropil or neuronal density. Magnetoencephalography findings suggested that both ASD (n = 13) and TD (n = 14) individuals showed no apparent differences in primary visual cortex activity in response to simple visual stimuli, whereas frontal regions of the ASD brain showed more deviations in gamma oscillations, providing some evidence for the executive dysfunction theory of ASD. Magnetic Resonance Spectroscopy results revealed elevated glutamate levels in primary visual cortex and medial prefrontal cortex in ASD (n = 11) compared to TD individuals (n = 13), as well as elevated creatine levels in the medial prefrontal cortex, which may be linked to hyperactivity of glial cells. ASD individuals also showed superior performance on a visual task, which correlated with glutamate levels in medial prefrontal cortex, and both of these measurements correlated with autism severity scores, providing evidence for the specificity of these findings to the disorder.

Immunohistochemistry was used to study the distribution of parvalbumin cells – a subset of fast-spiking GABAergic cells – in 14 ASD and 15 TD post-mortem cases. No significant group differences were found in any of the three regions of interest. These results taken together with the neuroimaging findings support the idea that hyperexcitability in ASD is a complex interplay between several cell-types.

TABLE OF CONTENTS

Abbreviations

Θ_{rad} – Angle of Radiality
%SD – Estimate of Standard Deviation in Percentage
ADI-R – Autism Diagnostic Interview-Revised
ADOS – Autism Diagnostic Observation Schedule
ASD – Autism Spectrum Disorder
BA – Brodmann Area
CHIPS – Cortical Hi-Profile Intensity Segmentation
CSF – Cerebrospinal Fluid
CSPG – Chondroitin Sulphate Proteoglycan
d' – Detection Sensitivity
$D_{\perp}$ – Vector Component of Θ_{rad} that is Perpendicular to v_{surf}
D_{PDD} – Tensor Component of the Principal Diffusion Direction
DAB – 3,3'-Diaminobenzidine
DSM-IV – Diagnostic and Statistical Manual of Mental Disorders, 4th Edition
DSM-V – Diagnostic and Statistical Manual of Mental Disorders, 5th Edition
DTI – Diffusion Tensor Imaging
ECG – Electrocardiogram
EEG – Electroencephalography
EOG – Electrooculogram
FA – Fractional Anisotropy
FG – Fusiform Gyrus
FID – Free Induction Decay
FMRIB – Oxford Centre for Functional MRI of the Brain
fMRI – Functional Magnetic Resonance Imaging
FOV – Field of View
FSL – FMRIB Software Library
GABA – Gamma-Aminobutyric Acid
Gln – Glutamine
Glu – Glutamate
IMS – Industrial Methylated Spirits
L – Left
MD – Mean Diffusivity
MEG – Magnetoencephalography
mM – mmol per Kg wet weight
MNI – Montreal Neurological Institute
MPFC – Medial Prefrontal Cortex
MPRAGE – Magnetisation-Prepared Rapid Gradient-Echo
MRI – Magnetic Resonance Imaging
MRS – Magnetic Resonance Spectroscopy
NAA – N-acetylaspartate
OHBA – Oxford Centre for Human Brain Activity
PBST – Phosphate Buffered Saline with Triton-X
PDD – Pervasive Developmental Disorder
PDDNOS - PDD Not Otherwise Specified
PHG – Parahippocampal Gyrus
PMI – Post-Mortem Interval
PV – Parvalbumin
V1 – Primary Visual Cortex
R – Right
rmAN(C)OVA – Repeated-Measures Analysis of (Co)variance
RGB – Red Green Blue
ROIs – Regions of Interest

SCQ – Social Communication Questionnaire
SD – Standard Deviation
SE – Standard Error
SE-EPI – Spin Echo Echo-Planar Imaging
SNPs –Single Nucleotide Polymorphisms
SRS – Social Responsiveness Scale
T – Tesla
TE – Echo Time
TR – Repetition Time
ToM – Theory of Mind
TD – Typically Developing
TWOBC – Thomas Willis Oxford Brain Collection
WASI – Wechsler Abbreviated Scale of Intelligence
WCC – Weak Central Coherence

Chapter 1: Introduction

Introduction to Autism Spectrum Disorder

During the 1900s, many attempts were made to describe the different forms of child psychosis. Scientists wrote about children who initially showed normal development, but then lost their language and social abilities later on in childhood. Despite efforts by many individuals, Dr. Leo Kanner is credited as the first individual to describe the characteristics of autism, likely due to his writings that contained exceptional details on the condition (Wing, 1997). In his descriptive accounts, Kanner wrote about children who seemed socially aloof and had varying degrees of intelligence (Kanner, 1968). Kanner's accounts in 1943 were followed by those of Dr. Hans Asperger in 1944. Asperger described individuals with average to high intelligence that acted inappropriately in social situations, spoke frequently about their own interests, and used body language inappropriately. Over the years, it became clear that what both Kanner and Asperger were describing fell under an umbrella term called Autism Spectrum Disorder (ASD). ASD today is known as a behavioural disorder, defined by repetitive and stereotyped behaviour and impaired communication.

In 1967, Victor Lotter published the first epidemiological study on autism and found that in the UK, 5 in 10,000 individuals were affected with the disorder described by Kanner (Lotter, 1967). Since then, many studies have reported on the prevalence of ASD in different countries. From 1991 to 1997, there was a 556% increase in paediatric prevalence of ASD in the US, likely due to increased awareness of the disorder and changes that broadened the diagnostic criteria (Stokstad, 2001). A study published in 2005 found that the rate of diagnosis had jumped to 6/1,000 individuals (Fombonne, 2005), suggesting again that this increase was due to changes in diagnostic criteria as well as better awareness of the disorder. Some of the latest consensus reports in the UK suggest that the prevalence of ASD is approximately 1 out of every 100 people (Office for National Statistics, 2011). These changes in prevalence over the years may reflect the complexity of the disorder. In order to fully understand this complexity, it is important to survey

the literature on topics including the aetiology and subtypes, as well as the behavioural and neuroanatomical basis of ASD.

Aetiology

ASD is aetiologically heterogeneous, and is known to have a strong genetic and environmental basis, supported by studies involving monozygotic and dizygotic twins (Hallmayer et al., 2011). The first study that explored the genetic component of ASD was in the late 1970s and demonstrated that the monozygotic twin of a child diagnosed with ASD has an 82% chance of showing cognitive abnormalities. However, in dizygotic twins, the statistic drops to 10% (Folstein & Rutter, 1977), demonstrating a strong genetic component to the disorder. Since then, several brain imaging, genetic and epidemiological studies have corroborated the genetic basis of the disorder (Folstein & Rosen-Sheidley, 2001). Researchers have suggested that environmental factors that do play a role in the aetiology of developmental disorders must interact with genetics, especially during critical periods of child development (Kelada, Eaton, Wang, Rothman, & Khoury, 2003; Lawler, Croen, Grether, & Van De Water, 2004).

Epigenetic influences on the aetiology of ASD have been reported as well, one of the most common being "parent of origin" effects (Donnelly et al., 2000), resulting in genomic imprinting. This occurs when one of the two genes inherited from a parent is imprinted, or "silenced", and the other parental gene is expressed through epigenetic changes like histone methylation. Many imprinted genes have shown expression in the brain of individuals with ASD (Davies, Isles, & Wilkinson, 2001), and therefore may play a role in the observed neuroanatomical changes in these individuals. There also exists evidence to suggest that maternal alleles passed down to a foetus, combined with an unfavourable in utero environment can cause ASD. These alleles have been referred to as "teratogenic" (Johnson, 2003), since they negatively affect a foetus in a similar way to teratogenic drugs like valproate, ethanol, and thalidomide, which have all been linked to the aetiology of ASD (Dufour-Rainfray et al., 2011).

The interplay between genes and the environment may also be studied through Single Nucleotide Polymorphisms (SNPs), which are the natural allelic variations in genes (Lawler et al., 2004). Specifically, it may be necessary to look at environmental response genes, like those that have evolved to respond to environmental toxins or are involved in DNA repair, cell cycle function and replication, as well as cell apoptosis. Studying SNPs may also help in discovering the genetic basis for the different subtypes of ASD.

Subtypes

In the 4th edition of the Diagnostic and Statistical Manual of Mental Disorders (DSM-IV), individuals had to show the classic "triad of impairments" which were in social interaction, imaginative ability, and communication, in order to receive a diagnosis of ASD, which fell under a broader term called Pervasive Developmental Disorder (PDD) (American Psychiatric Association, 2000; Wing, 2004). There were five subtypes under PDD: 1) autistic disorder, encompassing the classic symptoms of autism, 2) Asperger Syndrome, for those that did not show intellectual disability and had a normal language development, 3) PDD Not Otherwise Specified (PDDNOS), characterizing individuals who did not fall under the other categories but had autistic traits, 4) Childhood Disintegrative Disorder, for children who regressed in cognitive, behaviour or language, and 5) Rett's Disorder, diagnosed in individuals with a single-gene defect that codes for methyl-CpG-binding protein 2 (Muhle, Trentacoste, & Rapin, 2004). The main problem with this classification system was that many of the features in these subgroups overlapped with one another.

The publication of the 5th edition of the DSM (DSM-V) in 2013[1] brought forth several revisions on the subtypes of ASD. The DSM-V now groups all individuals who were previously diagnosed with autism, Asperger Syndrome, or PDDNOS into ASD. Instead of presenting with the "triad of impairments", individuals now must present with 1) impairments in social behaviour and

[1] It is important to note that the classification of ASD under the DSM-V has diverged from the description

communication, and 2) restricted and repetitive interests and behaviour (Frazier et al., 2012; Grzadzinski, Huerta, & Lord, 2013). In addition, individuals with ASD can present with varying levels of severity, psychiatric comorbidities, language and cognitive impairment, as well as different types of onset and medical conditions. It is believed that this new classification system will add more dimension to clinicians' diagnoses, and better unify the common features of the disorder (Grzadzinski et al., 2013). Figure 1 illustrates this by specifying the core criteria for an ASD diagnosis, as well as other non-ASD specific features that individuals may present with (Grzadzinski et al., 2013), including language level and comorbid symptoms.

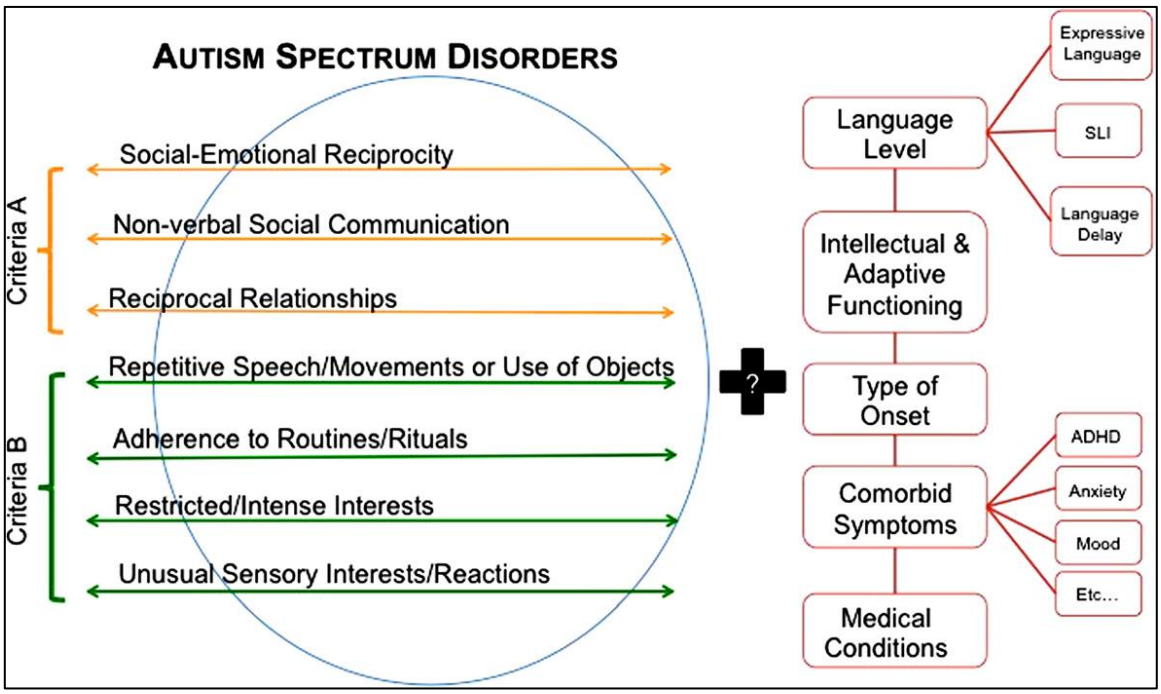

Figure 1. Characterization of ASD under DSM-V criteria. Figure was adapted from Grzadzinski et al., 2013.

Comorbidity with ASD

A comorbidity signifies the existence of two or more medical conditions in one individual, where the main symptoms of one condition are distinct from those of the other condition (Matson & Nebel-Schwalm, 2007). Up to 70% of individuals with ASD are thought to present with a co-occurring condition (Lai, Lombardo, & Baron-Cohen, 2014). Common comorbid conditions found in individuals with ASD are epilepsy, gastrointestinal disorders, sleep issues, feeding problems, and toileting issues. Though it is unclear why a large number of individuals on the spectrum also present with another condition, it is hypothesized that ASD may share

pathophysiology with some of the other conditions that individuals typically present with or may have overlapping diagnostic criteria with other conditions (Lai et al., 2014). Popular questionnaires used to determine comorbidity are Psychopathology in Autism Checklist and Autism Spectrum Disorders-Comorbidity of Adults (Mannion & Leader, 2013). These are often administered in addition to ASD screening and diagnostic tests.

Methods of Diagnosis

The type of screening used to diagnose individuals on the spectrum depends primarily on age and level of development. As reported in Lai et al. (2014), for young children, common screening tools are the Checklist for Autism in Toddlers, Early Screening of Autistic Traits, and the Screening Tool for Autism in Toddlers and Young Children. For older children, adolescents and adults, the screening tools often used are the Social Communication Questionnaire (SCQ), the Social Responsiveness Scale (SRS), and the child and adolescent versions of the Autism Spectrum Quotient. Additionally, tools like the Autism Spectrum Screening Questionnaire-Revised Extended Version have been developed to better identify the female autism phenotype, which is speculated to be distinct (Kopp & Gillberg, 2011). In terms of diagnosis, researchers and clinicians commonly use the Autism Diagnostic Interview-Revised (ADI-R), which requires an interview with the parent or caregiver, and the Autism Diagnostic Observation Schedule (ADOS), which is used by clinicians to observe the individual through interactions.

Difference Between Males and Females

Studies have found that ASD females show less restricted and repetitive behaviours and reduced problems in behavioural situations, questioning the validity of the current diagnostic tools. It is hypothesized that ASD females with average to above-average intelligence are underdiagnosed compared to males with similar intelligence (Kopp, Kelly, & Gillberg, 2010). This is somewhat in line with Kanner's and Asperger's initial reports on autism, which found that the disorder was much more common in males than females. The first epidemiological study conducted by Lotter

in 1967 also studied the differences in diagnosis between males and females, concluding that the ratio of male to female individuals with ASD is 2.6:1 (Lotter, 1967). Since this initial study, researchers have repeatedly found that the prevalence rates of ASD is 4-8 times higher in males than in females (Polleux & Lauder, 2004).

Some of these differences may be attributed to diagnostic tests. However, it also suggests that there is likely a genetic component to the disorder that is linked to the sex chromosome. For example, sex chromosome aneuploidies like 47 XYY syndrome represents approximately 20% of ASD cases, whereas Turner Syndrome (XO) and Klinefelter Syndrome (XXY) together represent less than 15% of cases. These statistics raise the possibility that ASD may be linked to genes in the Y chromosome, or that genes on the X chromosomes may play a protective role. This argument is further supported by the finding that X chromosome trisomy does not result in increased rates of ASD diagnosis (Bishop et al., 2011; Donnelly et al., 2000; van Rijn, Bierman, Bruining, & Swaab, 2012; Werling & Geschwind, 2013).

Another idea related to sex differences that is gaining popularity is the Extreme Male Brain Theory of ASD, which discusses the idea of "hypermasculinzation" in ASD aetiology (Simon Baron-Cohen, Knickmeyer, & Belmonte, 2005). Under this theory, TD females are thought to show a stronger ability to empathize than to systematize, whereas TD males are thought to show a higher ability to systemize than to empathize. This has been corroborated by a study, which showed that higher foetal testosterone levels negatively correlated with an individual's empathizing ability (Chapman et al., 2006). Others have shown that ASD individuals demonstrate higher systemizing ability and lower empathizing ability than TD males (Simon Baron-Cohen, Richler, Bisarya, Gurunathan, & Wheelwright, 2003; Simon Baron-Cohen & Wheelwright, 2004), hence providing support for the Extreme Male Brain in ASD.

Behavioural Theories

Several theories in addition to the Extreme Male Brain Theory exist to characterize ASD, like the Theory of Mind (ToM) (Baron-Cohen, 1989), Weak Central Coherence (WCC) (Frith, 1989), and executive dysfunction (Ozonoff, Pennington, & Rogers, 1991). While these three theories share characteristics, they are distinct and are hypothesized to work independent of one another (Happé & Frith, 2006).

ToM was a term initially used to describe a person's ability to recognize different mental states, like belief, thinking, doubt, and knowledge of oneself and others, and was hypothesized to be lacking in chimpanzees (Premack & Woodruff, 1978). Researchers believed that there must be a capability for individuals to understand and perceive the thoughts of others in order to engage in social situations (Leslie, 1987). Since these publications, the lack of ToM has been used in the context of several disorders, including ASD, right hemisphere damage, and traumatic brain injury (Baron-Cohen, 1989; Martin & McDonald, 2003).

WCC refers to ASD individuals' predisposition to detail processing, and hypothesizes that these individuals may have difficulties processing stimuli holistically (Frith, 1989). WCC has been tested in ASD using tasks that require participants to break down components of a larger picture (like the Embedded Figures Task) or a sentence (like the Homograph Task) (Happé, 1997). However, results on these tasks tend to vary based on experimental conditions and the ASD cohort's level of function (Burnette et al., 2005; White & Saldana, 2011).

The term executive function is often used in the context of working memory, planning, making decisions, self-reflection, and controlling emotions, which are all linked to the frontal cortex and require an ability to disengage with the immediate environment to take action (Hill, 2004; Rieger & Rabbitt, 1999). The theory of executive dysfunction in ASD was formally conceptualized by Ozonoff et al. (1991), though several groups have previously reported on similar ideas (Prior & Hoffmann, 1990; Rumsey & Hamburger, 1988). It was initially proposed that ASD individuals may have troubles inhibiting responses to external stimuli, and may show problems in self-

control and regulation, hence causing repetitive/stereotyped behaviours, and leading to lack of imaginative play.

This thesis will investigate another behavioural theory, called The Load Theory of Selective Attention (Lavie, 1995; Lavie, Hirst, de Fockert, & Viding, 2004), in ASD. The main principle of Load Theory is that increased perceptual load on the processing system results in insufficient attention capacities for distractor processing. This effect is modulated by age, where older participants require a lower level of perceptual load to reduce distractor processing (Maylor & Lavie, 1998). Studies on the effect of perceptual load on distractor processing in ASD have found enhanced perceptual capacity (Remington, Swettenham, Campbell, & Coleman, 2009; Remington, Swettenham, & Lavie, 2012). In one study, researchers presented a ring of letters, and asked participants to identify a certain letter as well as the presence or absence of a meaningless and subtle grey distractor stimulus. The number of letters presented in the ring modulated the perceptual load. They found that in high perceptual load conditions, ASD individuals performed significantly better than matched controls at identifying the grey stimulus, whereas in low perceptual load conditions, no group differences were found (Remington et al., 2012). The findings from this task are hypothesized to reconcile two contradictory ideas in the literature about ASD individuals showing superior ability in visual performance tasks (O'Riordan, Plaisted, Driver, & Baron-Cohen, 2001), as well as higher abnormalities in attention (Burack, 1994). This task, referred to as the "Complex Visual Task" in this thesis, was adapted in Chapter 3 to explore the neuroanatomical basis of this behavioural difference.

Neuroanatomical Basis

Studies have shown a wide range of brain regions implicated in the disorder, including the brainstem, cerebellum, different parts of the limbic system, and the cortex (Courchesne, 1997). One of the main findings from the cerebellum is the decreased number of Purkinje cells in individuals with ASD (Courchesne, 1997; Whitney, Kemper, Bauman, Rosene, & Blatt, 2008).

Other studies involving the limbic system suggest that children with ASD have an increased hippocampal and amygdala volume compared to Typically Developing (TD) children (Schumann et al., 2004). While these findings are worth further exploration, this thesis will focus on cortical differences in individuals with ASD. Several cortical regions have shown pathological differences in ASD, including the frontal lobe, superior temporal cortex, and the parietal cortex. These brain regions and their association with the triad of impairments are depicted in Figure 2, adapted from a previous publication (Amaral, Schumann, & Nordahl, 2008).

There is ongoing debate with regards to enlarged head size in ASD. A well-known theory is that the autistic brain undergoes a period of rapid growth, followed by a period of deceleration (Courchesne, Carper, & Akshoomoff, 2003). Studies have shown that 12-month old children with ASD start showing enlarged head sizes compared to TD children (Courchesne et al., 2003; Dawson et al., 2007). From 18 months – 4 years, ASD children showed a 5-10% increased brain volume, but it is unclear whether this relationship persists into adulthood (Courchesne et al., 2001; Palmen et al., 2005).

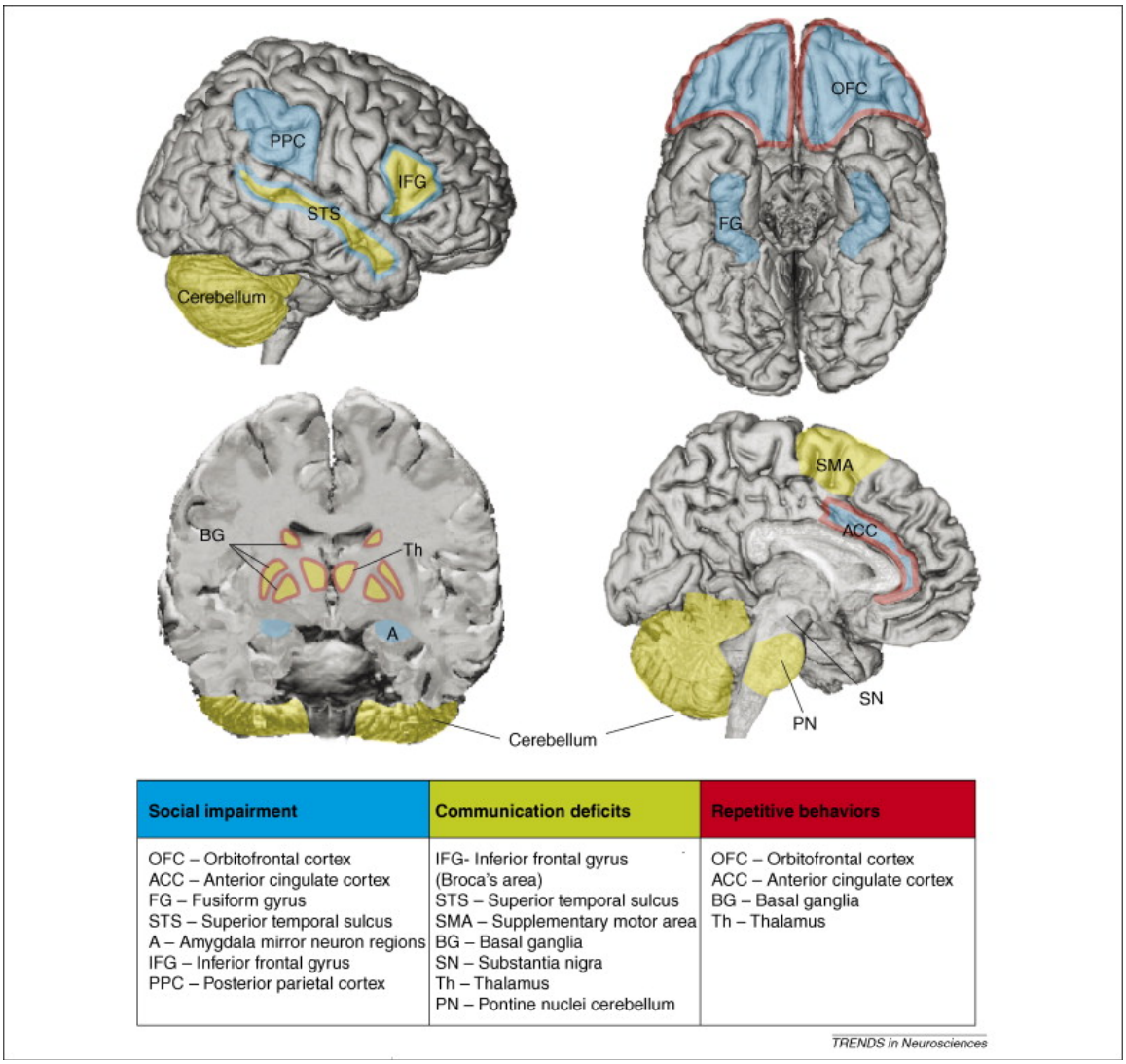

Figure 2. Summary of brain regions implicated in ASD. Regions have been organized based on their associations with the classic triad of impairments. Picture was adapted from Amaral et al. (2008).

Sensory Processing Deficits in ASD

ASD individuals demonstrate hypersensitivity to different types of stimuli. Given the language and communication impairments seen in ASD, many studies have focused on auditory processing in ASD. Underdevelopment of the auditory cortex may explain why ASD individuals have poor language skills (Rubenstein & Merzenich, 2003). Rat models show that the animals' exposure to sound frequencies during a certain critical period biases their abilities to recognize these sounds later on (Zhang, Bao, & Merzenich, 2001). Depending on whether these animals are presented with auditory noise in addition to behaviourally relevant sounds may determine whether the critical period closes or remains open indefinitely (Chang & Merzenich, 2003). Noise rearing yields a low signal/noise ratio, therefore resulting in poor development of auditory cortical

regions. Due to a lack of differentiation, neural activity in these regions are more likely to synchronize with other unrelated cortical regions, resulting in epileptic activity in the animals (Rubenstein & Merzenich, 2003). Two molecules of interest that play a role in critical period closure are brain derived neurotrophic factor (Maffei, 2002), and a component of the extracellular matrix called chondroitin sulphate proteoglycans (CSPG) (Pizzorusso et al., 2002).

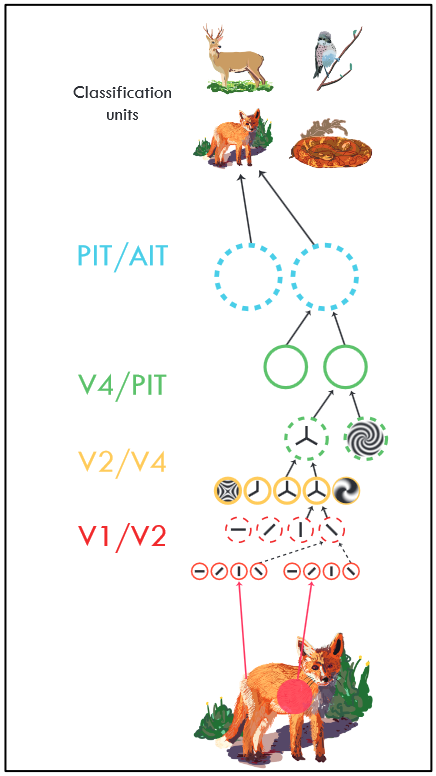

Figure 3. Cell types in different areas of the brain that respond to different features of a visual stimuli. Image adapted from Serre (2014) demonstrates that information from V1 travels to secondary and forth visual areas, and culminates at the posterior and anterior inferotemporal areas, named PIT and AIT respectively.

Altered tactile and visual processing have also been observed in ASD. Studies in the clinical setting show that individuals with ASD dislike activities involving physical contact to the head and body (Marco, Hinkley, Hill, & Nagarajan, 2011), and tend to have lower perceptual thresholds to tactile stimuli (Blakemore et al., 2006). Studies investigating visual deficits have mainly focussed on face processing tasks, given its relevance to social behaviour. While results on these tasks are mixed, there is evidence to suggest that the fusiform gyrus (FG) – hypothesized to play a role in face processing – may be hypoactive during these tasks, though other areas may also be involved in this deficit (Klin, 2008; Pierce & Redcay, 2008).

The Visual Processing Pathway

The following section will discuss the visual processing pathway, which will be the focus of the thesis. In a seminal paper published over 40 years ago, Hubel and Wiesel differentiated between two cell types – simple and complex (Hubel & Wiesel, 1962). Simple cells in primary visual cortex (V1) have receptive fields, which represent a defined area of visual space. Complex cells respond to several of these receptive fields, and are involved in higher-order processing of the

same visual stimuli. This was the foundation for their hierarchical model of vision and is depicted in Figure 3, which shows how information from more downstream areas are integrated upstream, and how cells further upstream in the pathway respond to increasingly larger receptive fields. The hierarchical model primarily involves these two types of cells, and extends from V1 all the way to temporal brain regions (Serre, 2014).

After the discovery of simple and complex cells, researchers established the principle that receptive fields of simple cells spatially represent Gabor-like shapes, and the firing pattern of these cells could be controlled by changing the spatial and temporal frequency of sinusoidal grating patterns, or Gabor patches (Movshon, Thompson, & Tolhurst, 1978). In order to code the information in the receptive field with millisecond precision, cells depend on their fast membrane potential changes. When these fast-spiking cells fire together, the result is neural synchronization at the gamma frequency (30-120 Hz), which will be discussed later in this Chapter and in Chapter 3.

Regions of Interest: V1, FG, and Dorsolateral Prefrontal Cortex

Visual information is first received in V1 (or BA17), and then is transmitted dorsally to parietal regions, and ventrally to temporal regions, including the FG, which extends to the occipital cortex. The FG has shown to play an important role in object recognition, especially when these objects have social saliency (Grill-Spector, Knouf, & Kanwisher, 2004; Parvizi et al., 2012). While both V1 and the FG have an established and direct role in visual processing, areas in prefrontal and frontal cortex play a more indirect and executive role in visual processing. Dorsolateral prefrontal cortex [roughly corresponding to Brodmann Area 9 (BA9)] has classically shown links to language processing (Brannen et al., 2001) and decision-making (Heekeren, Marrett, Bandettini, & Ungerleider, 2004). However this region may also be linked to visual processing and function. Studies of frontal areas, specifically regions involving BA9/10, show relationships to coordinate and categorical visual spatial memory (Slotnick & Moo, 2006). More

relevant to ASD, a study argued that individuals with ASD showed reduced connectivity between the fusiform and middle frontal gyrus while performing tasks involving response to faces (Koshino et al., 2008).

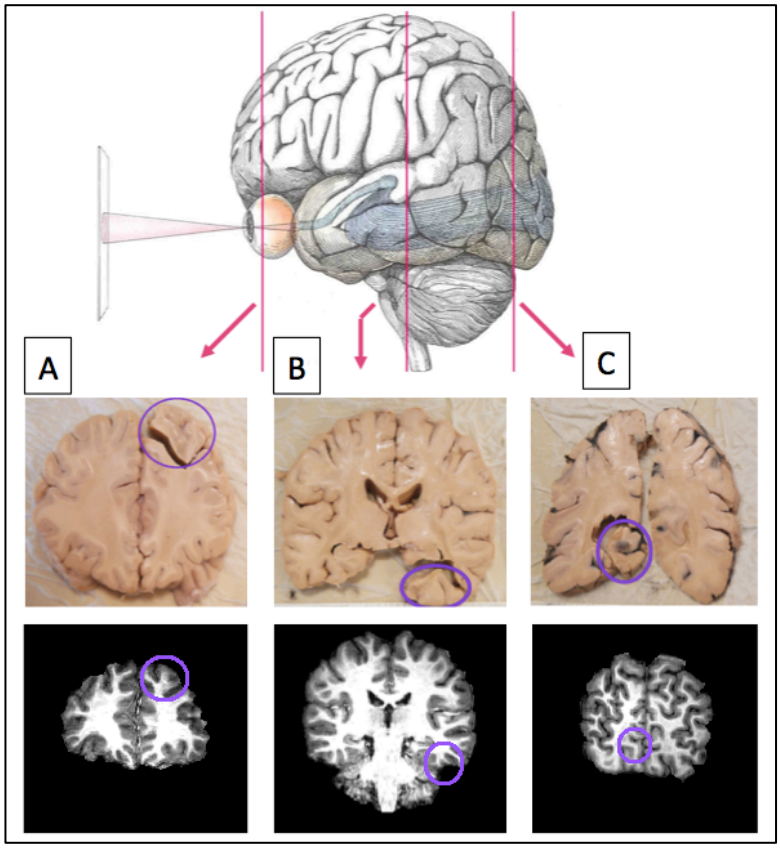

Figure 4. Regions of interest (ROIs) in this study. Coronal slices of both post-mortem tissue and Magnetic Resonance Imaging (MRI) scans of A) BA9, B) the FG, and C) V1 are shown below the main schematic of the brain. Purple circles outline the approximate location.

It seems evident that visual processing involves a pathway of brain regions that link V1, the FG, and BA9, despite their various functional roles, as depicted in Figure 4. V1 processes the basic features of a visual stimulus, whereas FG processes the visual stimulus in the context of its social saliency, and BA9 responds to visual stimuli in a highly specialized manner, and modulates the perception of the visual stimuli in a top-down approach (Gazzaley et al., 2007). These three regions will be studied in this thesis because they have all been implicated in ASD (Amaral et al., 2008; Hadjikhani et al., 2004; McKavanagh, Buckley, & Chance, 2015; Van Kooten et al., 2008), and all reside in anatomically distinct areas of the brain. In addition to diagnostic differences, any observed regional effects may provide insight into visual processing in ASD.

Neuropathological studies previously conducted within the Neuroanatomy and Cognition Group have shown that, contrary to a previous hypothesis that only frontal regions in ASD are compromised (Buxhoeveden et al., 2006), ASD individuals may show neuropathological

differences in both primary sensory and association cortices (McKavanagh et al., 2015). The purpose of this work is to further add to the discussion of primary sensory versus association deficits in ASD, specifically in the context of hyperexcitability and atypical connectivity.

Hyperexcitability in ASD

Results from neuroimaging, genetic, and pharmacological studies suggest that there may be an imbalance of excitatory to inhibitory activity in ASD (Rubenstein & Merzenich, 2003; Yizhar et al., 2011). The hyperexcitable state in ASD may be the result of several factors, including increased glutamatergic signalling, decreased Gamma-Aminobutyric acid (GABA)-ergic signalling, delayed synapse maturation, and abnormal myelination. Altered glutamatergic/GABAergic signalling may imbalance the amount of neurotransmitter release at the synapse, whereas abnormal myelination may disallow the proper development of synapses, and facilitate increased cortical noise (Rubenstein & Merzenich, 2003). The balance between excitation and inhibition can be investigated both at the cellular and systems levels. The following sections will review studies on hyperexcitability in the context of ASD using methodologies both at the cellular and systems level.

Gamma Oscillations

Gamma oscillations are hypothesized to reflect synchronized brain activity in response to attention-driven tasks (Headley & Paré, 2013; Polleux & Lauder, 2004), and are fine-tuned by interneuronal inhibitory activity (Buzsáki & Wang, 2012). At the systems level, studying gamma oscillations has shown to probe the excitation/inhibition balance in individuals. This type of oscillatory activity can be studied through both electroencephalography (EEG) as well as Magnetoencephalography (MEG), which will be the focus of this thesis. A recently published review summarizes gamma differences in individuals with ASD (Rojas & Wilson, 2014). Studies have shown reduced gamma oscillations in ASD both in response to simple visual stimuli involving Gabor Patches (Milne, Scope, Pascalis, Buckley, & Makeig, 2009; Snijders,

Milivojevic, & Kemner, 2013) as well as more complex visual stimuli involving perceptual closure, which requires the ability to perceive a complete object when an incomplete one is presented (Stroganova et al., 2012).

There is some discrepancy in the literature of the accepted gamma band frequency range, with some researchers expressing the belief that the neuronal mechanism producing high gamma frequencies (defined as above 80 Hz) must be different from those at the lower frequencies (defined as 30-80 Hz) (Freeman, 2007). Some researchers use 90 Hz as the point between low and high gamma frequencies (Buzsáki & Wang, 2012), while others do not differentiate between different gamma frequencies all together (Fontolan, Krupa, Hyafil, & Gutkin, 2013). Due to the lack of consensus in the literature, this thesis adapted a broad definition of the gamma range (30-120 Hz), in accordance with previously published papers on visual processing (Chaumon, Schwartz, & Tallon-Baudry, 2009; Honkanen, Rouhinen, Wang, Palva, & Palva, 2014).

Magnetic Resonance Spectroscopy Studies

Magnetic Resonance Spectroscopy (MRS) studies on ASD show that several brain metabolites are altered. However, these results vary depending on the scanning parameters, brain regions, age and gender of participants, as well as whether these individuals were taking medications or not (Baruth, Wall, Patterson, & Port, 2013). One study looked at occipital, frontal and temporal grey matter, and found widespread reduction of a marker of glutamate (Glu) (DeVito et al., 2007), suggesting altered glutamatergic neurotransmission. Other studies have reported on reduced markers of Glu in the anterior cingulate cortex (Bernardi et al., 2011), as well as reduced GABA in an area of the frontal lobe (Harada et al., 2011).

Molecular Studies

20% of all neocortical interneurons are GABAergic, as found in mice studies (Tamamaki et al., 2003), although this percentage varies depending on the species, with primates having a greater

number of GABAergic cells (Hendry, Schwark, Jones, & Yan, 1987; Jones, 2009). Calbindin, calretinin, and parvalbumin are the three main types of calcium-binding GABAergic interneurons and largely show non-overlapping expression in primates (Zaitsev et al., 2005). With regards to parvalbumin+ (PV+) cells – the main focus of Chapter 4 in this thesis – studies have showed a direct link between this cell type and gamma oscillations, making this subgroup of interneurons a point of interest in ASD studies (Sohal, Zhang, Yizhar, & Deisseroth, 2009).

Under the hyperexcitability framework of ASD, it is hypothesized that all or some of these interneurons should be decreased in ASD. However, the findings in the literature are varied. For example, all three of the calcium binding interneurons have shown to be increased (rather than decreased) in the hippocampus of post-mortem ASD cases (Lawrence, Kemper, Bauman, & Blatt, 2010), whereas other studies have shown no differences in PV+ cells in the posterior cingulate cortex and fusiform gyrus (Oblak, Rosene, Kemper, Bauman, & Blatt, 2011), as well as no differences in prefrontal cortex (Edmonson, Ziats, & Rennert, 2014). Other molecular studies have demonstrated decreased $GABA_A$ and $GABA_B$ receptors in the cingulate cortex of ASD (Oblak, Gibbs, & Blatt, 2009; Oblak, Gibbs, & Blatt, 2010), as well as decreased $GABA_B$ receptors in the fusiform gyrus (Oblak et al., 2010). These findings suggest that there is a complex interplay between several factors that control the balance, and that more work is required to understand the full mechanism at play.

Atypical Connectivity and Neuronal Organization in ASD

Neuroimaging Studies

ASD individuals are hypothesized to show hyperconnectivity in local networks, and hypoconnectivity in long-range networks (Belmonte et al., 2004). For example, a task-based functional MRI (fMRI) study showed hypoconnectivity between frontal, occipital and parietal regions when ASD individuals performed a cognitive control task, linked to executive function (Solomon et al., 2009). However, fMRI findings seem task specific. For example, in a visual

search task, ASD individuals showed hyperconnectivity in connections running from the posterior superior temporal sulcus (Shih et al., 2011). Other studies have theorized that age is important to consider, (Uddin, Supekar, & Menon, 2013), where children show increased connectivity within-network, and reduced between-network connectivity, adolescents show no differences in within-network connectivity, but do show decreased between-network connectivity, and adults show no within- or between-network connectivity differences (Nomi & Uddin, 2015).

Studies involving diffusion MRI provide a different perspective of atypical connectivity in ASD. A study using diffusion tractography to look at connectivity between cortical regions and at hemispheric asymmetry found that adolescents showed reduced leftward asymmetry in ASD in different fibre tracts, including those connecting 1) the orbitofrontal lobes, 2) the arcuate fasciculus, and 3) inferior frontal gyri. The study also found reduced interhemispheric connection in ASD individuals (Lo et al., 2011).

Minicolumns

A minicolumn refers to a group of 60-100 neurons organized vertically, and represents a repeating unit of structure in the neocortex (Jones, 2000; Mountcastle, 1997). Minicolumns are made up of four main components: 1) pyramidal neurons (layers 2-6), 2) interneurons (layers 1-6), 3) axons (stellate, double-bouquet and myelinated), and 4) dendrites. This organization is hypothesized to ensure that the firing of one cell in a minicolumn does not significantly differ in latency to a cell lying more deep or superficial to it, allowing for a well-timed response to a stimulus (Jones, 2000).

It is hypothesized that local inhibitory circuits control the function of minicolumns. Two common types of synapses that inhibitory interneurons make are perisomatic, where basket and chandelier cells synapse onto the cell soma, axon initial segment or axon hillock, allowing for a quick

inhibitory response, or dendritic, like double bouquet cells, which synapse onto the dendritic trees, allowing for a much weaker inhibitory response. The activity of these inhibitory interneurons plays a crucial role in the proper function of minicolumns.

In 2002, Casanova et al. found that in ASD cases, the spacing between minicolumns was narrower across different brain regions, specifically in frontal and temporal areas of the brain (Casanova, Buxhoeveden, Switala, & Roy, 2002). Since this publication, many have speculated on the specific neuropathology linked to ASD. More recent findings show that minicolumn spacing in ASD cases may actually be wider across a range of brain regions, with a pronounced effect at younger ages (McKavanagh et al., 2015). These contrasting findings emphasize the need for more work to be done on the neuropathological underpinnings of ASD.

Asymmetry in minicolumn width between the two hemispheres have been observed in several brain regions, including the FG, auditory cortex, and planum temporale in the healthy brain (Buxhoeveden, Switala, Litaker, Roy, & Casanova, 2001; Chance et al., 2013; Chance, Casanova, Switala, & Crow, 2008). This asymmetry is hypothesized to facilitate different functional roles, with narrower minicolumn spacing and overlapping neuropil space in one hemisphere resulting in lower resolution and higher holistic processing, and more widely spaced minicolumns and less overlapping neuropil space in the other hemisphere resulting in higher resolution processing (Chance, 2014). Given the ASD literature on impaired "central coherence" (or holistic processing), as well as altered minicolumn spacing, hemispheric asymmetry was a point of interest in this thesis. Though minicolumns were not directly investigated in this thesis, diffusion imaging in the grey matter was used as an in vivo method to study them, with particular interest to hemispheric asymmetry in diffusion measures for ASD and TD individuals.

Thesis Rationale and Hypotheses

This thesis will explore hyperexcitability and atypical connectivity in ASD through three neuroimaging modalities and through immunohistochemistry, focusing on brain areas involved in primary sensory and executive processing. Figure 5 provides an overview of the different techniques used across the Chapters, and their relationships to the main themes of this thesis.

Chapter 2 will investigate differences in diffusion measures (that are thought to represent cortical microstructure) in vivo between ASD and TD individuals, in order to better understand whether ASD individuals show atypical connectivity in the cortical ROIs. The aim of the multimodal-imaging project in Chapter 3 is to study the electrophysiological and biochemical measures of excitability, using MEG and MRS respectively, as well as to help determine whether diffusion imaging in the cortex may be linked to these other established markers of excitation/inhibition. The hypotheses are that ASD individuals 1) have reduced gamma oscillations in the cortex, reflecting a lack of balanced excitatory and inhibitory activity, 2) have reduced levels of GABA and/or increased levels of Glu in cortical regions, and 3) have altered patterns of diffusion in the cortex compared to their TD counterparts. Lastly, if diffusion imaging in the cortex is found to be linked to MEG and MRS, this modality may provide a unique link between hyperexcitability and atypical connectivity. Chapter 3 will also explore the possibility of linking the enhanced perceptual capacity of ASD individuals, which is a previously reported behavioural difference, with measures of hyperexcitability.

The purpose of Chapter 4 is to delve into the question of hyperexcitability in ASD further by examining brain function at the cellular level. Specifically, the distribution of PV+ cells will be studied in the three ROIs in ASD and TD cases. Given that PV+ cells are a marker of GABAergic activity and are linked to gamma oscillations, the hypothesis is that there may be reduced PV+ cells in ASD post-mortem brain tissue.

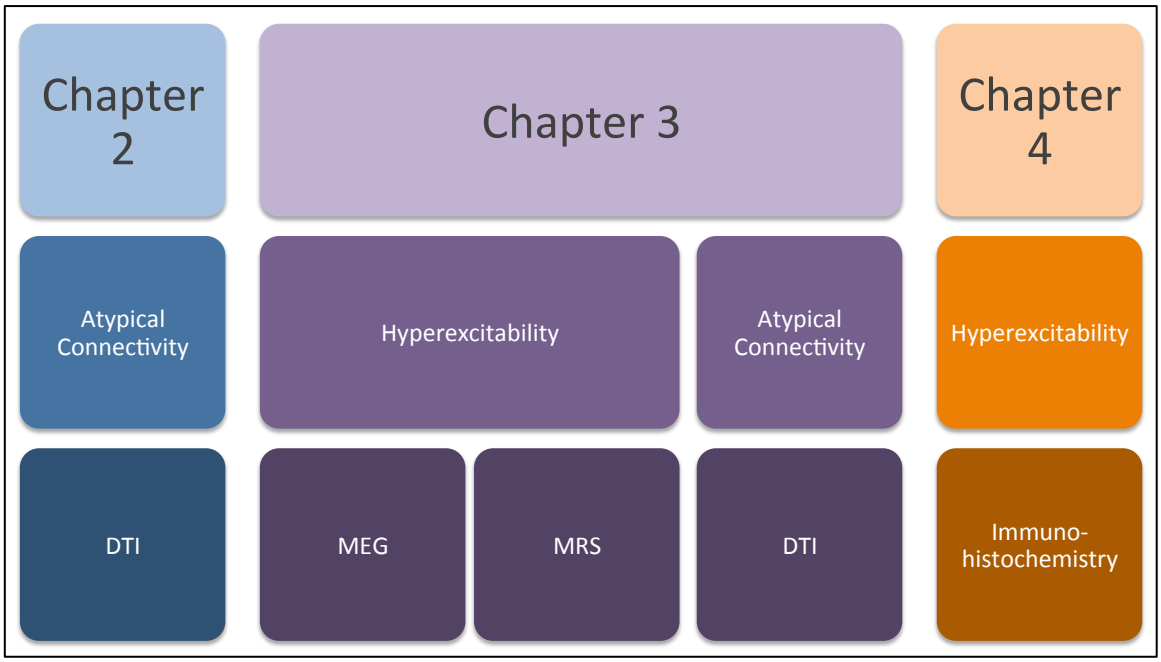

Figure 5. Flowchart of the different techniques used in this thesis to explore hyperexcitability and atypical connectivity in ASD.

Chapter 2: Diffusion Imaging in Cortex

Introduction

Diffusion MRI measures water movement to probe brain structure and connectivity. Based on the orientation, magnitude, and amount of directionality (or anisotropy) of water movement, information can be deduced on the way tracts are organized in the brain. Diffusion Tensor Imaging (DTI) is a popular method of achieving this and has been used extensively to study white matter connectivity.

In cortical grey matter, DTI studies have been limited due to the low resolution that conventional protocols involve and the lack of coherent diffusion patterns in this area of the brain. Hence, histological techniques have prevailed as the primary tool to study cortical microstructure. These techniques – while beneficial – are constrained by tissue sectioning, preservation, and degradation, and are limited to in vitro models. With the correct protocol and analysis tools, diffusion imaging can become a powerful auxiliary tool to study microstructure in cortical grey matter. Research is already underway to use diffusion imaging to reveal the layering patterns and microstructural organization of cortex in vivo.

For example, researchers have reported that diffusion patterns both tangential and radial to the cortex differentiate different laminae in V1 (Leuze et al., 2014). The authors found that diffusion patterns near the surface of the cortex were primarily tangential, whereas deeper laminae revealed more radial patterns of diffusion. Other groups have used cortical diffusion imaging to study both the levels of cortical anisotropy (McKinstry et al., 2002; Shimony et al., 1999), and the direction of diffusion at different stages of infant development and adulthood (McKinstry et al., 2002).

The combination of both diffusion and histological techniques may provide a unique insight into the biological significance of diffusion imaging in the cortex. One novel application currently being established in Oxford is the use of DTI to study the structure and spacing of minicolumns

in post-mortem brain tissue (McKavanagh, 2015). As discussed in Chapter 1, minicolumns characterize the radial microstructure in the cortex, and their altered arrangement in ASD is hypothesized to be one of the pathological underpinnings (Buxhoeveden et al., 2006; McKavanagh et al., 2015). Previous work has shown that certain diffusion measures correlate with minicolumn measurements, specifically the axon bundle width, in the post-mortem brain (McKavanagh, 2015), as depicted in Figure 6. The goal of this Chapter was to use those same diffusion measures in an in vivo dataset with ASD and TD adolescents.

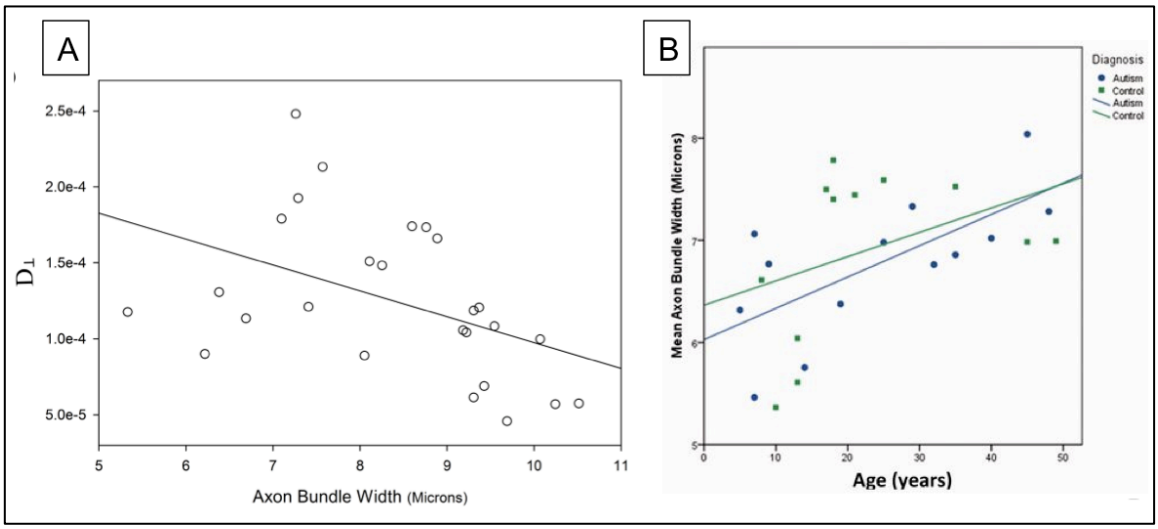

Figure 6. Relationship between diffusion measures and biological factors. A) was adapted from McKavanagh (2015) and shows the negative relationship between a diffusion measure as a function of axon bundle width in microns. B) was adapted from McKavanagh et al. (2015) and shows a positive relationship between age and axon bundle width.

In this Chapter, both an automated and manual masking technique were used to study diffusion patterns in cortex. While both have their benefits, it was hypothesized that the manual masking technique would be particularly useful in understanding cortical microstructure organized radially, for reasons that will be explained in the Methods and Discussion of this Chapter.

Research Questions

1. Are there general differences in diffusion measures, specifically those relating to minicolumnar spacing/axon bundle width, between ASD and TD individuals?
2. Are there hemispheric differences in diffusion measures, specifically those relating to minicolumnar spacing, between ASD and TD individuals?
3. Are there differences in diffusion measures in the three ROIs (BA17, FG, and BA9)?

Methods

Participants

Collaborators at the University of Leuven, in Belgium, acquired the 3 tesla (T) MRI scans. The database was downloaded from the Autism Brain Imaging Data Exchange at the University of Belgium. The data represents a total of 20 ASD and 26 TD adolescents, with demographic information available for 15 ASD and all 26 TD individuals. All ASD participants previously received a diagnosis in the clinical setting in accordance with DSM-IV criteria. In order to confirm diagnosis for ASD individuals and a lack of symptomatology for TD individuals, the SCQ and SRS were administered to all individuals. ASD individuals had to receive a score above 14 on the SCQ or above 60 on the SRS. Diagnosis of ASD was confirmed for 14 of the 15 individuals, and lack of ASD symptoms was confirmed for 25 of the 26 TD individuals. The demographics information for the eligible participants is summarized in Table 1.

Handedness information was not provided in the dataset. All TD individuals had no medical conditions, and all recruited ASD individuals did not have any comorbid psychiatric or neurological conditions. Before partaking in the study, participants were screened for MRI compatibility, which includes not having any surgeries or medical procedures that left behind metal implants.

MRI Acquisition Parameters

The 3T MRI scanner used in the study had an 8-channel phased-array head coil. Structural T1-weighted images were acquired using a turbo field echo sequence with the following parameters: echo time (TE) = 4.6ms, repetition time (TR) = 9.7ms, field of view (FOV) = 250x250mm, resolution = 0.98x0.98x1.2mm. Diffusion images were acquired using a single-shot spin echo echo-planar imaging (SE-EPI) pulse sequencing with the following parameters: TE = 55ms, TR = 4,956ms, FOV = 220x220mm, resolution = 2x2x2mm. 45 gradient directions were applied to the

diffusion data (b = 800 s/mm^2) with one b = 0 s/mm^2 image. Two diffusion images with the same parameters were acquired for each individual.

ASD (n = 14, 11 M, 3 F)			TD (n = 25, 18 M, 7 F)		
	Age (years)	SRS, SCQ		Age (years)	SRS, SCQ
Mean	13.88	94.43, 21.29	Mean	14.37	16.24, 3.04
SD	1.36	32.68, 7.94	SD	1.38	12.71, 2.85

Table 1. Summary of demographic information for eligible participants used in the automated masking pipeline. Mean and standard deviation (SD) are presented for each group.

Processing 3T Diffusion Images

Before standard processing for diffusion images could take place, the MRI images, which were initially in Philips PAR/REC format, had to be converted to a NIFTII file format using the dcm2nii program[2]. The diffusion gradient directions (bvecs) and gradient strengths (bvals) used during the diffusion scans were then extracted using a Unix script. After this was obtained, the processing pipeline for the 3T diffusion dataset involved programs built into FSL [Oxford Centre for functional MRI of the Brain (FMRIB) Software Library]. The pipeline included:

1. Extracting the brain from the skull using a brain extraction tool (Smith, 2002),
2. Correcting for eddy currents (using FSL's "eddy correct" tool), which result from switching between gradients in diffusion imaging, and for gradient-induced heating drift,
3. Fitting the diffusion tensor model onto each voxel in the diffusion image, and producing fractional anisotropy (FA) and mean diffusivity (MD) maps,
4. Performing linear registration for all participants, using 6 degrees of freedom for diffusion to structural images, and 12 degrees of freedom for each individual's structural image to be registered to the standard 1mm Montreal Neurological Institute (MNI) 152 T1 scan, and lastly,
5. Creating new diffusion images in structural space using the matrices from step 4.

[2] This program can be found online at http://www.mccauslandcenter.sc.edu/mricro/mricron/dcm2nii.html.

Automated Masking

After this basic processing was completed, an automated masking technique was used to mask BA17, FG, and BA9, in both hemispheres. These masks were created using the Talairach Daemon Labels and the Harvard-Oxford Cortical Structural Atlas, and are showed in Figure 7. This automated masking pipeline included:

1. Performing a non-linear registration, using each participant's structural image and the standard 1 mm MNI 152 T1 scan,
2. Segmenting the brain into grey matter, white matter, and cerebrospinal fluid (CSF) using FMRIB's automated segmentation tool,
3. Registering each standard mask into structural space,
4. Binarising the mask in structural space, and
5. Refining the mask to only include voxels that were 100% grey matter, as determined by the segmentation process in step 2.

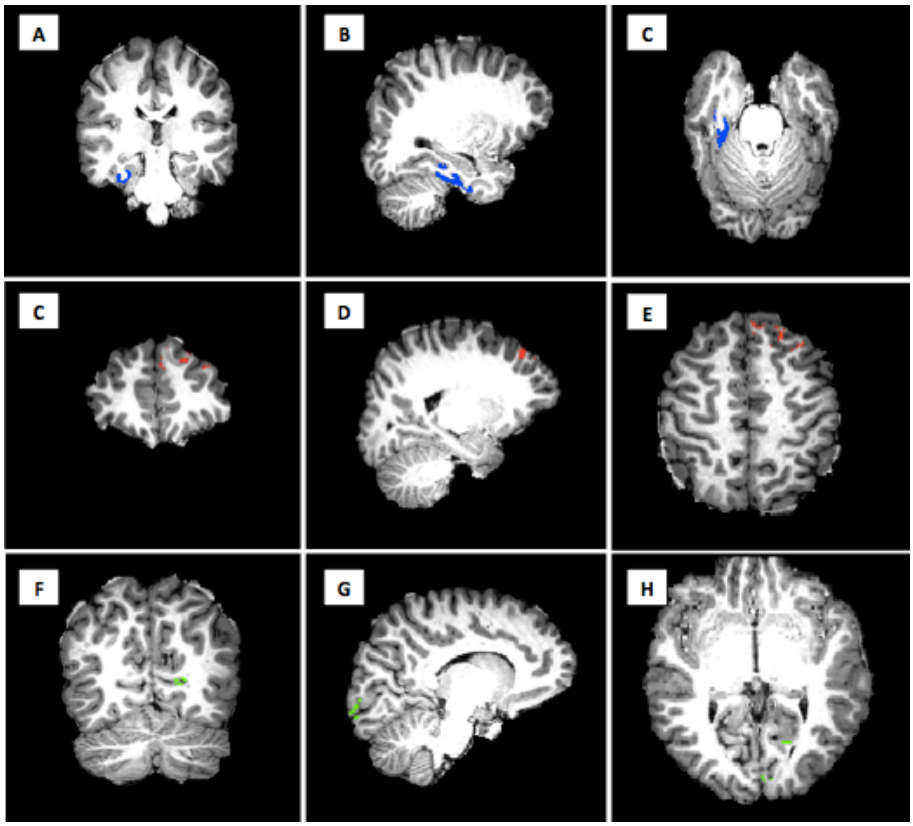

Figure 7. Screenshots of automated masks. A), B), and C) show the coronal, sagittal, and axial views respectively of the right FG mask. C), D), and E) are the same perspectives but for left BA9 in the same participant, and F), G), and H) are the same perspectives but for left BA17 in the same participant.

Manual Masking

The automated masking method was useful because it was quick and easy to complete. However, these masks were not anatomically precise, and often did not produce smooth and continuous outputs, which was required for an in-house program called Cortical High-Intensity Profile Segmentation (CHIPS). This program, described later on, was designed specifically to measure diffusion values that may be a proxy for cortical minicolumn spacing. Therefore, a manual masking method was also employed. The same images processed for diffusion artefacts in the previous section were used here. However, instead of using masks from a standard brain atlas, masks for BA17, FG, and BA9 for both left and right hemisphere were manually drawn on 10 TD and 10 ASD participants' structural images. Afterwards, the grey matter-CSF and grey matter-white matter boundaries were outlined with a pen tool on FSLView (Smith, 2002), which was required for CHIPS. The demographics information for the participants chosen for manual masking is outlined in Table 2.

ASD (n = 10, 7 M, 3 F)			TD (n = 10, 6 M, 4 F)		
	Age (years)	SRS, SCQ		Age (years)	SRS, SCQ
Mean	14.31	94.43, 21.29	Mean	14.42	20.10, 2.85
SD	1.33	32.68, 7.94	SD	1.22	15.09, 2.79

Table 2. Summary of demographic information for participants chosen for manual masking. TD individuals were matched on chronological age, and where possible, gender. SRS reflects total scores.

Anatomical Landmarks for Manual Masks

All grey matter masks were drawn primarily using the coronal view of the brain, although the sagittal and axial views helped in identifying and removing white matter and CSF voxels. The FG mask spanned 11-16 coronal slices, and was defined anteriorly by the ventral splenium of the corpus callosum on the midline, and posteriorly by the posterior limit of the cingulate gyrus on the midline (Chance et al., 2013). The parahippocampal gyrus (PHG) and inferior temporal gyrus were used to determine the medial and lateral boundaries of the FG, respectively.

Since the anatomical boundaries of BA9 and BA17 are defined by cytoarchitecture and the MRI scans acquired here did not provide resolution at that scale, it was decided that only 15 coronal slices would be used to mask these regions, since this number has shown to provide a stable result for CHIPS (McKavanagh, 2015). For BA9, the most dorsolateral gyrus eight slices anterior and seven slices posterior to the anterior boundary of the cingulate gyrus was masked. Care was taken to ensure the smoothness of the mask, which was essential for the CHIPS program. For BA17, the anterior limit was determined by the intersection of the parieto-occipital fissure with the calcarine sulcus at the midline. The gyrus around the calcarine sulcus on the subsequent 14 coronal slices towards the occipital pole were masked. When the retrocalcarine sulcus, which refers to the posterior tail of the calcarine sulcus (Iaria, Robbins, & Petrides, 2008), bifurcated into two, the gyri of both sulci was masked. These manual masks are depicted in Figure 8.

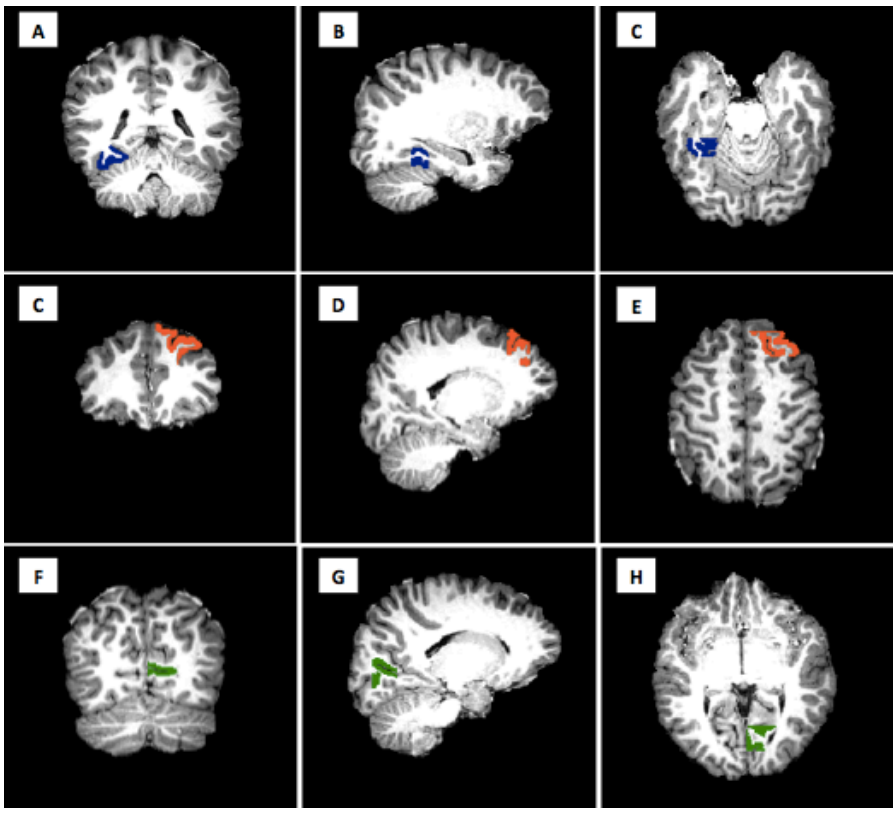

Figure 8. Screenshots of manually created masks. A), B), and C) show the coronal, sagittal, and axial views respectively of the FG mask. C), D), and E) are the same perspectives but for BA9 in the same participant, and F), G), and H) are the same perspectives but for BA17 in the same participant.

CHIPS

For each mask, CHIPS produced cortical profiles of several tensor-derived measurements across the cortex in a radial direction, perpendicular to the cortical surface. The average of these measurements was taken across the region, excluding the edges and the anterior and posterior limit of the mask. The measurements included FA and MD, as well as two measurements related to the principal direction of diffusion in each voxel: 1) the angle of

radiality in radians (Θ_{rad}), which is a measurement of the angle between the PDD and the radial direction of diffusion perpendicular to the cortical surface (v_{surf}), and 2) the vector component of Θ_{rad} that is perpendicular to v_{surf} ($D_{\perp}$). These measurements are described in Figure 9, which was adapted from McKavanagh (2015). FA, MD, Θ_{rad}, and $D_{\perp}$ outputted from CHIPS are interesting because they are thought to reflect differences in neuronal organization oriented radially in the cortex.

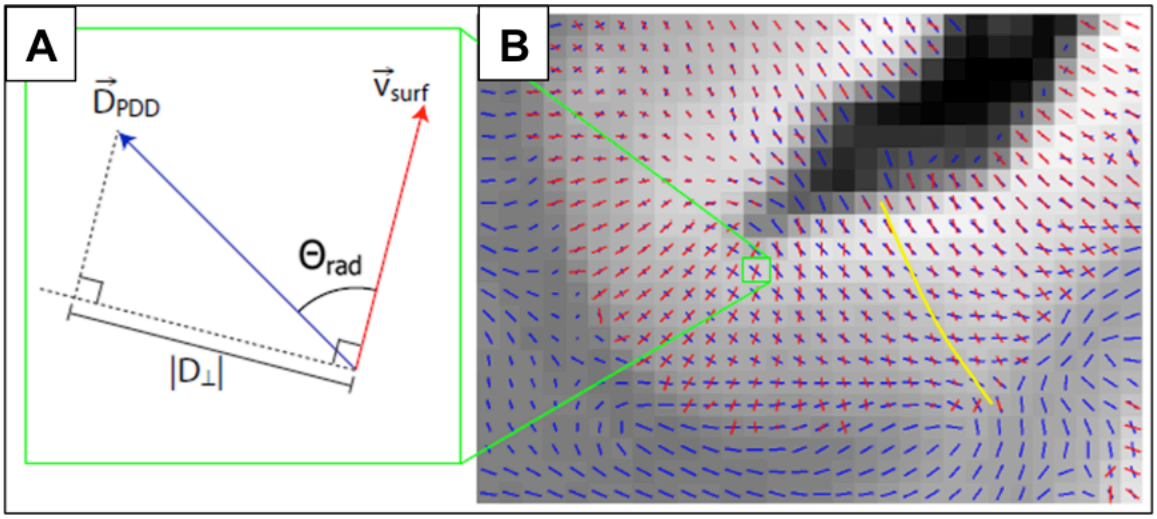

Figure 9. CHIPS outputs. B) shows diffusion patterns in a cortical surface, with v_{surf} in red and the tensor component of the principal direction of diffusion (D_{PDD}) in blue. An average of different measurements, including Θ_{rad} and $D_{\perp}$, is taken across a set of voxels in a radial direction in the cortex, delineated in yellow. A) shows a magnified view of the measurements in one voxel. The red and blue vectors show v_{surf} and D_{PDD}, respectively. The angle between the two shows Θ_{rad}, and $D_{\perp}$ shows the vector component of the principal direction of diffusion that is perpendicular to v_{surf}.

Statistical Analysis

SPSS version 20 for Windows was used for the analysis. A 2x3x2x2 repeated-measures analysis of covariance (rmANCOVA) was used for the different measurements, with hemisphere (2 levels – left and right hemisphere) and the ROIs (3 levels – BA17, FG, and BA9) as the within-subject factors, and diagnostic group (2 levels) and gender (2 levels) as the between-subject factors. Age and total grey matter volume were added as covariates. For the automated masking, data was analysed for the 14 ASD and 25 TD individuals who were eligible. For the manual masks, 10 ASD and 10 TD individuals were included in the analysis.

In order to probe the question of whether the automated and manual masks differed in anatomical location, six paired samples t-tests (3 regions x 2 hemispheres) were performed to compare the volumes between the automated and manual masks for the 20 individuals with both automated and manual masks available. Additionally, the overlapping volume between the automated and manual masks were calculated and graphed.

Results

Automated Masking

FA and MD across regions and hemispheres for each group are plotted in Figure 10. The assumptions of the rmANCOVA were checked and are summarized below.

Normality – The Shapiro-Wilk test confirmed the normality of FA and MD averaged across regions for both the ASD and TD group ($p > 0.05$).

Homogeneity of Variance – Levene's test suggested homogeneity of variance across diagnostic groups ($p > 0.05$).

Sphericity – In the cases where the null hypothesis for Mauchly's test of sphericity was rejected ($p < 0.05$), Greenhouse-Geisser and Huynh-Feldt adjustments were used, for epsilon values > 0.75, and < 0.75, respectively.

Homogeneity of the Covariate Regression Slopes (specific to ANCOVAs) – The test for the homogeneity of the regression slopes failed to reject the null hypothesis, suggesting that an ANCOVA would be appropriate.

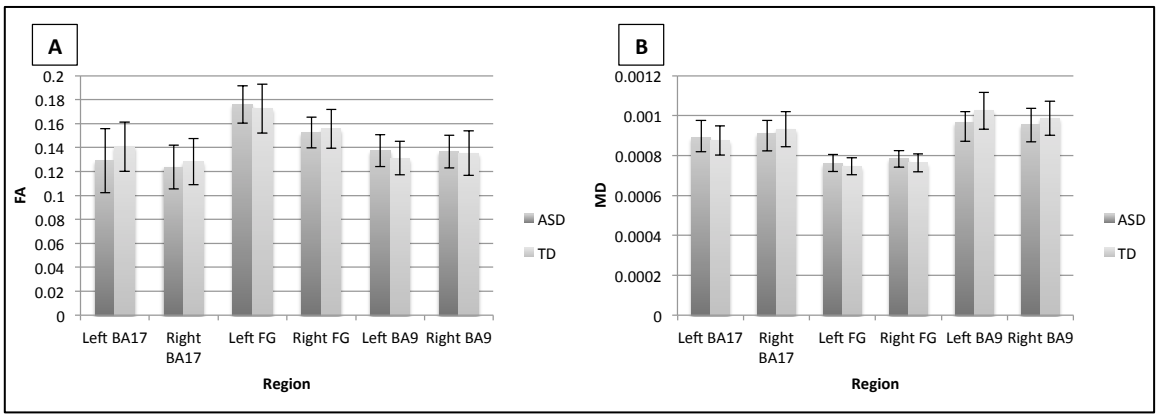

Figure 10. Results for automated masking. A) depicts FA, and B) depicts MD across regions and hemispheres. Error bars represent SE.

The rmANCOVA results for FA and MD across the ROIs are summarized in Table 3 below. For FA, the results suggest no main effect of hemisphere, brain region, gender, age or diagnosis, although the effect of age in years trended on significance ($p = 0.086$). The significant hemisphere by group by gender interaction was followed up with graphs, shown in Figure 11. The graphs show a mean leftward asymmetry for FA for both genders and diagnostic groups. To confirm this finding, a post-hoc paired samples t-test revealed that the mean FA value in left hemisphere was significantly higher compared to FA in the right hemisphere ($t(38) = 4.632$, $p < 0.001$). When this paired samples t-test was run, but split by gender, left hemisphere asymmetry for FA was still demonstrated in males ($t(28) = 4.188$, $p < 0.001$), but not in females ($t(9) = 2.50$, $p = 0.060$). For the left hemisphere, ASD males showed lower mean FA values than their TD counterparts, whereas ASD females had higher mean FA values, as seen by the graphs in Figure 9. It is important to note that the female group for both TD and ASD individuals are underpowered by low n-values. For MD, there were no main effects of hemisphere, brain region, gender, age or diagnosis, but the region by age interaction (not reported in Table 3) trended on significance ($p = 0.05$).

	Measures of Cortical Diffusion	
	FA	MD
Effect of hemisphere	$F(1,33) = 0.772$ **$p = 0.386$** $\eta^2 = 0.023$	$F(1,33) = 0.646$ **$p = 0.427$** $\eta^2 = 0.019$
Effect of brain region	$F(2,66) = 0.821$ **$p = 0.445$** $\eta^2 = 0.024$	$F(2,66) = 1.088$ **$P = 0.343$** $\eta^2 = 0.032$
Effect of gender	$F(1,33) = 0.192$ **$p = 0.664$** $\eta^2 = 0.006$	$F(1,33) = 0.023$ **$p = 0.881$** $\eta^2 = 0.001$
Effect of age	$F(1,33) = 3.129$ **$p = 0.086$** $\eta^2 = 0.087$	$F(1,33) = 0.090$ **$p = 0.766$** $\eta^2 = 0.003$
Effect of grey matter volume	$F(1,33) = 0.006$ **$p = 0.936$** $\eta^2 < 0.001$	$F(1,33) = 0.007$ **$p = 0.932$** $\eta^2 < 0.001$
Effect of diagnosis	$F(1,33) = 0.019$ **$p = 0.890$** $\eta^2 = 0.001$	$F(1,33) = 0.368$ **$p = 0.548$** $\eta^2 = 0.011$
Hemisphere by diagnosis interaction	$F(1,33) = 1.645$ **$p = 0.209$** $\eta^2 = 0.047$	$F(1,33) = 0.112$ **$p = 0.740$** $\eta^2 = 0.003$

Hemisphere by gender by diagnosis interaction	F(1,33) = 4.312 **p = 0.046*** η^2 = 0.116	F(1,33) = 0.681 **p = 0.415** η^2 = 0.020

Table 3. Summary of rmANCOVA results for automated masking.

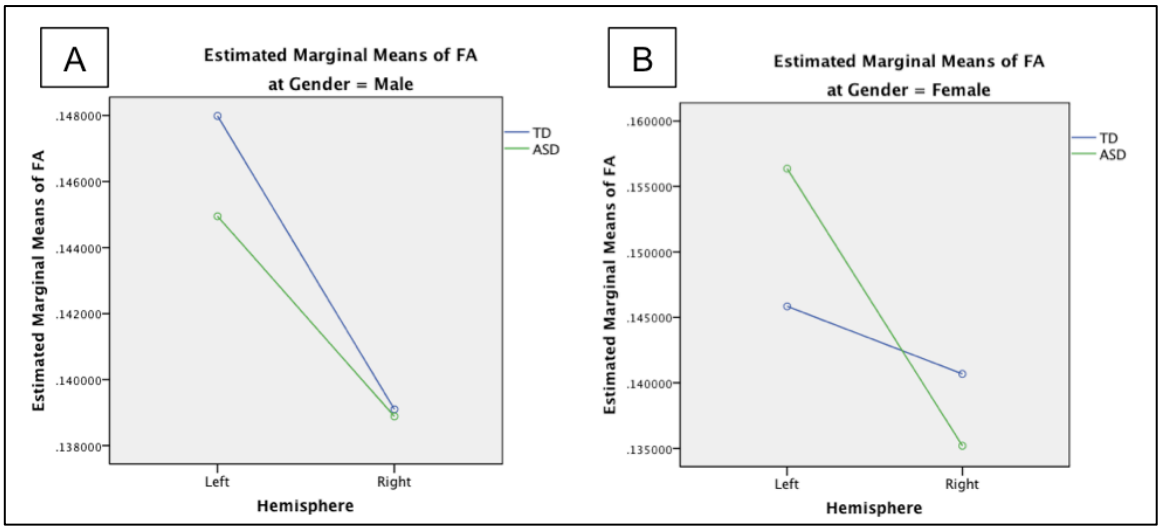

Figure 11. Graphs showing the significant hemisphere by gender by diagnosis interaction for FA. A) shows the interaction for males, and B) shows the interaction for females.

Lastly, to explore the relationship between diffusion measures and diagnostic scores, four Pearson's bivariate correlations were run for SRS and SCQ scores, with FA and MD values (averaged across regions) from automated masking. None of these relationships were significant (all p-values > 0.400).

Manual Masking

A 2x3x2x2 rmANCOVA was run for the four main outputs of CHIPS: FA, MD, Θ_{rad} and $D_{\perp}$, with hemisphere (2 levels) and brain region (3 levels) as within-subject factors, and diagnostic group (2 levels) and gender (2 levels) as the between-subject factors. Age in years and total grey matter volume were added as covariates because these factors are known to affect diffusion measures in the cortex (Pal et al., 2011; Pfefferbaum, Adalsteinsson, Rohlfing, & Sullivan, 2010). The mean values of each diffusion measure are plotted in Figure 12, and the results of the rmANCOVA are summarized in Table 4.

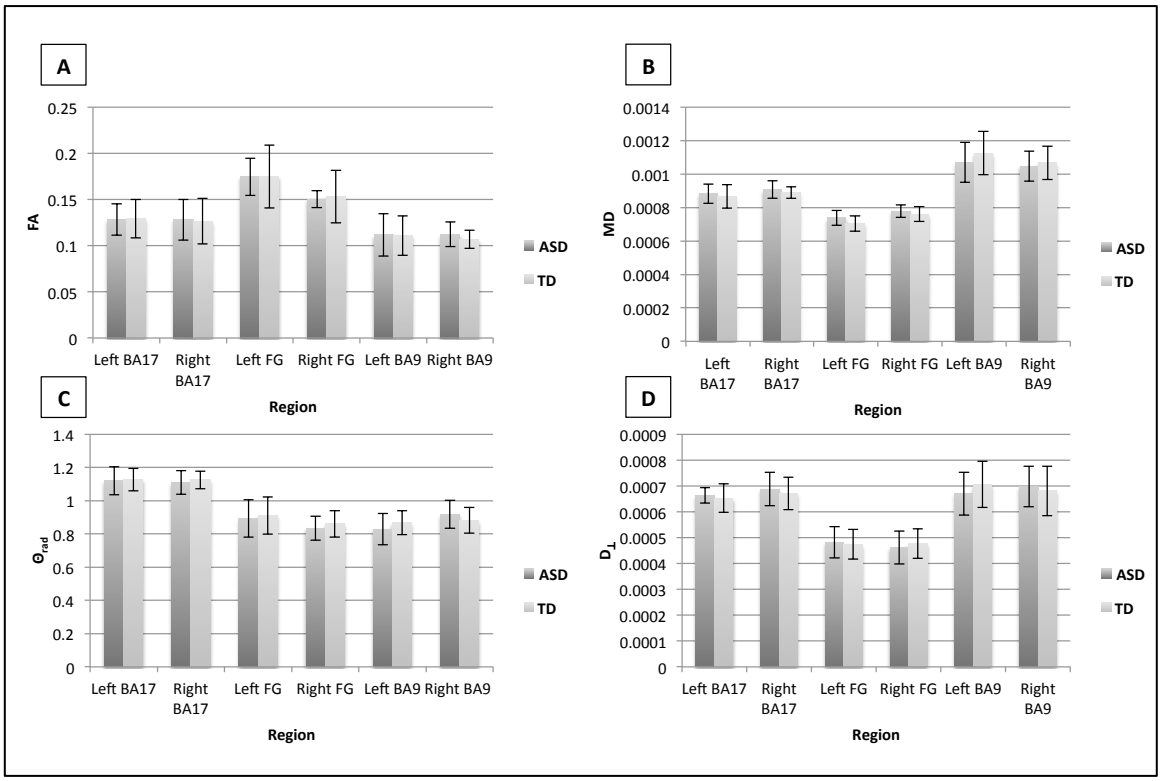

Figure 12. Results for manual masking. A) depicts FA, B) depicts MD, C) depicts Θ_{rad}, and D) depicts $D_{\perp}$ across regions and hemispheres. Error bars represent SE.

	Measures of Cortical Diffusion			
	FA	MD	Θ_{rad}	$D_{\perp}$
Effect of hemisphere	F(1,14) = 0.013 **p = 0.910** η^2 = 0.001	F(1,14) = 0.115 **p = 0.739** η^2 = 0.008	F(1,14) = 0.252 **p = 0.625** η^2 = 0.021	F(1,14) = 0.136 **p = 0.718** η^2 = 0.010
Effect of brain region	F(2,28) = 2.268 **p = 0.122** η^2 = 0.139	F(2,28) = 0.910 **p = 0.414** η^2 = 0.061	F(2,28) = 0.219 **p = 0.805** η^2 = 0.018	F(2,28) = 0.449 **p = 0.643** η^2 = 0.031
Effect of gender	F (1,14) = 0.014 **p = 0.909** η^2 = 0.001	F (1,14) = 0.471 **p = 0.504** η^2 = 0.033	F (1,14) = 0.617 **p = 0.447** η^2 = 0.049	F(1,14) = 0.216 **p = 0.649** η^2 = 0.015
Effect of age	F(1,14) = 0.585 **p = 0.457** η^2 = 0.040	F(1,14) = 0.189 **p = 0.671** η^2 = 0.013	F(1,14) = 2.183 **p = 0.165** η^2 = 0.154	F(1,14) = 1.080 **p = 0.316** η^2 = 0.072
Effect of grey matter volume	F(1,14) = 1.935 **p = 0.186** η^2 = 0.121	F(1,14) = 1.533 **p = 0.236** η^2 = 0.099	F(1,14) = 0.005 **p = 0.945** η^2 < 0.001	F(1,14) = 0.724 **p = 0.409** η^2 = 0.049
Effect of diagnosis	F(1,14) = 0.673 **p = 0.426** η^2 = 0.046	F(1,14) = 0.471 **p = 0.504** η^2 = 0.033	F(1,14) = 1.144 **p = 0.306** η^2 = 0.087	F(1,14) = 0.680 **p = 0.423** η^2 = 0.046
Hemisphere by age interaction	F(1,14) = 2.851 **p = 0.113** η^2 = 0.169	F(1,14) = 6.30 **p = 0.025*** η^2 = 0.310	F(1,14) = 0.076 **p = 0.788** η^2 = 0.006	F(1,14) = 0.508 **p = 0.488** η^2 = 0.035
Brain region by age interaction	F(2,28) = 0.184 **p = 0.833** η^2 = 0.013	F(2, 28) = 1.145 **p = 0.333** η^2 = 0.076	F(2,28) = 1.608 **p = 0.221** η^2 = 0.118	F(2,28) = 4.425 **p = 0.021*** η^2 =0.240

Hemisphere by diagnosis interaction	F(1,14) = 0.307 **p = 0.588** η^2 = 0.021	F(1,14) = 1.043 **p = 0.325** η^2 = 0.069	F(1,14) = 0.758 **p = 0.401** η^2 = 0.059	F(1,14) = 0.744 **p = 0.403** η^2 =0.050
Hemisphere by gender by diagnosis interaction	F(1,14) = 6.753 **p = 0.021*** η^2 = 0.325	F(1,14) = 10.393 **p = 0.006**** η^2 = 0.426	F(1,14) = 0.223 **p = 0.645** η^2 = 0.018	F(1,14) = 0.911 **p = 0.356** η^2 = 0.061

Table 4. Summary of rmANCOVA results for manual masking.

For FA, the rmANCOVA revealed no significant main effects. However, there was a significant hemisphere by gender by diagnosis interaction, as reported in the automated masking results. Graphs were plotted to understand this interaction and are shown in Figure 13. Both genders and diagnostic groups showed a leftward asymmetry, except for ASD females. From the graphs, it seems that FA values in the left hemisphere for ASD males were higher compared to their TD counterparts. For ASD females, FA values were higher in the right hemisphere, and lower in the left hemisphere, compared to their TD counterparts. Again, it is important to note the low n-value for the female subgroup.

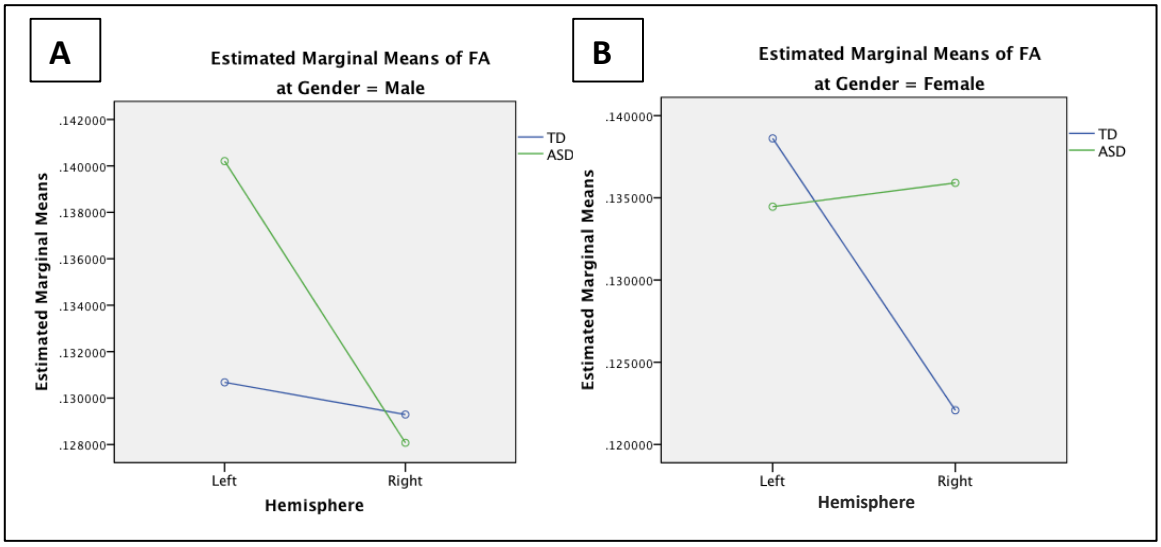

Figure 13. Graphs showing the significant hemisphere by gender by diagnosis interaction for FA from manual masking. A) shows the interaction for males and B) shows the interaction for females.

There was a significant interaction between hemisphere and age in years for MD levels. A Pearson's bivariate correlation was performed between the left hemisphere MD values (averaged across regions) and age, as well as the right hemisphere MD values and age. The Bonferroni adjusted alpha level was 0.025 (0.05/2 = 0.025). Neither correlation showed significance at the adjusted alpha level. The significant hemisphere by group by gender interaction for MD was

followed up with graphs, shown in Figure 14. These graphs show that ASD males and TD females had rightward asymmetry, and TD males and ASD females had leftward asymmetry.

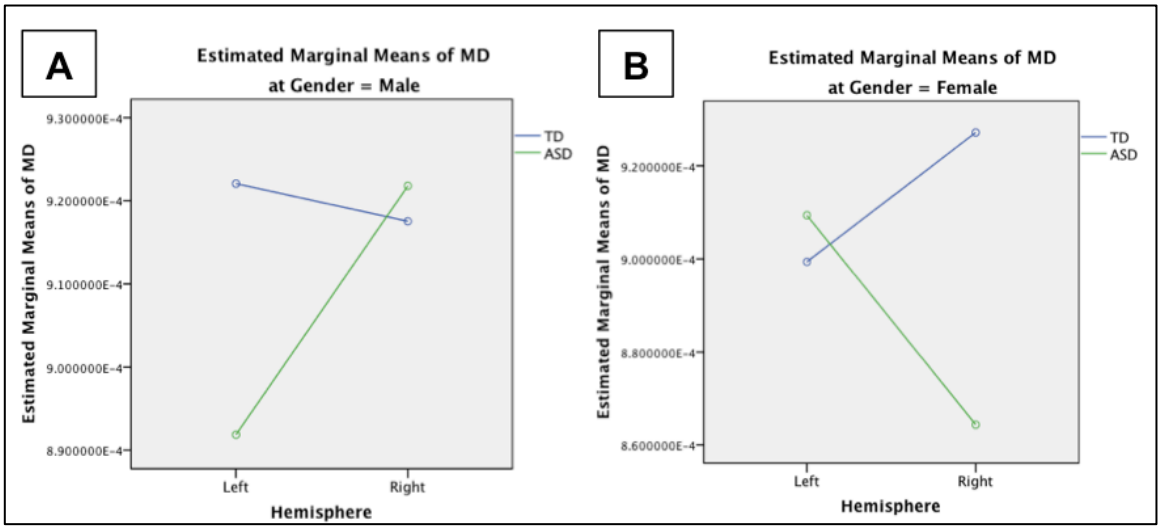

Figure 14. Graphs showing the significant hemisphere by gender by diagnosis interaction for MD. A) shows the interaction for males, and B) shows the interaction for females.

The significant interaction between brain region and age for $D_{\perp}$ was further explored using post-hoc tests. A 2-tailed Pearson's bivariate correlation was performed between age and $D_{\perp}$ for each brain region. Three correlations were run and the Bonferroni-adjusted alpha level was 0.017 (0.05/3 = 0.017). While there was a negative correlation between mean $D_{\perp}$ in BA9 and age, this did not pass the Bonferroni correction for multiple comparisons.

Lastly, an exploratory approach was taken to determine if there were any relationships between SRS and SCQ scores with any of the diffusion measures. Eight Pearson's bivariate correlations were run between total SRS and SCQ scores, with FA, MD, Θ_{rad} and $D_{\perp}$ averaged across regions. None of these relationships were significant (all p-values > 0.100.

Comparing the Automated and Manual Masking Volumes

Figure 15 shows the overlapping automated and manual left hemisphere masks for one participant. Figure 16 depicts the average volume of the masks for the different regions, for the automated and masking technique, and Table 5 summarizes the paired samples t-test results from

comparing the two techniques. All manual masks were significantly greater in volume compared to their automated counterparts. Additionally, the overlapping masks between the automated and manual masks for each region were calculated, and are shown in Figure 17. Figure 15, Figure 17, and Table 5 suggest that the masks from the two techniques did not significantly overlap with one another.

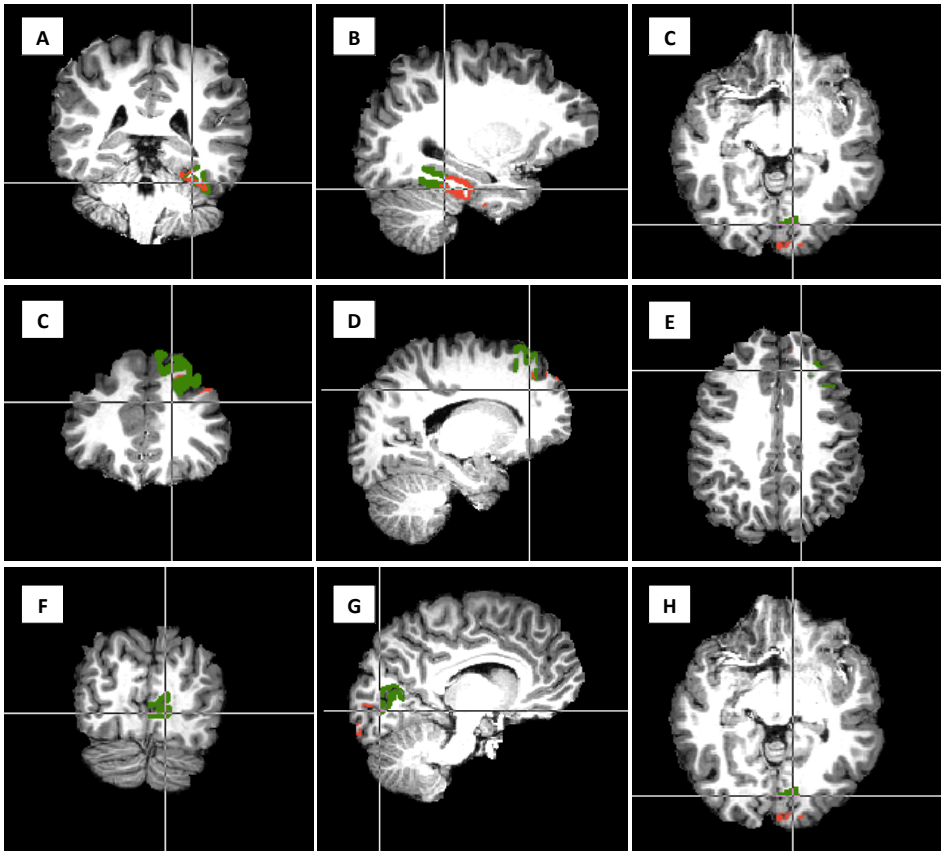

Figure 15. Figures showing the automated and manual mask overlapped for one participant. A), B), and C) show the coronal, sagittal, and axial views respectively of the left FG mask. D), E), and F) are the same perspectives but for left BA9, and F), G), and H) are the same perspectives for left BA17.

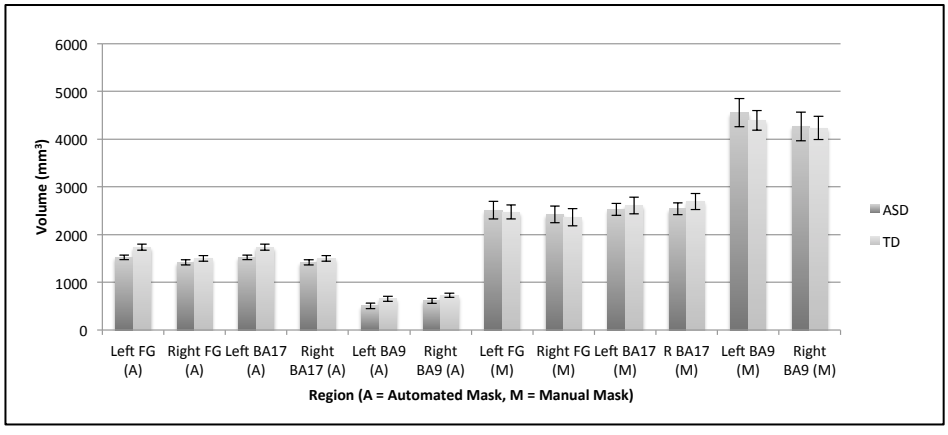

Figure 16. Average mask size for each of the brain region and masking technique. Error bars represent SE.

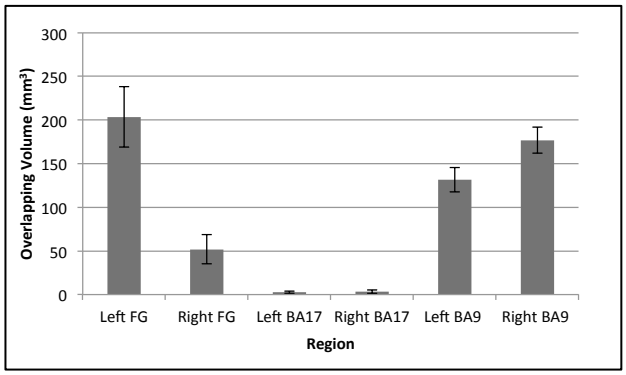

Figure 17. Overlapping volume between automated and manual masks across the different regions.

Comparisons	Results
Left BA17	t(21) = 9.354 **p < 0.001****
Right BA17	t(21) = 11.177 **p < 0.001****
Left FG	t(21) = 6.947 **p < 0.001****
Right FG	t(21) = 8.125 **p < 0.001****
Left BA9	t(21) = 20.469 **p < 0.001****
Right BA9	t(21) = 19.974 **p < 0.001****

Table 5. Main results from comparing the volume differences between automated and manual masks.

Discussion

The purpose of this Chapter was to automatically and manually mask the three ROIs (BA17, FG, and BA9) and to determine whether there were differences in cortical diffusion measures between ASD and TD individuals. The automated technique was used to extract average FA and MD values across each cortical mask, whereas the manual technique used the CHIPS program to extract FA and MD values, calculated in a novel way, as well as Θ_{rad} and $D_{\perp}$ values. The automated technique is quick and can provide useful clues to cortical differences in diffusion between ASD and TD individuals. However, it was hypothesized that the manual masking technique in conjunction with the CHIPS method would reveal more useful information about the radial organization of the cortex. While the manual technique was much more time-consuming, the employment of CHIPS[3] probed the question of cortical organization, and helped determine whether any differences seen with the automated masking

[3] CHIPS can also be used with automated masks. However, CHIPS requires smooth masks in order to delineate the white matter/grey matter as well as the grey matter/CSF boundary clearly. Since automated masks are less continuous than manual masks, CHIPS was only run on the manual masks. Moreover, unlike manual masking, the automated masking technique lacks in precision of anatomical boundaries.

were related to biologically relevant structures, like axon bundle width, which has previously shown a negative correlation with $D_{\perp}$ values.

The automated masking technique revealed that both gender and diagnostic group play a role in FA cortical grey matter asymmetry. There was a general leftward asymmetry for FA values across regions, and this relationship was much more pronounced for males than females. This finding is supported by a voxel-based morphometry study, which showed that males had greater leftward asymmetry than females in certain grey matter areas (Good et al., 2001). TD females showed less leftward asymmetry compared to the ASD females. These results suggest that ASD females are more similar to ASD and TD males than they are to TD females. When broadly interpreted, this may provide some support for the Extreme Male Brain hypothesis, which states that ASD females and males may show the most extreme male traits (Simon Baron-Cohen et al., 2005; Baron-Cohen, 2002; Beacher et al., 2012). The CHIPS data from the manual masking showed slightly different results for FA values. A significant interaction between hemisphere, gender, and diagnosis was found. Female ASD individuals showed a mean rightward asymmetry across regions, while TD males, ASD males, and TD females showed a mean left asymmetry. These results are supported by other work (Hu, Sarachana, Sherrard, & Kocher, 2015), and suggest that the female ASD brain is atypical from the other subgroups.

The manual masking method also resulted in a significant interaction between hemisphere, gender, and diagnosis for MD values. ASD males and TD females showed a mean rightward asymmetry, whereas TD males and ASD females showed a mean leftward asymmetry. These results, taken together with the other hemisphere by gender by diagnosis interactions for the other diffusion values, imply that analyses of ASD studies should be stratified by gender whenever possible. Overall, the diffusion data from manual compared to automated masking showed more sensitivity to diagnostic, hemispheric, and gender differences (judged by the number of significant effects found using each method), providing some support for the manual masking technique.

No significant main effect of diagnosis was found for Θ_{rad} and $D_{\perp}$values, which have previously shown to reflect microstructural differences, like axon bundle width (McKavanagh, 2015). A recent publication showed that minicolumn spacing differences between ASD and TD individuals were more pronounced at a young age (≤16 years, similar to the age group of the cohort in this study). Specifically, the mean axon bundle width was wider for ASD adolescents compared to age-matched controls (McKavanagh et al., 2015). In light of this publication, the lack of significant differences on these diffusion measures between ASD and TD adolescents are surprising. However, this may be because the resolution of the diffusion scans used in this study (2x2x2mm) was lower compared to the resolution of scans that were previously used to establish the relationship between diffusion and histology measures (0.94x0.94x0.94mm) (McKavanagh, 2015). The average cortical thickness is approximated at 2.5mm (Fischl & Dale, 2000), therefore suggesting that one voxel in the diffusion image from this study (with resolution 2x2x2mm) spans almost the entire cortical thickness.

In order to determine whether the automated and manual masks were anatomically similar, the volumes of the automated and manual masks were compared. It was evident that the manual masks on average were significantly larger than the automated masks, and that the overlapping volume between the two masks were small, with the least overlap for BA17. Therefore, it was evident that the same regions in the different masking techniques were characterized by different anatomical boundaries. This is a confounding factor and may be a potential explanation for the differing results between the two techniques. Future work should involve trying to better fine-tune the automated masking technique to better reflect the more precise anatomical boundaries used for the manual masks.

The biggest caveat when interpreting the effects found in this study is the small sample size, especially for female individuals in both the ASD (n = 3) and TD (n = 7) group. Future work should involve recruiting more ASD women in neuroimaging studies and stratifying analyses

based on gender as well as diagnosis. Another limitation is that handedness information was not provided, making it difficult to determine whether this factor played a role in any of the brain asymmetry patterns. However, a previous study using voxel-based morphometry did not find a main effect of handedness, or a significant interaction between handedness and asymmetry in grey or white matter (Good et al., 2001).

Conclusions

DTI, and specifically the manual masking technique used with the CHIPS program, may be a useful method to study microstructural differences in the cortex. It is hypothesized that the diffusion measures unique to CHIPS, like Θ_{rad} and $D_{\perp}$, may be used to study columnar organization in the cortex, which have been reported to be altered in neuropathological studies of ASD. While the work presented in this Chapter did not show differences between ASD and TD individuals in Θ_{rad} and $D_{\perp}$, the main results suggest that there are hemispheric, gender, and diagnostic differences in other cortical diffusion measures like FA and MD. No regional effects were found – however, given the small sample size and the number of covariates used in the analyses, it may be due to a lack of statistical power. Future work should focus on combining high resolution DTI scans with histology to further understand the significance of these diffusion measures, and to fine-tune the analysis methods currently being used to study microstructure in the cortex.

Chapter 3: Multimodal Imaging Project

Introduction

The purpose of multimodal brain imaging is to acquire structural and functional data of the brain using different instruments (Uludağ & Roebroeck, 2014). As shown in Figure 18, imaging techniques differ from one another in their temporal and spatial resolution. For example, while MEG has better temporal resolution compared to MRI techniques, its spatial resolution is less good. Multimodal imaging benefits from combining imaging techniques that complement one another in the temporal and spatial domain.

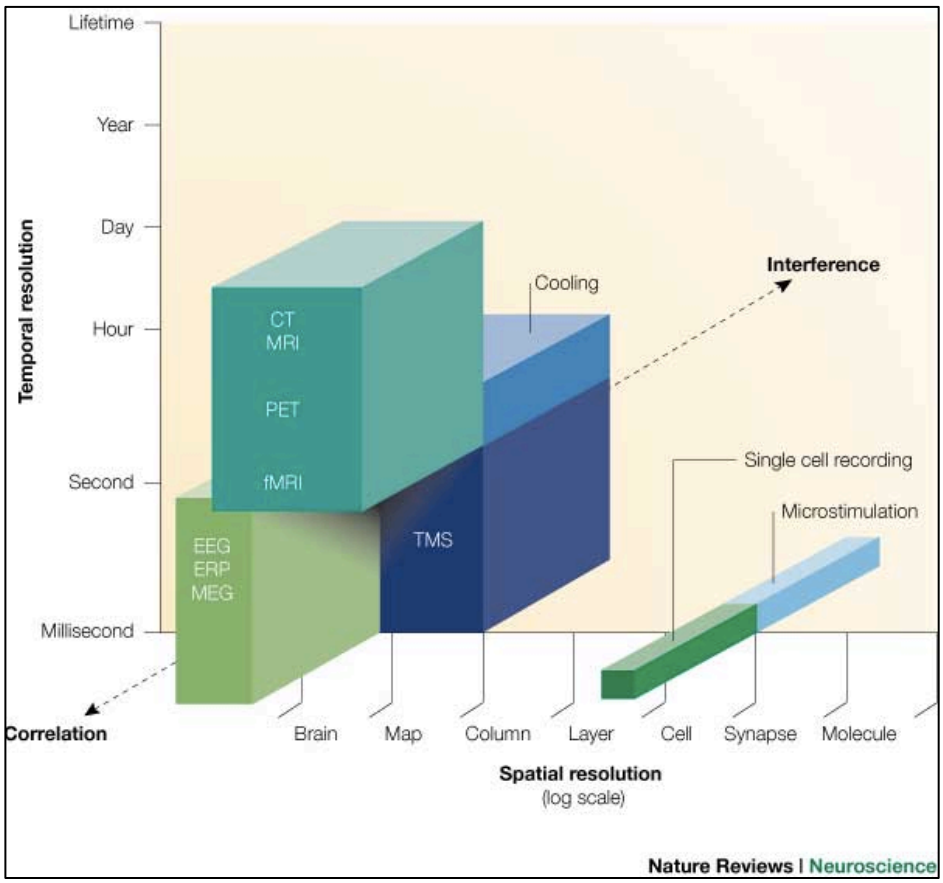

Figure 18. Spatial and temporal resolution of different imaging techniques. This picture is adapted from another publication (Walsh & Cowey, 2000).

The purpose of this Chapter was to study findings relevant to hyperexcitability and structural connectivity in ASD across different modalities. Specifically, this Chapter explored the relationships between MEG, MRS, and DTI findings in the same group of individuals. It also

explored the neural underpinnings of heightened perceptual capacity in ASD, which has previously been reported on (Remington et al., 2012).

The amplitude and frequency of these gamma oscillations have shown relationships with different markers of inhibition through in vitro (Whittington, Traub, & Jefferys, 1995) and in vivo studies (Muthukumaraswamy, Edden, Jones, Swettenham, & Singh, 2009). Muthukumaraswamy et al. (2009) found that there was a positive correlation with the amount of GABA levels and the frequency of gamma oscillations in V1 (Muthukumaraswamy et al., 2009). This seminal paper was the first to establish a direct relationship between two different neuroimaging markers of excitation/inhibition. However, the results have been difficult to replicate, and a recent publication has refuted the initial paper's findings (Cousijn et al., 2014). Figure 19 outlines the results from the two papers. One of the aims of this thesis was to shed light into the relationship between MRS and MEG measurements of excitation and inhibition, and to determine whether there are diagnostic differences in this relationship. No study to date has looked at these different modalities together in the same group of ASD individuals.

Another aim of this Chapter was to determine whether the perceptual load theory of ASD was related to a marker of the excitation/inhibition imbalance in ASD. The previous publication on the perceptual load theory of ASD suggested that high-functioning ASD individuals and TD individuals perform similarly on visual tasks where the perceptual load is low. However, for high perceptual load conditions, ASD individuals show superior performance in visually detecting distractor stimuli.

Lastly, DTI was incorporated in this study to determine whether any of the cortical diffusion measures (discussed in length in Chapter 2) showed group differences in this cohort, and whether these measures related to the excitation and inhibition imbalance. The background information for using this modality can be found in Chapter 2.

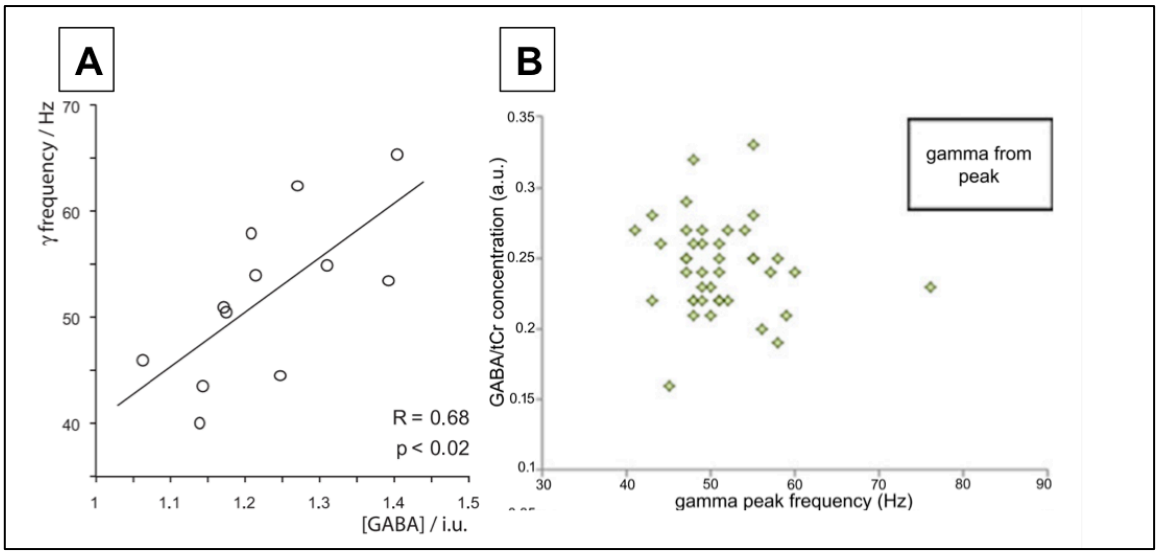

Figure 19. Different relationships between GABA and gamma oscillations. A) was adapted from Muthukumaraswamy et al. (2009), and illustrates a positive correlation between GABA and gamma frequencies. On the contrary, B) shows no correlation between GABA concentrations and gamma peak frequencies, adapted from Cousijn et al. (2014).

Two commonly used terms in the MEG literature are induced activity and evoked activity. While some researchers use these terms interchangeably, other studies adapt the term induced activity to refer to changes in power from baseline, and evoked to refer to changes in phase-locking values (Milne et al., 2009). This thesis refers to evoked activity as time-locked and phase-locked oscillations to a certain stimulus onset/offset, and to induced activity as oscillations that are centred around a certain time, but have a jitter in latency (Bertrand & Tallon-Baudry, 2000). Evoked oscillatory gamma activity was explored in this thesis by performing an analysis in signal space.

One of the main advantages of the MEG analysis used in this thesis is that it examines significant bands of interest, without having a-priori regions of interest (in the time-frequency plane). The bands of interest in this analysis look at interesting regions both in the time and frequency domain rather than just looking at peak frequency alone, which is what other studies have used. For example, in this thesis, the frequency data was analysed and represented globally as a function of time, and particular attention was given to gamma bands strictly at the stimulus onset and offset, emphasizing the importance of the time domain. Some of the disadvantages are that this type of analysis may be more conservative, and is more relevant for data in signal rather than

source space. A general disadvantage for analyses performed in signal space is that there may be volume conduction effects, which are not taken into consideration in the analysis.

A good complement to MEG is MRS, which can probe the biochemistry of the brain. MRS works under the principle that a proton's chemical environment determines its resonating frequency. Since different metabolites in the brain provide different environments for their protons, each proton's unique splitting pattern can act as a chemical signature for different metabolites in the brain. Protons are excited using a radio frequency pulse, and then detected through the free induction decay (FID) pattern. A Fourier transformation is applied to the FID pattern, which results in the total chemical spectrum for an individual, as depicted in Figure 20. This total spectrum can be broken down into the individual metabolite components. An MRS spectrum from V1 for a participant in this study is depicted in Figure 21.

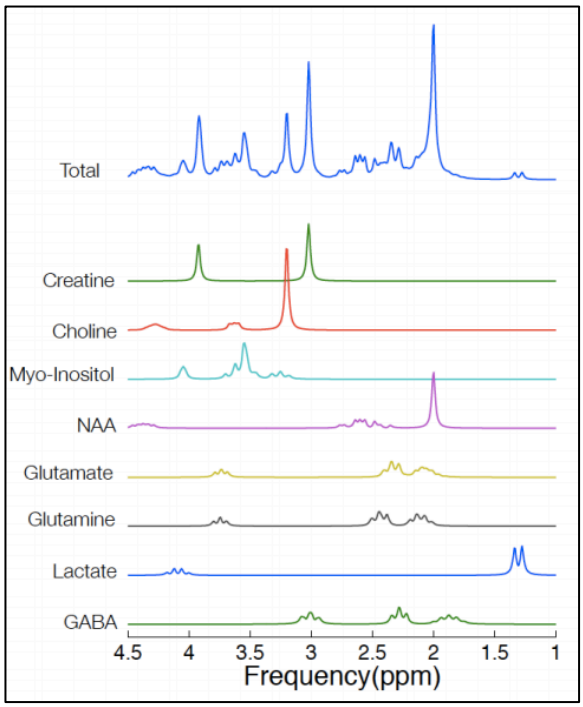

Figure 20. Image of an MRS spectrum and its individual components adapted from a lecture (Near, 2010). The main metabolites investigated in this study are creatine (Cr), Glu, gamma-aminobutyric acid (GABA), n-acetylaspartate (NAA).

Three common types of sequences used for single-voxel localization in MRS are 1) Stimulated Echo Acquisition Mode (STEAM), 2) Point Resolved Spectroscopy (PRESS), and 3) Semi-Localized by Adiabatic Selective Refocusing (semi-LASER), which is the type used in this study. STEAM uses three 90° excitation pulses, whereas PRESS uses one 90° excitation pulse and two 180° refocusing pulses. The challenge with these two techniques used at high magnetic fields (3T or higher) is maintaining a homogeneous magnetic field, due to wavelength effects in the receiver coils. The semi-LASER technique

uses one 90° excitation pulse, followed by two pairs of 180° refocusing pulses, and may be more powerful in establishing a homogeneous excitation (Zhu & Barker, 2011).

The majority of MRS studies on ASD have been completed on 1.5 T and 3 T, which can limit the spectral quality. For example, many MRS studies have reported differences in the Glx peak, which is the summation of glutamine (Gln) and Glu peaks. This is because at lower magnetic fields, these metabolites have overlapping chemical signatures that are difficult to separate. Since Glu is more abundant in the brain, differences in Glx have been attributed to Glu (Baruth et al., 2013). Using ultra-high field MRI scanners for spectroscopy, like the 7T in this study, can help increase the signal-to-noise ratio and increase the spectral resolution. This means there is greater potential to resolve peaks of molecules that have historically been reported together as one (Li, Xu, Chen, Vigneron, & Nelson, 2008).

The purpose of MRS in this study was to specifically look at the following metabolites: GABA, Glu, n-acetylaspartate (NAA), and Cr. The first two are the main inhibitory and excitatory neurotransmitters in the brain. NAA is hypothesized to reflect neuronal differences, and Cr levels are thought to reflect glial density, which have shown alterations in ASD (Menassa, 2013).

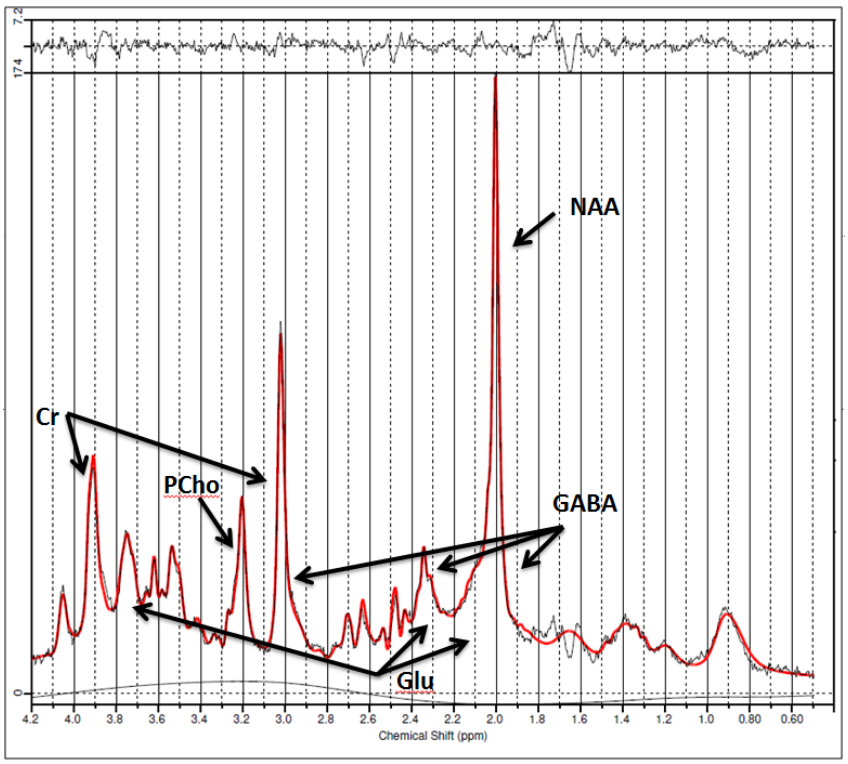

Figure 21. MRS spectrum for an individual in this study, acquired from V1. Arrows point to the location of significant peaks for the metabolites of interest, as well as phosphocholine (PCho). The red outline shows the fit of the data.

Research Questions

MEG:

1. Are there differences (or reductions) in gamma oscillations from a simple visual task between ASD and TD individuals, in V1 or in other regions?

Behavioural Data:

2. Do ASD individuals have a higher perceptual capacity, as described in Remington et al. (2012), compared to TD individuals, when performing a complex visual task?

MRS:

3. Do ASD individuals have reduced GABA levels, or increased Glu levels in V1 and medial prefrontal cortex (MPFC)[4], as predicted by the hyperexcitability model? Do they also show altered levels of NAA, a neuronal marker, or Cr, a marker for glial cells, in these brain regions?

DTI:

4. Are there differences in diffusion measures, specifically those relating to minicolumnar spacing as described in Chapter 2, between ASD and TD individuals in BA17, FG, or BA9?

Multimodal Research:

5. Are similar trends in diffusion measures observed from the dataset in Chapter 2 and this dataset?
6. Are there any relationships between GABA/Glu measures and gamma oscillations, as described in a previous publication?
7. Are there any relationships between gamma oscillations and diffusion measures in occipital cortex?
8. Taking an exploratory approach, are there any other interesting relationships between the different modalities in this study?

---

[4] MPFC rather than dlPFC was used for MRS due to image acquisition constraints in this region.

Methods

The following steps provide a summary of the chronological events with regards to data collection in this multimodal imaging study.

1. Individual expressed interest in the study (through phone, e-mail, or post) in response to an advertisement (paper or online).
2. Individual was provided with a detailed information sheet of the study and confirmed interest and eligibility.
3. Individual was contacted via phone for study eligibility.
4. Individual was tested for IQ, using the Wechsler Abbreviated Scale of Intelligence (WASI), and if in the ASD group, for diagnosis as well.
5. Participant came to the Oxford Centre for Human Brain Activity (OHBA) and performed the Simple Visual Task while in the MEG scanner.
6. Participant performed the Complex Visual Task while in the MEG scanner.
7. Participant was taken to FMRIB and screened for MRI contraindications by a trained radiographer.
8. Participant laid in the MRI scanner for MRS.
9. Participant laid in the MRI scanner for diffusion imaging.

The following Methods section goes into detail about participant recruitment, data collection, experimental design, neuroimaging parameters, and statistical analyses of the results from each modality of this study.

Data Collection

The Medical Sciences Inter Divisional Research Ethics Committee at the University of Oxford provided ethics approval for the study with identification number MSD-IDREC-C2-2013-015. Advertisements were placed on websites, including www.dailyinfo.co.uk and www.autism.org.uk, and on bulletin boards in different hospitals, grocery stores and public areas in Oxford. The final cohort involved 13 ASD individuals and 16 TD individuals. ASD

individuals were recruited and scanned first to ensure that it would be possible to recruit TD individuals who matched for chronological age, gender and IQ. Individuals who expressed interest in the study were sent an electronic or paper copy of the detailed information sheet. After the individual read the information sheet and confirmed interest and eligibility, (s)he was contacted via phone and was screened for eligibility. An individual became ineligible if (s)he: 1) was currently taking non-contraceptive medication, 2) had visual impairments that could not be corrected with glasses available at the MEG scanner (i.e. any visual impairments other than near and far-sightedness, including colour blindness and strabismus), 3) had any contraindications for an MRI (i.e. surgeries involving metal implants), or 4) had major dental work.

All ASD individuals who partook in the study previously attained a clinical diagnosis of high-functioning autism or Asperger Syndrome according to DSM-IV criteria. Four ASD individuals were recruited from a previous Oxford study and had both ADOS and ADI-R scores available. All interested and eligible individuals were tested for IQ with WASI and newly recruited ASD individuals were additionally tested for autism diagnosis with Module 4 of ADOS. These tests always took place before the neuroimaging to ensure eligibility. All ASD individuals made cut-offs with the ADOS or the ADI-R. Since the research questions in this project did not involve language processing or development, it was decided to recruit both native and non-native speakers of English. All participants in this study had a verbal IQ score ≥ 75 and non-verbal IQ score ≥ 85. The WASI took approximately 45 minutes to complete, while the ADOS for newly recruited ASD individuals took one hour to complete. Table 6 summarizes the demographic information for all the participants. All were right-handed except ASD05 and ASD012. Table 7 summarizes what data is available from each individual in the multimodal imaging project.

Modality 1: MEG

MEG Data Acquisition

After IQ and diagnostic scores were collected, individuals were connected to electrodes and coils to undergo the MEG scan at OHBA. One electrode was placed on each wrist to record heartbeats for an electrocardiogram (ECG) and two electrodes were placed above and below the left eye respectively to record eye blinks for an electrooculogram (EOG). The ground electrode was positioned in the middle of the forehead to measure baseline electrical activity. Coils were used to register the head to scanner space. The ECG and EOG were used to measure physiological artefacts that would later be filtered out during data analysis. All data was recorded using the Elekta Neuromag-306 VectorView^{TM} system. This consists of a 306 helmet-shaped channel Superconducting Quantum Interference Device, with 102 pairs of orthogonal gradiometers and 102 magnetometers. A sampling rate of 1,000 Hz was used, with a 0.03-Hz anti-alias filter.

Simple Visual Task Experimental Design

Stimuli for the Simple Visual Task were adapted from a previous study investigating gamma oscillations in individuals (Cousijn et al., 2014). The stimuli were projected on a screen using a Panasonic DLP projector model PT-D7700E with a 1280 x 1024 pixel resolution and 60 Hz frequency. The viewing distance was 120cm. During this task, participants were asked to stare at a small black circle positioned in the middle of the screen, and to press the button "X" when the black circle turned into an open circle. The purpose of this task was to fix the participant's attention to the centre of the screen. Concurrently, one of three different types of visual stimuli appeared on the screen: 1) a Gabor patch in the left visual field, 2) a Gabor patch in the right visual field, or 3) no Gabor patch. Each of these stimuli appeared on the screen for a 2s period, interspersed with a period of no stimulus presentation for 2s. The stimuli occurred in blocks of 5 at the same time, and in a pseudorandom order. In total, 45 presentations of each of the three stimuli occurred, and the total task took 10 minutes to complete. The visual stimuli in the Gabor patches consisted of stationary and vertical gratings (with maximum contrast) of 2.4

cycles/degree with 5.4° visual angles, and were presented on a grey background. The stimuli are shown in Figure 23.

Data Analysis for Simple Visual Task

The data analysis for the Simple Visual Task consisted of both analysing the behavioural results as well as the MEG brain activity. The processing pipeline for the Simple Visual Task was performed through one of OHBA's in-house software called MEG Plotter, which has been used in previous publications (Braeutigam, Rose, Swithenby, & Ambler, 2004; Braeutigam, 2013). The following summarizes the steps.

1. The accuracy of participants' button presses was analysed using Matlab (R2014b) and coded into a spreadsheet.
2. A processing script was run, which incorporated MaxFilter™ and MaxMove™, two programs that aid in removing movement artefacts and cleaning the MEG epochs.
3. Physiological artefacts (including eye blinks and heart beats) as well as gradiometer/magnetometer artefacts were identified using MEG Plotter, and corrected for using a principal component analysis based approach. This step is crucial in ensuring quality when analysing the MEG signal.
4. MEG epochs were extracted for subjects for each of the three conditions (Gabor patch in the left visual field, Gabor patch in the right visual field, and no Gabor patch) and for each of the 306 channels.
5. The data for each individual was combined using a Gabor wavelet transform, which demonstrates phase with respect to the stimuli and the power, represented in time and frequency.
6. A bootstrapping approach was used to assess the standard error (SE) of the data and to identify densities of gamma phase-locking.
7. Different statistical tests were then performed for each channel. Wilcoxon tests were run to evaluate each of the following within-group differences: difference in gamma phase-locking activity between Gabor patch in left visual field and no Gabor patch for the A) ASD, and B)

TD group, as well as difference in gamma phase-locking activity between Gabor patch in right visual field and no Gabor patch for the C) ASD group, and D) TD group. Additionally, Mann-Whitney U tests were run for between diagnostic group differences in phase-locking for 1) Gabor patch presentation in the left visual field, 2) Gabor patch presentation in the right visual field, and 3) no Gabor patch presentation.

8. Channels were combined using a chi-square like method, in order to obtain global (i.e., whole-head) statistics.

In order to investigate gamma activity in the occipital cortex, gamma phase-locking values were extracted from one channel in the left occipital region and one channel in the right occipital region, with consultation of the sensor elements (see Figure 22). This was done to ensure that the task elicited an occipital gamma response from all participants, and to explore whether there were any relationships with these values and data from other modalities, like MRS and DTI.

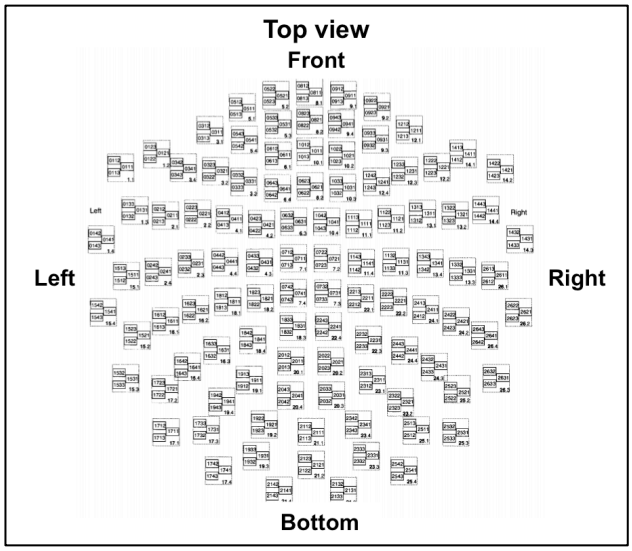

Figure 22. Diagram adapted from the Elekta Neuromag System Hardware for the layout of the sensor elements. The Elekta Neuromag System specifies the channel numbers for the different sensors. This information was used to extract phase-locking values from different participants.

Additionally, the TF-planes for phase-locking values across all channels were examined, with particular attention given to any significant differences between diagnostic groups in the gamma range (30-120 Hz), within 300ms of stimulus onset and within 300ms of stimulus offset. This was more of an exploratory approach to determine whether there were any localized group differences. All analyses for the three stimuli conditions were done separately, since atypical laterality in gamma oscillations have previously been reported (Maxwell et al., 2013).

Complex Visual Task Experimental Design

After the Simple Visual Task, participants took a break and prepared for the Complex Visual Task. This dual-paradigm task was adapted from previously published work (Macdonald & Lavie, 2008; Remington et al., 2012). On any trial of this task, there was an "X" or an "N" (referred to as "target letters") in one of the six positions of a ring centred in the middle of the screen. A participant was presented with one of the four following options during any given trial: 1) one target letter and five small letter Os that were easy to distinguish from the target, 2) one target letter, one non-target letter (K, Y, Z, H, or V) that looked similar to the target letter and four Os, 3) one target letter, three non-target letters, and two Os, or 4) one target letter, five non-target letters and no Os. The set size of these four options was 1, 2, 4, and 6 (determined by the number of letters presented), respectively, where set size 1 reflected the lowest perceptual load and set size 6 the highest. On some of these trials, there was also a small, grey, meaningless squiggle, called the critical stimulus (CS) that appeared anywhere outside the ring of letters. Each participant had to make two decisions during every trial – first, decide whether there was an X or an N in the ring of letters, and second, decide whether the CS was present or absent. The stimuli used in this task are shown in Figure 23. The CS was presented at 0.3° x 0.4° visual angles, the Os were presented at 0.3° x 0.4° visual angles, and the letters (both target and non-target) were presented at 0.6° x 0.6° visual angles. Stimuli were presented at a 120cm viewing distance on the same projector as the Simple Visual Task.

The Complex Visual Task was programmed using Matlab and the Psyctoolbox. All letters in the ring were equally spaced from one another, and each had a radius of 1.7° visual angles. The CS appeared in any one of six positions on an imaginary circle with a radius of 5.4° visual angles, around the ring of letters. Letters appeared in black Courier New text on a grey background, with the red green blue (RGB) values of 205, 205 and 205 while the CS appeared with RGB values of 153, 153, and 153. Participants were asked to decide as quickly as possible whether there was an X or an N on the screen. After presentation of the stimulus on each trial, a black mesh pattern

appeared on the screen to mask the relevant visual stimuli, and then a screen with a question mark appeared. At this point, participants were asked to decide if the CS was present or absent.

The order and duration of stimuli presented on the screen was as follows. Participants were presented with 1) a fixation cross for 1,000ms, 2) the relevant visual stimuli for 100ms, 3) the block mesh pattern for 500ms, 4) a blank screen for 1,400ms, 5) a screen with a question mark for 100ms, and lastly 6) a blank screen for 1,900ms. This is shown in Figure 24.

There were 72 trials in total for each of the four set sizes, divided into two blocks of 36 trials each. In total, there were eight blocks (two blocks x four set sizes) where participants had to make a decision about the target letter and the presence of the CS. These eight blocks were presented in a pseudorandom order, where the first four blocks always included all four set sizes, and the last four blocks reflected the reverse order of the set size in the first four blocks. For example, if the first four blocks presented set size 1, 2, 4, and 6, respectively, the last four blocks would represent set size 6, 4, 2, and 1 in that order. At the end of the eight blocks, all participants were presented with a "control block" of 18 trials, and were asked to only decide whether the CS was present and to ignore the letters. This block ensured that an incorrect decision about the presence of the CS in blocks 1 – 8 were due to the perceptual load and not due to a general inability to detect the CS. The CS was presented in 50% of all the trials.

Data Analysis for Complex Visual Task

For this task, only the behavioural data was analysed (analysis of the MEG data accompanying this task exceeded the scope of this project and may form the subject of future studies). The analysis for behavioural data was done with both Matlab as well as SPSS. The steps for analysis followed closely to those used in the publication that this test is based off of (Remington et al., 2012). Before running any of the statistical tests, the results from the "control block" was analysed for each individual to determine validity of results. After determining which individuals had valid behavioural results, 4 mixed-model ANOVAs were run, and are outlined below.

1. To test the effect of set size on the reaction time of correctly identifying letters in the ring, a 4x2 rmANOVA was run with set size (1, 2, 4, and 6) as a within-subject factor, and diagnostic group (ASD and TD) as the between-subject factor.
2. To test the effect of set size on correct letter identification, a 4x2 rmANOVA was run with set size as a within-subject factor, and diagnostic group as the between-subject factor.
3. To test the effect of set size on correct CS identification, a 4x2 rmANOVA was run with set size as a within-subject factor, and diagnostic group as the between-subject factor.
4. To test the effect of set size on the detection sensitivity (d'), which takes into account both the correct identification of the CS when present and the correct rejection of it when absent, a 4x2 rmANOVA was run with set size as a within-subject factor, and diagnostic group as the between-subject factor.

Modality 2: MRS

MRS Data Acquisition

After the MEG scan, participants were taken to FMRIB, were asked to change into scanner-safe clothing provided by the centre, and were screened again by a trained MRI radiographer for any metal implants or devices in the body. Before entering the scanner, participants were given earplugs and were told how to signal for help if they experienced discomfort. All ^{1}H-MRS data was acquired using a 7T system (Magnetom 7T manufactured by Siemens), which has a 32-channel head array receiver coil. The MRI protocol first began with the acquisition of a T1-weighted structural image, using the magnetisation-prepared rapid gradient-echo (MPRAGE) sequence with the following parameters: TE = 2.82ms, TR = 2,200ms, inversion time = 1,050ms, flip angle = 7°, 192mm x 192mm x 176mm FOV, bandwidth = 240 Hz/pixel, resolution = 1mm x 1mm x 1mm. The ^{1}H-MR spectra were obtained using the semi-LASER sequence with the following parameters: TE = 50ms, TR = 8,000ms, spectral width = 6,000 Hz, number of spectral points = 2,048. The MRS voxel (20mm x 20mm x 20mm) was positioned using the coronal, sagittal and axial views of the MPRAGE scans in two brain regions.

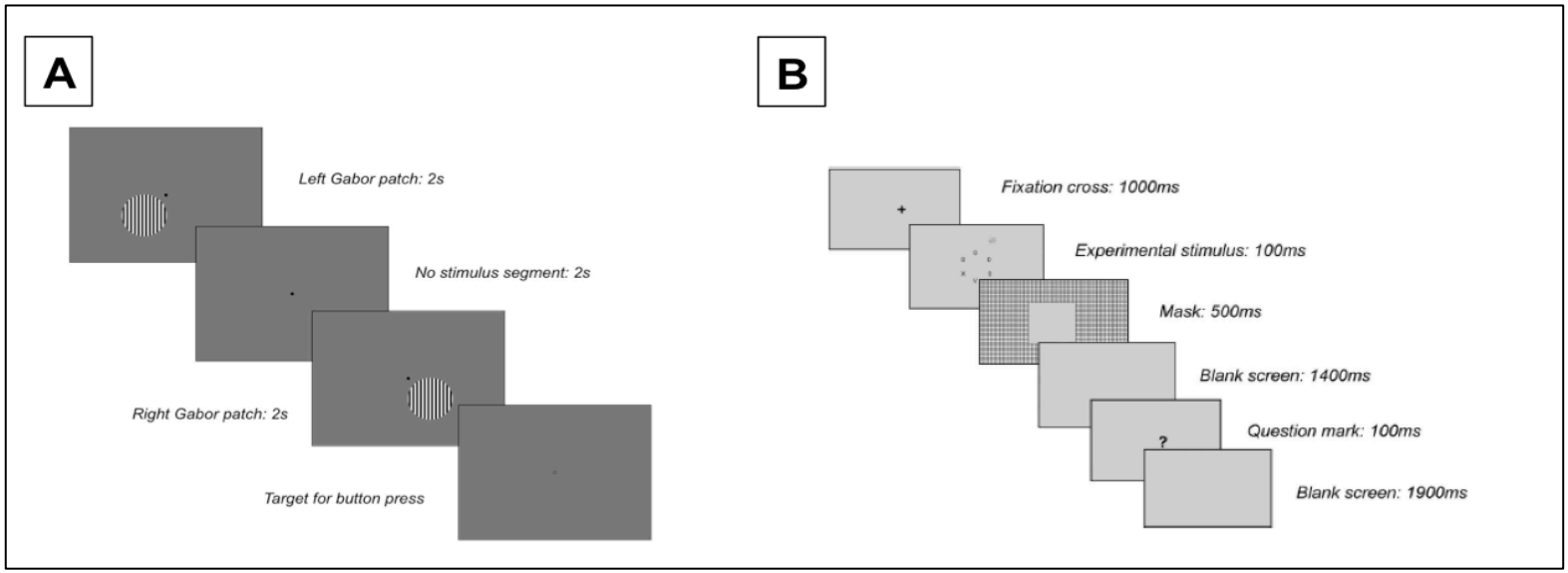

Figure 23. Stimuli presented for the A) Simple Visual Task, and B) Complex Visual Task. A) was adapted from a previous thesis (Doherty, 2013), and shows the order of events for the Simple Visual Task, while B) adapted from Remington et al. (2012) shows the order of events for the Complex Visual Task for a block with set size 2.

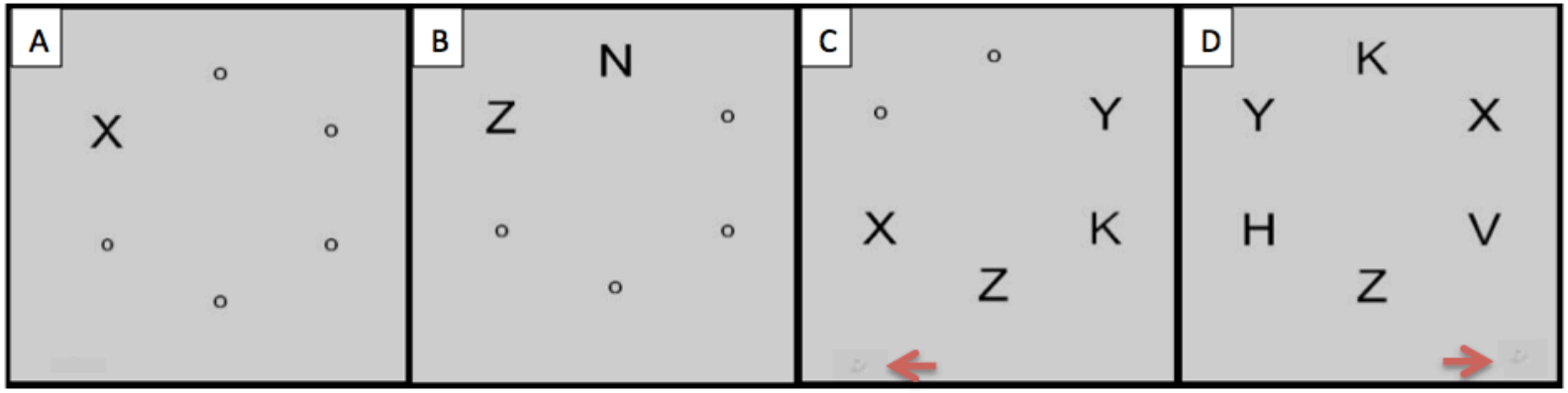

Figure 24. Visual stimuli with different set sizes. A), B), C), and D) shows a set size of 1, 2, 4, and 6, respectively. Red arrows in C) and D) have been added for this thesis to point out the CS, which may appear in any of the trials across any of the set sizes.

Case – MEG ID, MRI ID	Group	Age (years)	Gender	WASI (Non-verbal)	Total ADOS, ADI-R Score*	Case –MEG ID, MRI ID	Group	Age (years)	Gender	WASI (Non-verbal)
ASD01 – 013,014	ASD	18	M	112	15, N/A	TD01 – 003,004	TD	19	M	99
ASD02 – 008,008	ASD	20	M	125	7, 51	TD02 – 011,012	TD	19	M	88
ASD03 – 015,016	ASD	21	M	127	7, 52	TD03 – 001,002	TD	21	M	88
ASD04 – 004,005	ASD	21	M	115	3, 68	TD04 – 002,N/A	TD	21	M	103
ASD05 – 014,015	ASD	23	M	135	9, N/A	TD05 – 016,017	TD	22	M	125
ASD06 – 025,025	ASD	23	M	107	9, N/A	TD06 – 023,024	TD	23	M	129
ASD07 – 007,009	ASD	28	M	116	9, 45	TD07 – N/A,003	TD	24	F	129
ASD08 – 010,011	ASD	29	F	116	15, N/A	TD08 – 021,023	TD	24	M	128
ASD09 – 017,018	ASD	30	F	136	10, N/A	TD09 – 026, N/A	TD	25	M	106
ASD10 – 022,N/A	ASD	32	M	126	9, N/A	TD10 – N/A,001	TD	26	F	139
ASD11 – 019,020	ASD	34	M	138	10, N/A	TD11 – 005,006	TD	28	M	112
ASD12 – 027,N/A	ASD	35	M	96	16, N/A	TD12 – 018,019	TD	28	M	123
ASD13 – 009, 010	ASD	44	M	118	7, N/A	TD13 – 020,021	TD	31	F	132
						TD14 – 006,007	TD	33	F	104
						TD15 – 012,013	TD	33	M	123
						TD16 – 024,026	TD	33	M	123
Total: 13		**Mean:** 27.54 **SD:** 7.48	**Total:** 11 M, 2 F	**Mean:** 120.54 **SD:** 12.18	**Mean:** 10.23 **SD:** 3.79	**Total:** 16		**Mean:** 25.13 **SD:** 4.64	**Total:** 12 M, 4 F	**Mean:** 115.31 **SD:** 15.44

Table 6. Summary of demographic information for each participant in the study. *Total ADOS score reflects the sum of the communication and social interaction subscore. Total ADI-R score reflects the total reciprocal social interaction, communication (verbal), communication (nonverbal), and restricted, repetitive and stereotyped patterns of behaviour. Since the DSM-V was recently published, distinction between high-functioning autism and Asperger Syndrome was not explicitly made in this thesis. Age was calculated based on the day an individual came in for the first neuroimaging scan.

Case	Simple Visual Task	Complex Visual Task (behavioural data + MEG)	MRS	Diffusion imaging	All Modalities	Case	Simple Visual Task (behavioural data + MEG)	Complex Visual Task (behavioural data + MEG)	MRS	Diffusion imaging	All Modalities
ASD01	✓	Not valid	✓	✓	No	TD01	✓	✓	✓	✓	✓
ASD02	✓	✓	✓	✓	✓	TD02	✓	✓	✓	✓	✓
ASD03	✓	✓	✓	✓	✓	TD03	✓	Not valid	✓	Only one DTI image	No
ASD04	✓	✓	✓	✓	✓	TD04	✓	Not valid	No	No	No
ASD05	✓	✓	✓	✓	✓	TD05	✓	✓	✓	One image was not completed	✓
ASD06	✓	Not valid	✓	Not valid	No	TD06	✓	✓	✓	✓	✓
ASD07	✓	✓	✓	✓	✓	TD07	Not acquired	Not acquired	✓	Only one DTI image	No
ASD08	✓	✓	✓	✓	✓	TD08	✓	✓	✓	✓	✓
ASD09	✓	Not valid	✓	✓	No	TD09	✓	✓	Not acquired	Not acquired	No
ASD10	✓	Not valid	Not acquired	Not acquired	No	TD10	Not acquired	Not acquired	Only V1 voxel	Only one DTI image	No
ASD11	✓	✓	✓	✓	✓	TD11	✓	✓	✓	✓	✓
ASD12	✓	Not valid	Not acquired	Not acquired	No	TD12	✓	✓	✓	✓	✓
ASD13	✓	✓	✓	✓	✓	TD13	✓	Not valid	✓	✓	No
						TD14	✓	Not valid	✓	✓	No
						TD15	✓	Not valid	✓	✓	No
						TD16	✓	✓	✓	✓	✓
	Total: 13	Total: 8	Total: 11	Total: 10	Total: 8		Total: 14	Total: 9	Total: 13	Total: 10	Total: 8

Table 7. Summary of available data from all participants. The full multimodal dataset was acquired from eight ASD individuals and eight TD individuals. For a full list of reasons why it was not possible to acquire the complete data from participants, please refer to this Chapter's Appendix.

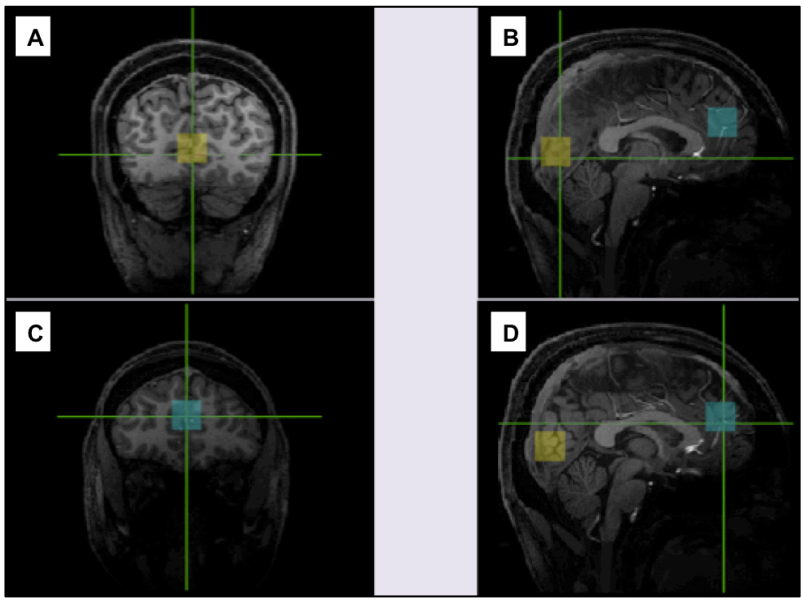

Figure 25. MRS voxel location. A) shows the coronal view of the V1 voxel, whereas B) shows the coronal view of the MPFC voxel in the same participant. C) and D) show the sagittal views of the brain. MRS voxel size was 20mm by 20mm by 20mm.

MRS data was first collected from V1, roughly following the boundaries used to manually mask BA17 (outlined in Chapter 2), and secondly from MPFC, roughly following the boundaries used to manually mask BA9 (outlined in Chapter 2), but using the medial rather than the dorsolateral gyrus. Figure 25 shows the voxel placements for the two regions in the same individual. A shimming technique called FASTEST MAP was used in the procedure to enhance the main magnetic field homogeneity in the voxel and improve the signal acquired from different metabolites (Mekle, Gambarota, Mlynarik, & Gruetter, 2008).

Data Analysis for MRS Data

All spectra were analysed using the LCModel program (Provencher, 2001) and corrected for the amount of CSF fraction in the MRS voxel. Unsuppressed water spectra were used for metabolite quantification. Between-group differences in metabolites both in V1 and MPFC were investigated using SPSS. Four mixed-model ANCOVAs were run, one for each of the four the metabolites of interest (GABA, NAA, Glu, Cr). A 2x2 rmANCOVA was run with brain region (V1 and MPFC) as a within-subject factor, and diagnostic group as the between-subject factors. Age as well as grey matter volume were added as covariates.

Modality 3: DTI

DTI Data Acquisition

After the MRS data was acquired, two diffusion images were acquired on the 7T, using a SE-EPI pulse sequencing with the following parameters: TE = 64ms, TR = 7,900ms, bandwidth = 1,698 Hz/pixel, FOV = 192x192x120mm**,** image resolution of 1.5x1.5x1.5mm, number of slices = 80, echo spacing = 67ms, and EPI factor = 128. 64 gradient directions were applied to the diffusion data (b = 1,500 s/mm^2) with four b = 0 s/mm^2 images. Two diffusion images with reversed phase encoding directions (referred to as blip-up/blip-down images) were acquired in the Anterior → Posterior and the Posterior → Anterior phase-encode directions. Given the resolution of the diffusion image, one voxel would span approximately 60% of the cortical thickness, if the average thickness is approximated at 2.5mm (Fischl & Dale, 2000).

Processing 7T Diffusion Images

The processing pipeline of the 7T diffusion data was very similar to the pipeline used for the 3T dataset. However, the 3T dataset used the FSL tool called "eddy correct", whereas the pipeline here used the "topup" and "eddy" tool in conjunction. The following outlines the steps.

1. A basic processing normalised the intensity of the diffusion images across the series.
2. B0 images were extracted from both diffusion files, and an index file was created, which was used for both topup and eddy.
3. The B0 files were concatenated together.
4. Using the "topup" tool, the susceptibility-induced off-resonance field was estimated using a previously described method (Andersson, Skare, & Ashburner, 2003) and implemented in FSL (Smith, 2002). Then, the two diffusion images were combined into a single corrected one.
5. Images were corrected for eddy currents with the "eddy" tool, and resampled into one diffusion image.
6. The resulting diffusion image from step 5 was used in dtifit, which fits the diffusion tensor model onto each voxel, producing FA and MD maps.

7. Linear registration took place for all participants' diffusion to structural image, and for all participants' structural image to be registered to the standard 1mm MNI 152 T1 scan.
8. New diffusion images were resampled in structural space using the matrices from step 7.

Automated Masking of 7T Data

After the 7T data was processed for eddy currents and susceptibility-induced currents, the pipeline used to automatically mask the 7T data was the same as the pipeline used for the 3T dataset in Chapter 2. Please refer to the "Automated Masking" part of the Methods section in Chapter 2 for more details.

Manual Masking of 7T Data

The pipeline used to manually mask the 7T data was the same as the pipeline used for the 3T dataset, with the exception that instead of masking both hemispheres of each individual, only the left hemisphere was masked. The left hemisphere of BA17, FG, and BA9 were manually masked by a visiting student in the laboratory, with the same anatomical boundaries outlined in Chapter 2. The CHIPS software was used to output the following values: FA, MD, Θ_{rad}, and $D_{\perp}$.

Statistical Analysis

For the automated masking, a 2x3x2 rmANCOVA was run, with hemisphere and brain region (BA17, FG, and BA9) as the within-subject factors, and diagnostic group as the between-subject factors. Age and total grey matter volume were added as covariates. The dependent variables were FA and MD values. The same statistical model was used for the manually masked 7T data, with the exception that hemisphere was not included as a within-subject factor, since only one hemisphere was masked. The dependent variables were FA, MD, Θ_{rad} and $D_{\perp}$.

Bringing the Modalities Together

Planned correlations were run for measures in the different modalities to explore the relationships across modalities in this Chapter. Specifically, the following relationships were explored: 1) diffusion measures from Chapter 2 and from this Chapter, 2) gamma phase-locking values in occipital cortex, as well as GABA and Glu values in occipital cortex, and 3) gamma phase-locking values in occipital cortex and diffusion measures in BA17.

Results

Modality 1: MEG

Simple Visual Task – Behavioural and MEG Results

ASD (n = 13)				TD (n = 14)		
	Age (years)	WASI (non-verbal)	ADOS (total)		Age (years)	WASI (non-verbal)
Mean	27.54	120.54	10.23	Mean	25.71	113.07
SD	7.48	12.18	3.79	SD	5.43	15.10

Table 8. Demographics information for individuals who participated in the Simple Visual Task.

The demographics information and the behavioural data of the 13 ASD and 14 TD individuals who participated in the Simple Visual Task are summarized in Table 8 and Figure 26, respectively. All 13 ASD and 14 TD individuals were used in the MEG analysis, despite some variance between participants in the number of correct button presses for the task. An independent samples t-test showed no statistical differences in the number of correct responses between groups ($t(25) = 1.804$, $p > 0.05$).

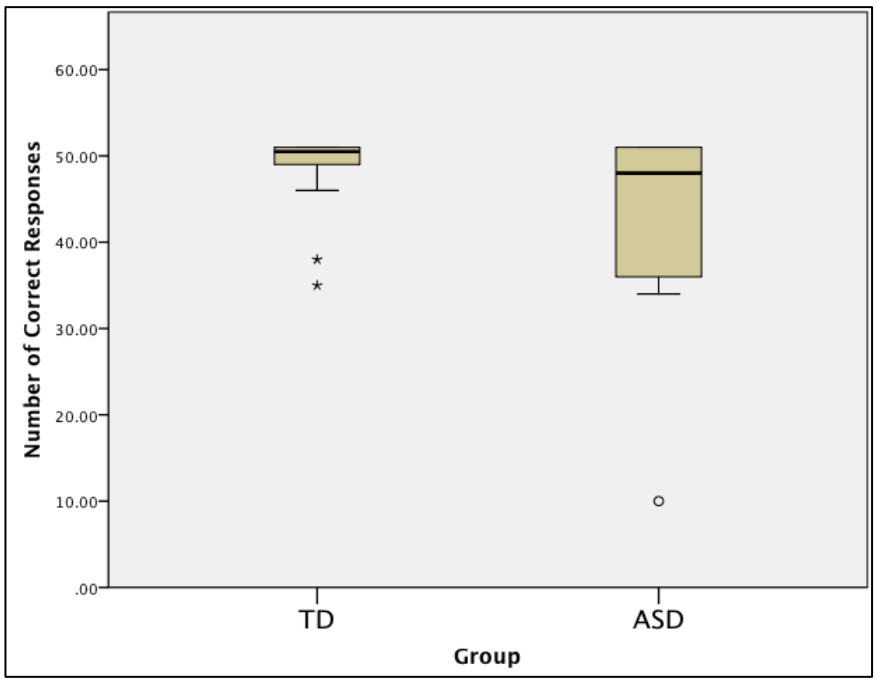

Figure 26. Number of correct button presses for each group. The maximum number of correct responses was 51. The outlier in the ASD group noted that he struggled to see the target and was instructed to fixate on the middle of the screen for the duration of the task.

Occipital Gamma Phase-Locking Values

Figure 27 shows the time-frequency plane across all channels for Gabor patch presentation relative to no stimulus presentation (or baseline). After stimulus onset at 0s, the most prominent gamma band was within the 35-80 Hz frequency range and the 60-100ms time range, as delineated by the black circle in Figure 27. In order to determine whether this significant gamma activity was localized to the occipital brain region, topographic plots were created by integrating over the specified time and frequency ranges. These plots are shown in Figure 28, which depicts the statistical difference of gamma activity compared to baseline, and in Figure 29, which shows the grand means for gamma phase-locking. Both ASD and TD individuals demonstrated significant gamma phase-locking activity ($p < 0.05$) for left and right visual stimuli compared to baseline, in the contralateral occipital area.

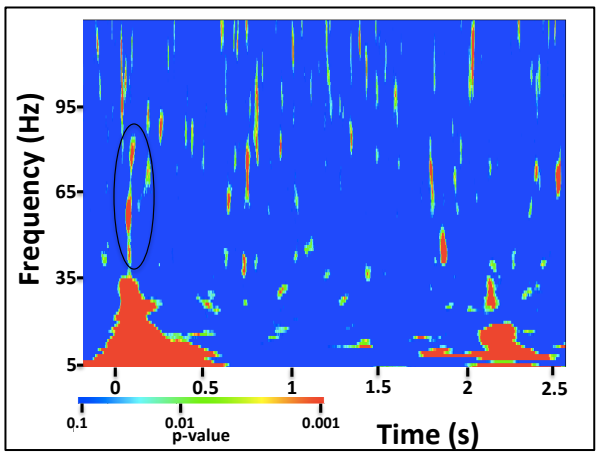

Figure 27. Time-frequency plane for within-group effects of simple visual stimuli presentation versus no stimuli presentation for ASD individuals. The plane for TD individuals looked very similar. The black circle shows the gamma-band of interest for analysis, which corresponds to 60-100ms, and 35-80 Hz.

Occipital gamma phase-locking values were extracted from both left and right occipital cortex in order to determine whether there were any relationships between MEG and the other modalities in this study, which will be further discussed in the "Bringing the Modalities Together" section. These values were also used for correlation analyses with ASD diagnostic scores. Values were extracted from the channel corresponding to the highest gamma phase-locking activity, shortly after visual stimulus onset (60-100ms) from the 35-80 Hz range. The grand means in occipital gamma phase-locking are summarized in Table 9.

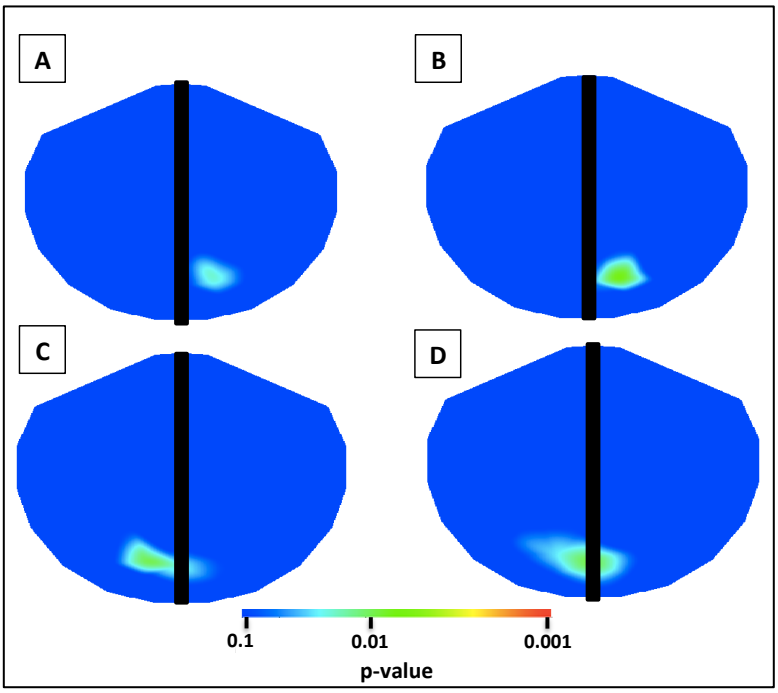

Figure 28. Topographic plots for statistical difference in gamma phase-locking, specifically integrated over the 60 – 100ms time range and the 35-80 Hz frequency range. The different plots represent the statistical difference of left Gabor patch presentation versus baseline for A) ASD, or B) TD individuals, as well as the statistical difference of right Gabor patch presentation versus baseline for C) ASD, or D) TD individuals. Hemisphere divisions are depicted by the black bar in each plot in order to visualize the contralateral occipital response.

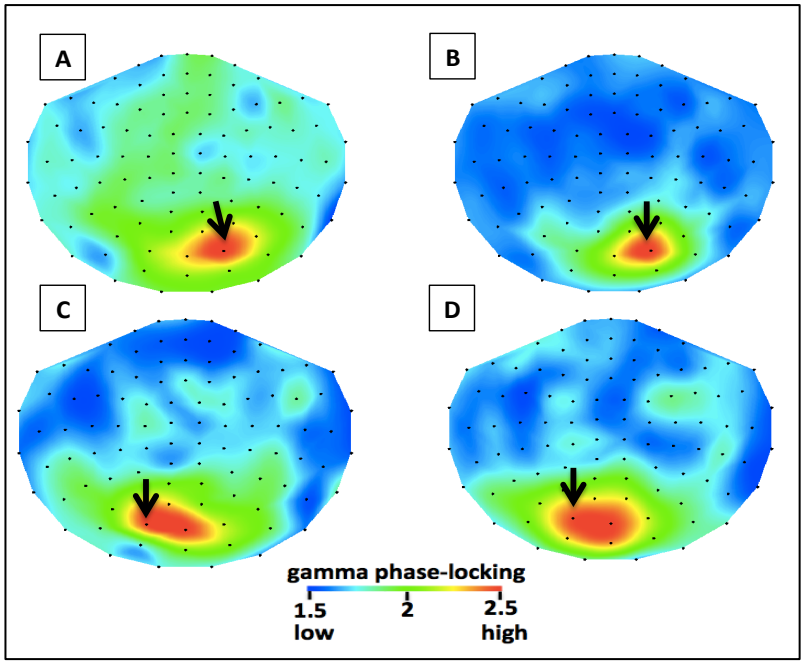

Figure 29. Topographic plots of grand mean gamma phase-locking values, integrated over the 60 – 100ms time range and the 35-80 Hz frequency range. The different plots represent gamma phase-locking activity with left Gabor patch presentation for A) ASD, or B) TD individuals, as well as gamma phase-locking activity with right Gabor patch presentation for C) ASD, or D) TD individuals. Black arrows point to the channel where gamma phase-locking values were extracted from. A node grid was overlaid on each topographic plot to help determine the corresponding channel.

	Phase-locking in Left Occipital Cortex		Phase-locking in Right Occipital Cortex	
	ASD	TD	ASD	TD
Mean	2.370	2.507	2.447	2.834
SD	0.797	0.674	0.844	1.109

Table 9. Summary of mean and SD phase-locking for each diagnostic group. For both left and right occipital cortex, TD individuals on average demonstrated higher phase-locking. However, this difference was not significant at the p = 0.01 level.

Correlations with Diagnostic Scores

The literature suggests that measures of gamma activity may correlate with ADOS symptom severity scores (Rojas & Wilson, 2014). Pearson's bivariate correlations were used to explore these relationships in this dataset. None of the relationships survived the test for multiple comparisons. The results are summarized in Table 10 and the relationship between gamma in left occipital cortex and ADOS scores, which trended on significance, is graphed in Figure 30.

	ADOS (Total Score)	ADOS (Communication Subscore)	ADOS (Social Interaction Subscore)
Gamma Phase-Locking in Right Occipital Cortex	r = -0.492 **p = 0.088**	r = -0.507 **p = 0.077**	r = -0.374 **p = 0.208**
Gamma Phase-Locking in Left Occipital Cortex	r = -0.606 **p = 0.028**	r = -0.610 **p = 0.027**	r = -0.472 **p = 0.103**

Table 10. Correlations between occipital gamma phase-locking and ADOS scores. P-values reflect unadjusted levels.

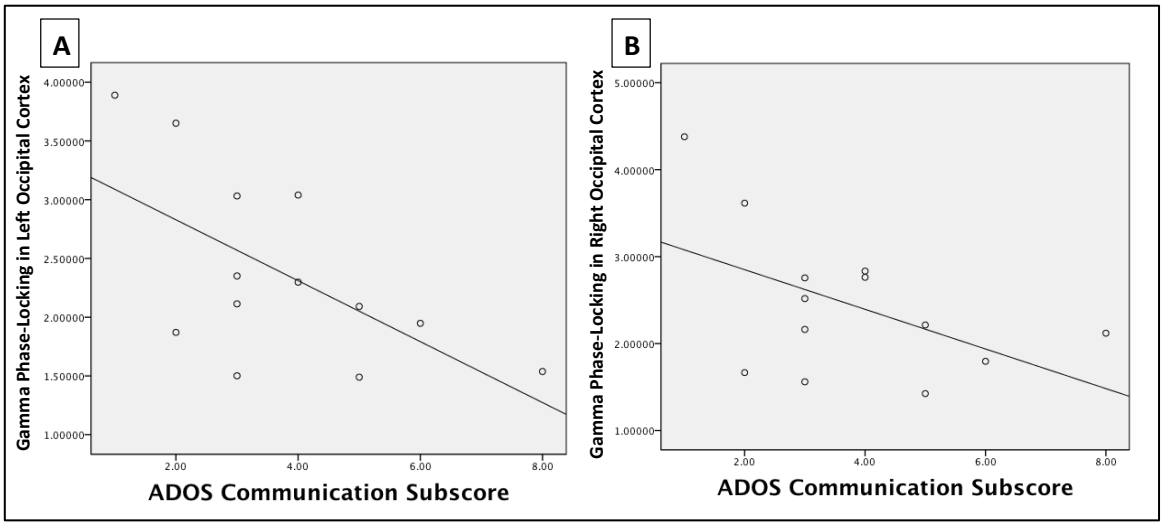

Figure 30. Correlation between ADOS communication subscore and gamma phase-locking in A) left, and B) right occipital cortex. The correlation was stronger in left.

Between-Group Differences in Gamma Phase-Locking Values

In order to fully understand between-group differences, time-frequency planes for each of the three conditions were plotted: A) Gabor Patch presentation in left visual field, B) Gabor Patch presentation in right visual field, and C) no Gabor patch presentation. The time-frequency plane for A) is depicted in Figure 31. Gamma-bands within 300ms of stimulus onset and offset with significant difference at the p = 0.001 level were of interest and further scrutinized. In total, six gamma bands (two for each condition) were examined across different times and frequencies, which are described in Table 11, and are visually depicted on topographic plots in Figure 32. Gamma phase-locking values for each participant were extracted from the orange and red areas in topographic plots A2, B2, C1, and C2 shown in Figure 32, since these regions corresponded to the most localized significant difference (p = 0.03 to p = 0.01) in gamma activity between ASD and TD individuals. The mean and SD of gamma phase-locking values corresponding to these regions are summarized in Table 12. Significant group differences in gamma phase-locking were mainly found in frontal cortex and not in occipital cortex. Across all four regions that were identified, TD individuals showed higher gamma phase-locking activity, as seen in Table 12.

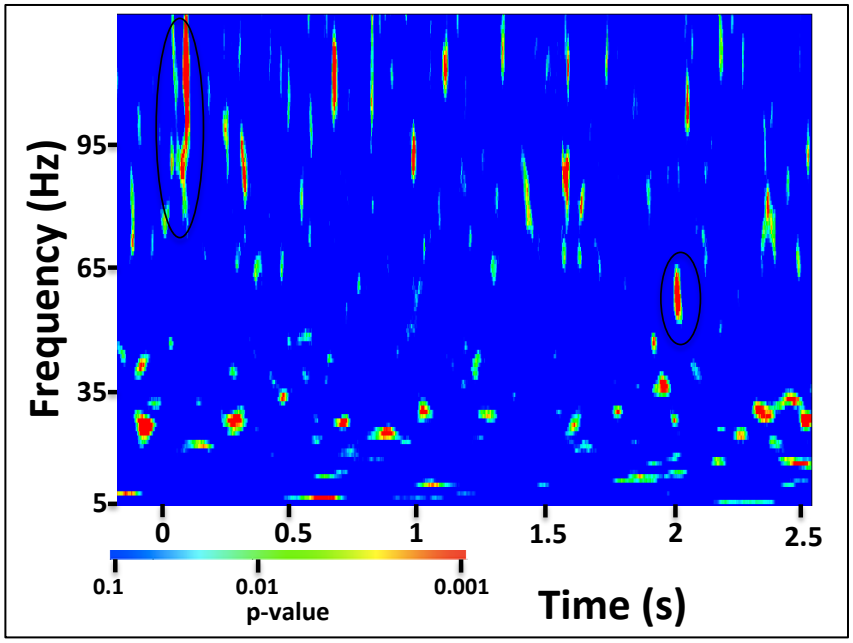

Figure 31. Time-frequency plane representing between-group differences for Gabor Patch presentation in left visual field. Black circles show the gamma bands of interest that are within 300ms of visual stimuli onset and offset, and are significantly different between groups at the p = 0.001 level across all channels.

Gamma-bands of Interest	Time Range (ms)	Frequency Range (Hz)
A1	41-85	80-115
A2	1,950-2,000	45-60
B1	85-110	80-100
B2	240-280	70-80
C1	95-120	75-85
C2	190-210	65-75

Table 11. Summary for gamma-bands chosen for further analyses. A1 and A2 correspond to between-group differences in gamma-band activity when Gabor patches were presented in the left visual field, B1 and B2 when Gabor patches were presented in the right visual field, and C1 and C2 when there were no Gabor patches.

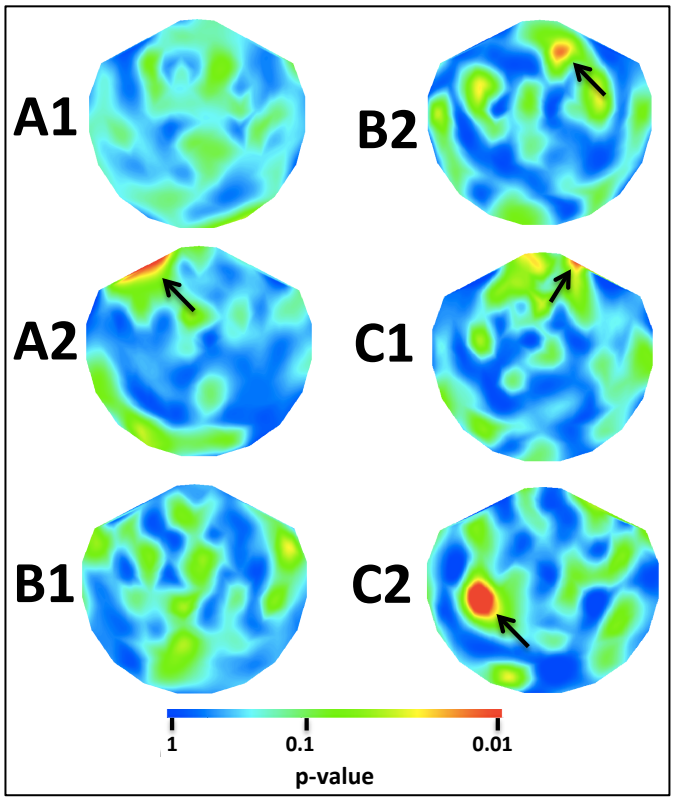

Figure 32. Topographic plots of statistical difference between ASD and TD individuals in brain activity, across different time and frequencies outlined in Table 11. Black arrows point to the most significant differences between groups. Plots A2, C2, C1, and C2 showed most localized significant differences, as pointed out by the black arrows. Gamma phase-locking values were extracted for each participant from the channels that corresponded to these regions.

	A2		B2		C1		C2	
	ASD	TD	ASD	TD	ASD	TD	ASD	TD
Mean Phase-Locking Value	1.342	1.88	1.440	1.60	1.368	1.576	1.413	1.604
SD	0.372	0.740	0.297	0.370	0.467	0.414	0.572	0.382

Table 12. Summary of mean and SD gamma phase-locking values in different times and frequencies. TD individuals showed higher phase-locking in all areas.

Correlations with Diagnostic Scores

Pearson's bivariate correlations were used to explore whether the gamma phase-locking values that showed most significant differences between groups had any relationships with ADOS

scores. The results are summarized in Table 13. The relationship between gamma phase-locking in A2 and ADOS scores (both total and the social subscore) was significant, after correcting for multiple comparisons.

	ADOS (Total Score)	ADOS (Communication Subscore)	ADOS (Social Subscore)
Gamma Phase-Locking in A2	r = 0.747 **p = 0.003***	r = 0.574 **p = 0.040**	r = 0.707 **p = 0.007***
Gamma Phase-Locking in B2	r = -0.118 **p = 0.702**	r = 0.171 **p = 0.577**	r = -0.427 **p = 0.145**
Gamma Phase-Locking in C1	r = 0.361 **p = 0.226**	r = 0.073 **p = 0.813**	r = 0.527 **p = 0.064**
Gamma Phase-Locking in C2	r = 0.546 **p = 0.054**	r = 0.364 **p = 0.222**	r = 0.563 **p = 0.045**

Table 13. Correlations between gamma phase-locking and ADOS scores. A positive correlation was seen between gamma phase-locking in A2 and ADOS scores, with the social subscore driving the relationship. P-values reflect unadjusted values.

Complex Visual Task – Behavioural Results

Of all the individuals who participated, a total of eight ASD individuals and nine TD individuals had valid behavioural results. The demographic information of these participants is summarized in Table 14. All participants with valid behavioural results were right-handed, except for one ASD individual who was left-handed. Validity of behavioural results was determined by the control block, which consisted of 18 trials. During this block, participants were asked to specifically focus on looking for the CS and to ignore the letters. The 18 trials in the control block consisted of nine trials where the CS was present and nine trials where the CS was not. Behavioural results were considered valid if participants correctly identified the CS on >50% of the trials where it was present, and if participants did not identify false positives (i.e. pressing for the CS when it was not present) on <50% of the trials where the CS was absent.

ASD (n = 8)				TD (n = 9)		
	Age (years)	WASI (non-verbal)	ADOS (total)		Age (years)	WASI (non-verbal)
Mean	27.50	123.75	9.25	Mean	24.56	114.78
SD	8.26	9.04	3.88	SD	4.56	14.44

Table 14. Summary of demographic information of participants used in the Complex Visual Task analysis.

Next, the assumptions of the rmANOVA were checked for the 17 participants who had valid behavioural results.

Normality – The Shapiro-Wilk test confirmed the normality of the average reaction time (across all set sizes) when participants correctly responded to letters, accuracy rate of identifying letters in the ring, correct identification of the CS, and average detection sensitivity values (all p-values > 0.05).

Homogeneity of Variance – Levene's test suggested homogeneity of variance across diagnostic groups ($p > 0.05$).

Sphericity – In the cases where the null hypothesis for Mauchly's test of sphericity was rejected ($p < 0.05$), Greenhouse-Geisser and Huynh-Feldt adjustments were used, for $\epsilon < 0.75$, and > 0.75, respectively.

	Behavioural Measures			
	Reaction Time	Accuracy Rate	CS Detection	d'
Effect of set size	$F(1.37,20.51) = 28.55$ **$p < 0.001$**** $\eta^2 = 0.656$	$F(3,45) = 46.537$ **$p < 0.001$**** $\eta^2 = 0.756$	$F(1.60,23.98) = 3.77$ **$p = 0.046$*** $\eta^2 = 0.021$	$F(3,45) = 9.38$ **$p < 0.001$**** $\eta^2 = 0.385$
Effect of diagnosis	$F(1,15) = 2.617$ **$p = 0.127$** $\eta^2 = 0.149$	$F(1,15) = 0.223$ **$p = 0.643$** $\eta^2 = 0.015$	$F(1,15) = 4.60$ **$p = 0.049$*** $\eta^2 = 0.235$	$F(1,15) = 5.027$ **$p = 0.041$*** $\eta^2 = 0.251$
Set size by diagnosis interaction	$F(1.37,20.51) = 1.149$ **$p = 0.316$** $\eta^2 = 0.071$	$F(3,45) = 0.052$ **$p = 0.984$** $\eta^2 = 0.003$	$F(1.60,23.98) = 2.616$ **$p = 0.104$** $\eta^2 = 0.148$	$F(3,45) = 1.618$ **$p = 0.198$** $\eta^2 = 0.097$

Table 15. Summary of rmANOVA results for the Complex Visual Task.

Two independent samples t-tests were run for non-verbal IQ and for age between ASD and TD individuals and no significant differences were found. The main effects of set size and diagnosis, as well as set size by diagnosis interactions, are summarized in Table 15.

Reaction time and CS Detection failed the Mauchly's test of sphericity ($p < 0.001$). Therefore, Greenhouse Geisser corrections were used ($\epsilon < 0.75$). The 2012 Remington et al. paper found a significant set size by group interaction in CS Detection and in d', where ASD individuals performed significantly better than TD individuals in both parameters only at set size 6. These interactions were not seen with this dataset, but planned independent samples t-tests showed that ASD and TD individuals did not differ in CS Detection and in d' at set size 1, 2, and 4 (all p-values > 0.05), but ASD individuals were significantly better in both metrics at set size 6 (both p-values < 0.02). These findings are similar to those reported in Remington et al. (2012). The main findings from this and the previous study are depicted in Figure 33. Graphs for the letter task accuracy as well as reaction time are shown in the Appendix in Figure 43.

Correlations with Diagnostic Scores

Pearson's bivariate correlations were run for ASD severity scores and 1) CS Detection, and 2) d' values at set size 1 and set size 6[5]. The results for this are summarized in Table 16. No correlations were significant at the adjusted alpha level.

	ADOS (Total Score)	ADOS (Communication Subscore)	ADOS (Social Subscore)
CS Detection (set size 1)	r = 0.286 **p = 0.492**	r = 0.314 **p = 0.448**	r = 0.219 **p = 0.602**
CS Detection (set size 6)	r = 0.710 **p = 0.048**	r = 0.658 **p = 0.076**	r = 0.607 **p = 0.110**
d' (set size 1)	r = 0.222 **p = 0.596**	r = 0.309 **p = 0.456**	r = 0.138 **p = 0.745**
d' (set size 6)	r = 0.393 **p = 0.335**	r = 474 **p = 0.235**	r = 0.280 **p = 0.501**

Table 16. Summary of correlations between ADOS scores and measurements of distractor processing at low (set size 1) and high (set size 6) perceptual load conditions. Reported p-values are unadjusted for multiple comparisons.

[5] Correlations were not run for set size 2 and 4 to reduce the number of correlations that were performed. The main purpose of running a correlation for set size 1 and set size 6 was to determine whether performance at low or high perceptual load was related to severity scores.

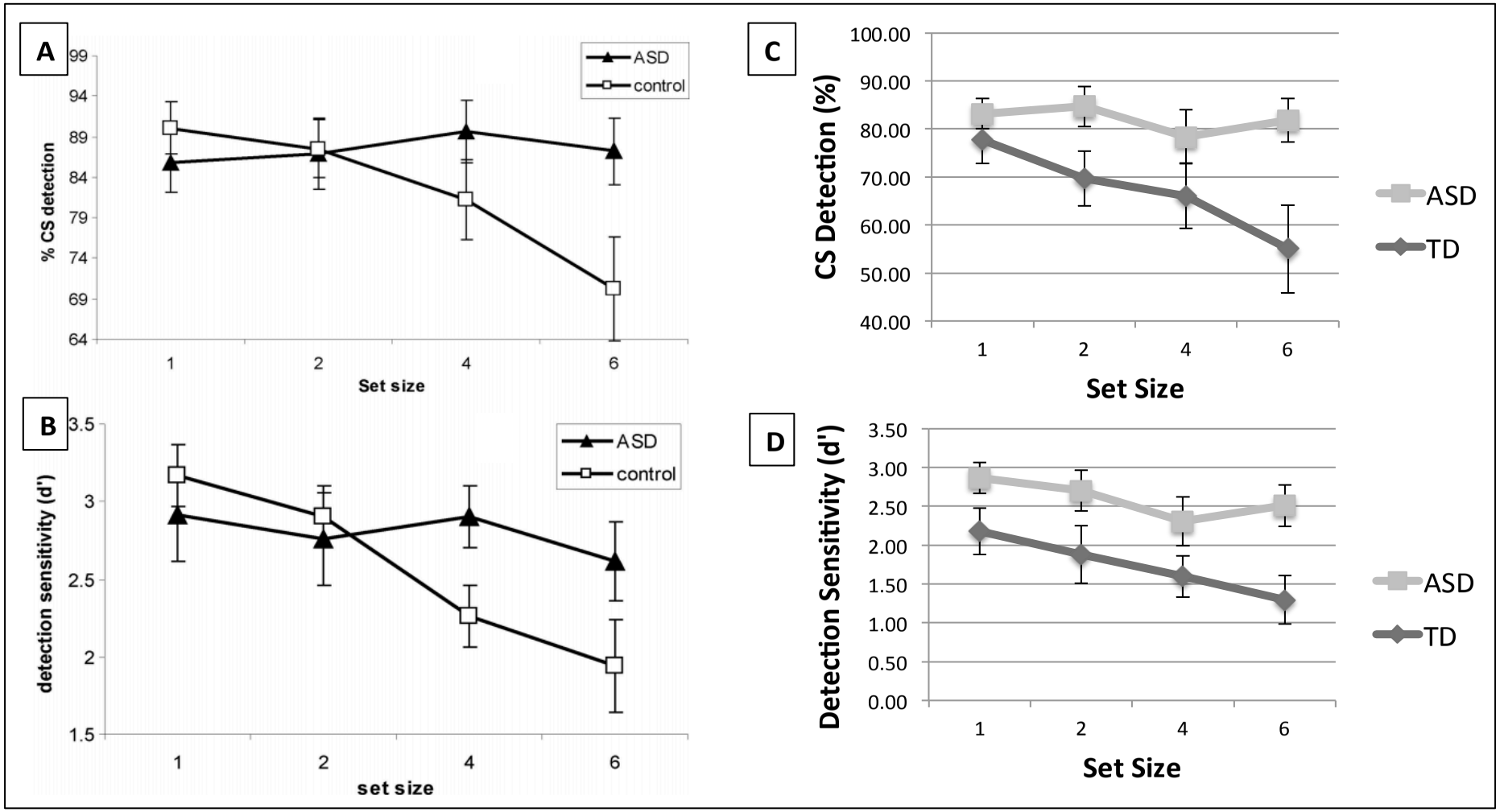

Figure 33. Comparison of results from this study and those in Remington et al. (2012). A) and B) are figures adapted from the previous study while C) and D) reflect the results from this study. Error bars represent SE in all graphs.

Modality 2: MRS

ASD (n = 11)				TD (n = 13)		
	Age (years)	WASI (non-verbal)	ADOS (Communication + Social Interaction)		Age (years)	WASI (non-verbal)
Mean	26.45	122.27	9.82	Mean	26.00	114.60
SD	7.63	10.56	3.68	SD	5.08	15.71

Table 17. Summary of demographic information for individuals with valid MRS data.

Table 17 summarizes the demographic information of the individuals with MRS data available. The quality of the metabolite estimation varied between participants, and between brain regions of the same participant. In order to determine whether the goodness of fit for metabolite measurements were valid, the estimate of standard deviation in percentage (%SD) – known as the Cramer-Rao lower bounds – for each metabolite was used (Provencher, 2014). Metabolite concentrations with %SD values >50% are thought to be unreliable (Srinivasan, Sailasuta, Hurd, Nelson, & Pelletier, 2005), and were excluded from statistical analysis. Therefore, while Table 17 summarizes the demographics from all individuals with MRS data, for GABA, a different combination of individuals were included in the analysis due to GABA levels for some individuals having %SD values > 50%. All concentrations are reported in mM, representing the mmol per kg wet weight (Provencher, 2014). Figure 34 shows the V1 and MPFC spectra for one participant, and Figure 35 shows the different levels of metabolites in V1 and MPFC that were quantified using LCModel. Statistical tests were only run for the metabolites of interest, however. Before running these tests, assumptions for the rmANCOVA were checked.

Normality – The Shapiro-Wilk test confirmed the normality of all metabolite concentrations of interest in V1 and MPFC, for both groups ($p > 0.05$), except for GABA levels both in V1 and in MPFC for TD individuals. However, since ANOVAs are generally robust to small violations of normality, rmANCOVAs were still used for GABA differences.

Homogeneity of Variance – Levene's test was used to test for homogeneity of variance. If the null hypothesis was rejected, equal variances would not be assumed.

Sphericity – In the cases where the null hypothesis for Mauchly's test of sphericity was rejected ($p < 0.05$), Greenhouse-Geisser and Huynh-Feldt adjustments were used, for $\epsilon < 0.75$, and > 0.75, respectively.

Homogeneity of the Regression Slopes – The test for the homogeneity of the regression slopes failed to reject the null hypothesis.

Additionally, independent samples t-tests were run between diagnostic groups for the amount of grey matter and CSF in the V1 and MPFC voxels – no significant differences were found (all p-values > 0.200).

Absolute Metabolite Values

	GABA	Glu	NAA	Cr	GABA/Glu
n-values	ASD = 6 TD = 9	ASD = 13 TD = 11	ASD = 11 TD = 13	ASD = 11 TD = 13	ASD = 6 TD = 9
Effect of brain region	F(1,11) = 2.161 **p = 0.170** $\eta^2 = 0.164$	F(1,20) = 1.092 **p = 0.309** $\eta^2 = 0.052$	F(1,20) = 0.724 **p = 0.405** $\eta^2 = 0.035$	F(1,20) = 2.802 **p = 0.110** $\eta^2 = 0.123$	F(1,11) = 1.184 **p = 0.300** $\eta^2 = 0.097$
Effect of age	F(1,11) = 2.092 **p = 0.176** $\eta^2 = 0.160$	F(1,20) = 2.364 **p = 0.140** $\eta^2 = 0.106$	F(1,20) = 0.004 **p = 0.951** $\eta^2 < 0.001$	F(1,20) = 0.068 **p = 0.797** $\eta^2 = 0.003$	F(1,11) = 2.082 **p = 0.177** $\eta^2 = 0.159$
Effect of diagnosis	F(1,11) = 2.975 **p = 0.113** $\eta^2 = 0.213$	F(1,20) = 1.935 **p = 0.180** $\eta^2 = 0.088$	F(1,20) = 0.607 **p = 0.445** $\eta^2 = 0.029$	F(1,20) = 0.774 **p = 0.390** $\eta^2 =0.037$	F(1,11) = 0.977 **p = 0.344** $\eta^2 = 0.082$
Region by age interaction	F(1,11) = 0.359 **p = 0.561** $\eta^2 = 0.032$	F(1,20) = 2.962 **p = 0.101** $\eta^2 =0.129$	F(1,20) = 0.785 **p = 0.386** $\eta^2 = 0.038$	F(1,20) = 0.035 **p = 0.854** $\eta^2 = 0.002$	F(1,11) = 1.262 **p = 0.285** $\eta^2 = 0.103$
Region by diagnosis interaction	F(1,11) = 0145 **p = 0.710** $\eta^2 = 0.013$	F(1,20) = 3.151 **p = 0.091** $\eta^2 = 0.136$	F(1,20) = 1.091 **p = 0.309** $\eta^2 =0.052$	F(1,20) = 7.320 **p = 0.014*** $\eta^2 = 0.268$	F(1,11) = 0.593 **p = 0.457** $\eta^2 = 0.051$

Table 18. Summary of rmANOVA results for the metabolites of interest in absolute value.

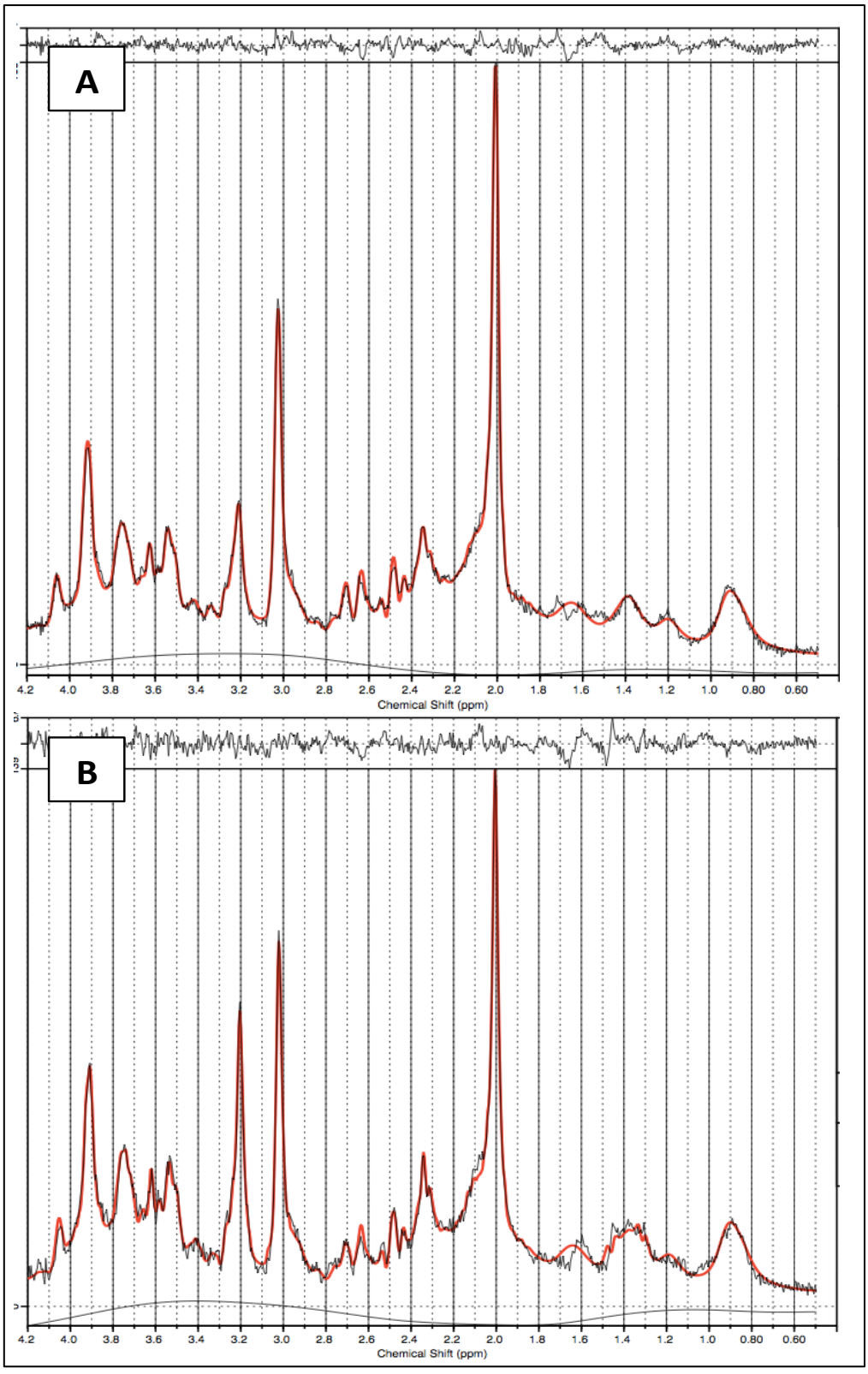

Figure 34. Spectra for A) V1 and B) MPFC from the same participant.

For the absolute value metabolites (results summarized in Table 18) a significant region by diagnosis effect was found for Cr, which was followed up with independent samples t-tests. These tests showed that ASD and TD individuals showed no differences in Cr values in V1 ($p > 0.05$), but did show a significant difference in MPFC ($t(23) = 0.352$, $p = 0.017$). The region by diagnosis interaction for Glu levels reached significance ($p = 0.091$). Given the a-priori hypothesis that Glu levels may be higher in ASD individuals, an independent samples t-test for both V1 and MPFC were run separately, and revealed that there was a greater concentration of Glu in MPFC for ASD individuals compared to TD individuals ($t(22) = 2.162$, $p = 0.042$), but not in V1 ($t(23) = 0.171$, $p = 0.866$).

When one metabolite value negatively correlates with another in MRS, it may be that the signal for one is being "stolen" from the signal of the other. In order to investigate whether this was happening in this dataset, Spearman's correlations were run for GABA and Glu for both V1 and MPFC. A non-significant positive correlation was found for V1 ($rho = 0.329$, $p = 0.135$), and a non-significant negative correlation was found for MPFC ($rho = -0.409$, $p = 0.116$).

Standardized Metabolite Values

It is important to note that the metabolite concentrations used for the analysis were the absolute values. One way of standardizing the concentration levels in order to compare metabolite differences between individuals is by dividing metabolites by a baseline metabolite value like NAA, which is thought to reflect neuronal integrity (Gazdzinski et al., 2010). Therefore, additional rmANOVAs were run for GABA/NAA and Glu/NAA values. The results are summarized in Table 19. No significant main effects were found for metabolites standardized for NAA values.

	Metabolites standardized for NAA	
	GABA/NAA	Glu/NAA
n-values	ASD = 6 TD = 9	ASD = 11 TD = 13
Effect of brain region	F(1,19) = 0.154 **p = 0.703**	F(1,19) = 1.899 **p = 0.065**

	$\eta^2 = 0.015$	$\eta^2 = 0.012$
Effect of age	F(1,19) = 2.134 **p = 0.175** $\eta^2 = 0.176$	F(1,19) = 1.024 **p = 0.324** $\eta^2 = 0.051$
Effect of diagnosis	F(1,19) = 0.768 **p = 0.402** $\eta^2 = 0.071$	F(1,19) = 0.040 **p = 0.844** $\eta^2 = 0.002$
Region by age interaction	F(1,19) = 1.112 **p = 0.316** $\eta^2 = 0.100$	F(1,19) = 2.345 **p = 0.142** $\eta^2 = 0.110$
Region by diagnosis interaction	F(1,19) = 0.061 **p = 0.811** $\eta^2 = 0.006$	F(1,19) = 0.464 **p = 0.504** $\eta^2 = 0.024$

Table 19. Summary of rmANCOVA results for metabolites of interest standardized for NAA.

Correlations with Diagnostic Scores

In order to determine if either of the diagnostic differences with MPFC Glu and MPFC Cr were linked to ADOS scores, Pearson's bivariate correlations were run. The Bonferroni-adjusted alpha level for multiple comparisons was set to 0.025. At the new alpha level, absolute Glu levels in MPFC correlated with both Total ADOS Score and the Communication Subscore. The results are summarized in Table 20.

	ADOS (Total Score)	ADOS (Communication Subscore)	ADOS (Social Subscore)
MPFC Glu	r = 0.772 **p = 0.005***	r = 0.745 **p = 0.009**	r = 0.657 **p = 0.028**
MPFC Cr	r = 0.409 **p = 0.212**	r = 0.131 **p = 0.701**	r = 0.500 **p = 0.117**

Table 20. Correlations between diagnostic scores and metabolites that showed significant differences between ASD and TD individuals.

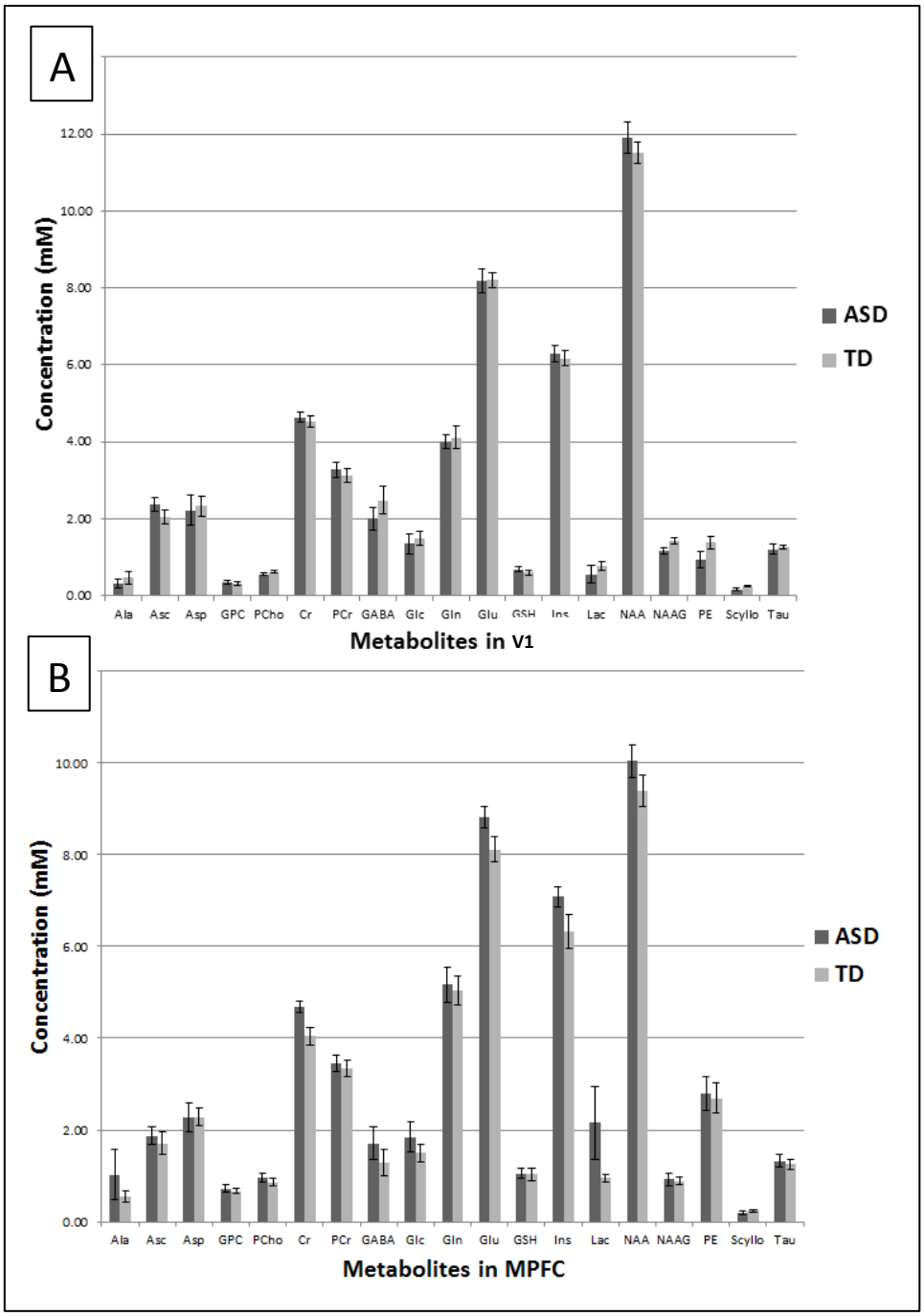

Figure 35. Mean concentration of absolute metabolite levels in A) V1 and B) MPFC across ASD and TD individuals. Error bars in the graphs represent the SE. Measurements of several metabolites are shown. Abbreviations used are as follows: Ala = alanine, Asc = ascorbate, Asp = aspartate, GPC = glycerophosphophorylcholine, PCr = phosphocreatine, Glc = glucose, GSH = glutathione, Ins = insulin, Lac = lactate, NAAG = n-acetylaspartylgutamate, PE = phosphorylethanolamine, Scyllo = scylloinositol, Tau = taurine.

Modality 3: DTI

Only participants with complete diffusion scans in the Anterior → Posterior and Posterior → Anterior phase-encode direction were used for the automated and manual masking of the 7T dataset. Therefore, TD03, TD07 and TD10 were excluded from the dataset, since they only had one of two diffusion scans available. The second diffusion scan (in the Posterior → Anterior phase-encode direction) was interrupted towards the end for TD05, who was unable to come back for the complete scan. However, this participant's data was still included in the analysis. The demographic information is summarized in Table 21 and the automated and manual data are shown graphically in Figure 36 and 38, respectively.

Automated Masking of 7T Data

ASD (n = 10)				TD (n = 10)		
	Age (years)	WASI (Non-verbal)	ADOS (Communication + Social Interaction)		Age (years)	WASI (Non-verbal)
Mean	27.50	123.75	9.25	Mean	24.56	114.78
SD	8.26	9.04	3.88	SD	4.56	14.44

Table 21. Summary of the demographic information of participants in the multimodal imaging diffusion dataset.

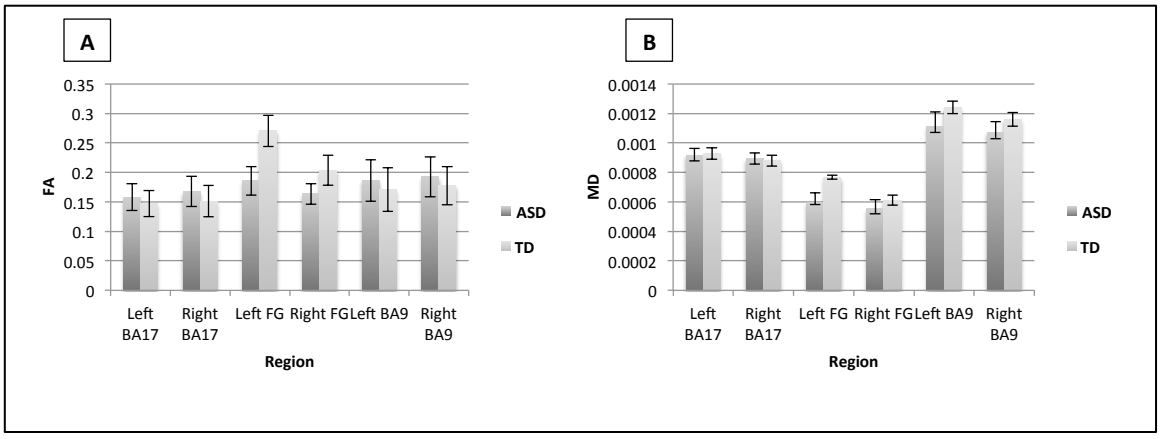

Figure 36. Results for automated masking. A) depicts FA, and B) depicts MD across regions and hemispheres. Error bars represent SE.

First, the assumptions of the rmANCOVA were checked. The statistical results are summarized in Table 22.

Normality - The Shapiro-Wilk test confirmed the normality of the average FA and MD (across regions) for the ASD group. For the TD group, the Shapiro-Wilk test was significant for FA values ($p < 0.001$). However, given the robustness of ANOVAs towards violations of normality, parametric tests were still used for FA analysis. Moreover, this would make it easier to compare results from the 7T dataset with the results in the 3T dataset in Chapter 2.

Homogeneity of Variance – Levene's test suggested homogeneity of variance for both diagnostic groups ($p > 0.05$) for MD and FA.

Sphericity – In the cases where the null hypothesis for Mauchly's test of sphericity was rejected ($p < 0.05$), Greenhouse-Geisser and Huynh-Feldt adjustments were used, for epsilon values > 0.75, and < 0.75, respectively.

Homogeneity of the Regression Slopes – The tests for the homogeneity of the regression slopes suggested no significant interaction between the covariate and diagnosis group on diffusion measures.

	Measures of Cortical Diffusion	
	FA	MD
Effect of hemisphere	$F(1,16) = 4.447$ **$p = 0.051$** $\eta^2 = 0.217$	$F(1,16) = 1.746$ **$p = 0.205$** $\eta^2 = 0.098$
Effect of brain region	$F(2,32) = 3.564$ **$p = 0.040$*** $\eta^2 = 0.182$	$F(2,32) = 7.770$ **$p = 0.002$**** $\eta^2 = 0.327$
Effect of diagnosis	$F(1,16) = 0.546$ **$p = 0.471$** $\eta^2 = 0.033$	$F(1,16) = 8.192$ **$p = 0.011$*** $\eta^2 = 0.339$
Hemisphere by diagnosis interaction	$F(1,16) = 0.274$ **$p = 0.608$** $\eta^2 = 0.017$	$F(1,16) = 7.963$ **$p = 0.012$*** $\eta^2 = 0.332$

Table 22. Summary of rmANCOVA statistics for FA and MD values in the three ROIs using an automated masking method.

There was a significant main effect of brain region on mean FA values. Paired-samples t-tests were run post-hoc, and showed that FA values were lowest for BA17 and highest for BA9. The

significant main effect of region on MD values showed that MD values in the FG was highest and lowest in BA9. The significant main effect of diagnosis for MD values was followed by a post-hoc independent samples t-test, which revealed that MD values were significantly lower for ASD individuals compared to TD individuals. The significant hemisphere by diagnosis interaction was followed up with post-hoc tests – this interaction suggests that the MD across regions in the left hemisphere for TD individuals was significantly higher compared to ASD individuals. MD values averaged across the left and right hemisphere for each ROI and group were plotted in Figure 37. MD values in the left hemisphere were larger for each ROI and group. However, the difference between hemispheres was least pronounced in BA17, for both TD and ASD individuals.

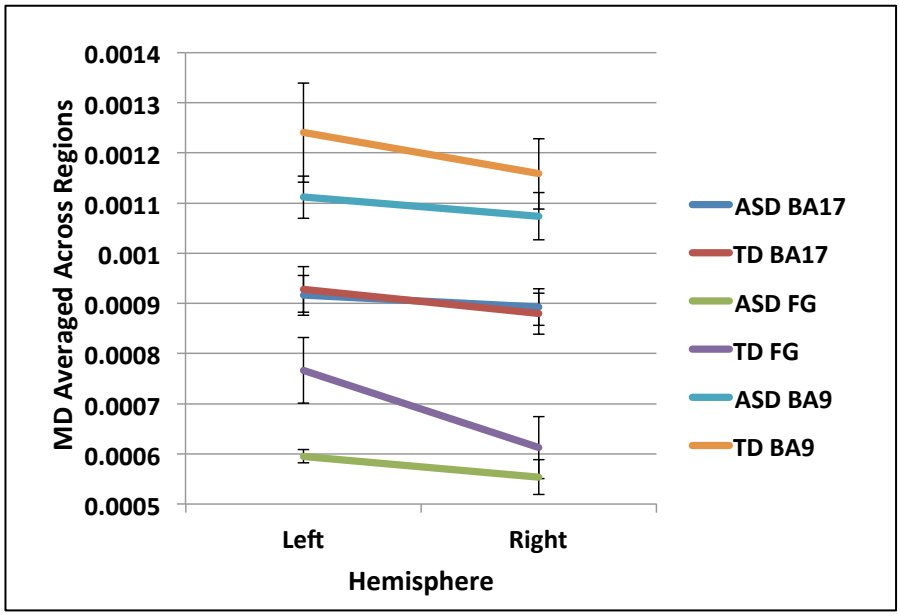

Figure 37. MD values averaged across the three regions. Error bars reflect SE.

Manual Masking of 7T Data

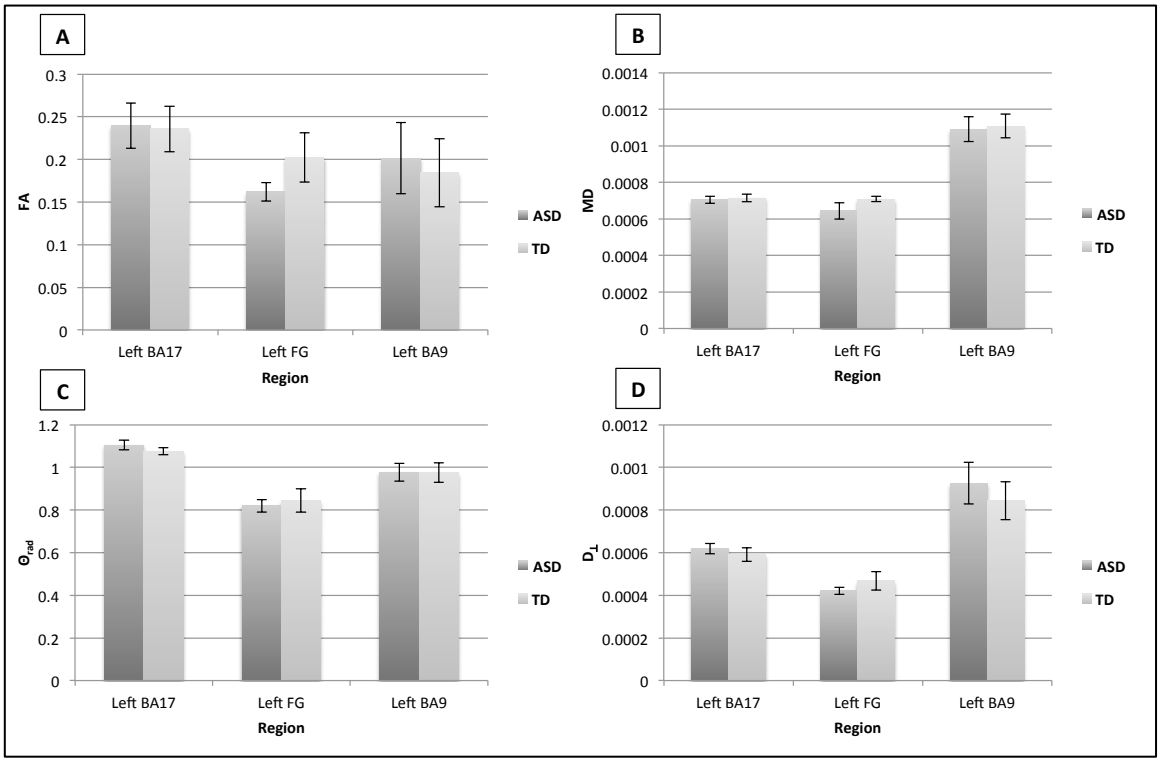

Figure 38. Results for manual masking. A) depicts FA, B) depicts MD, C) depicts Θ_{rad}, and D) depicts $D_\perp$ across regions and hemispheres. Error bars represent SE.

The mean values for each of the diffusion measures are shown in Figure 38, and the results from the statistical analyses are summarized in Table 23. The assumptions for the rmANCOVA were checked for each of the dependent variables. As was the case with the automated masking data, the mean FA values for TD individuals did not show a normal distribution. However, ANOVAs are generally robust against violations of normality and were still run. A 3x2 rmANCOVA was used for the manually masked 7T data, with brain region as a within-subject factor, and diagnostic group as the between-subject factor. Age was added as a covariate. Four rmANCOVAs were run for each of the dependent variables: FA, MD, Θ_{rad} and $D_\perp$. No significant main effects or interactions were found for the manual masking data.

	Measures of Cortical Diffusion			
	FA	MD	Θ_{rad}	$D_\perp$
Effect of brain region	$F(2,32) = 1.922$ **$p = 0.107$** $\eta^2 = 0.190$	$F(2,32) = 1.897$ **$p = 0.167$** $\eta^2 = 0.106$	$F(2,32) = 0.369$ **$p = 0.694$** $\eta^2 = 0.023$	$F(2,32) = 1.632$ **$p = 0.211$** $\eta^2 = 0.093$
Effect of age	$F(1,16) = 1.001$ **$p = 0.332$** $\eta^2 = 0.059$	$F(1,16) = 0.679$ **$p = 0.422$** $\eta^2 = 0.041$	$F(1,16) = 0.425$ **$p = 0.524$** $\eta^2 = 0.026$	$F(1,16) = 0.069$ **$p = 0.796$** $\eta^2 = 0.004$

Effect of diagnosis	$F(1,16) = 0.336$ **$p = 0.570$** $\eta^2 = 0.021$	$F(1,16) = 1.709$ **$p = 0.210$** $\eta^2 = 0.096$	$F(1,16) = 1.532$ **$p = 0.234$** $\eta^2 = 0.087$	$F(1,16) = 0.267$ **$p = 0.613$** $\eta^2 = 0.016$

Table 23. Summary of rmANCOVA results for manual masking.

Correlations with Diagnostic Scores

ASD individuals showed reduced MD across regions (through automated masking). In order to determine whether this was related to ADOS scores, Pearson's bivariate correlations were run. The results are summarized in Table 24. No significant correlations were found.

	ADOS (Total Score)	ADOS (Communication Subscore)	ADOS (Social Subscore)
Average MD (automated masking)	$r = 0.029$ **$p = 0.937$**	$r = 0.333$ **$p = 0.347$**	$r = -0.151$ **$p = 0.678$**

Table 24. Correlations between diagnostic scores and mean MD from automated masking.

Bringing the Modalities Together

Correlations Between Gamma and MRS Metabolites

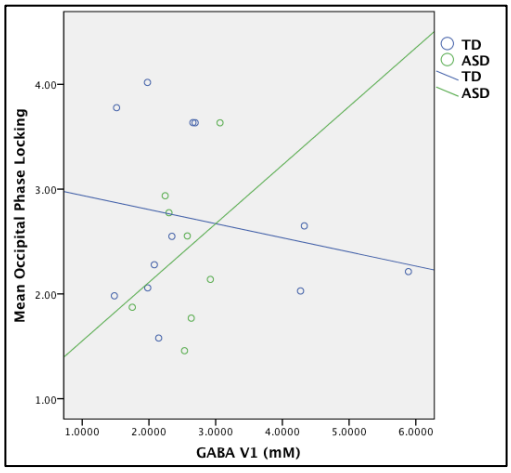

Figure 39. Correlation between mean gamma (35-80 Hz) phase-locking and GABA values in V1.

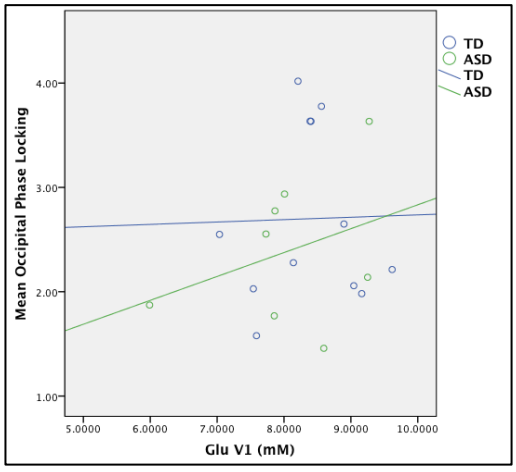

Figure 40. Correlation between mean gamma (35-80 Hz) phase-locking in occipital cortex and Glu values in V1.

In order to explore the relationship between gamma and GABA/Glu, partial correlations were run for different metabolite values and mean gamma phase-locking values (which were obtained by averaging the phase-locking values for the left and right occipital cortex), while controlling for grey matter volume. The correlation between GABA and gamma, and Glu and gamma, are depicted in Figure 39 and 40, respectively. The results of these tests are summarized in Table 25. Correlations were run for absolute metabolite values, as well as for values corrected for NAA values[6]. No significant correlations were found between mean gamma phase-locking values and GABA or Glu.

	Glu V1	Glu/NAA V1	GABA V1	GABA/NAA V1
Mean Gamma Phase-Locking in Occipital Cortex	r = 0.206 **p = 0.398**	r = 0.325 **p = 0.175**	r =-0.081 **p = 0.740**	r = -0.074 **p = 0.763**

Table 25. Correlations between gamma phase-locking and different metabolite values.

In vivo Minicolumn Measurements and Gamma Phase-Locking

To explore the relationship between gamma oscillations and in vivo minicolumn measurements through diffusion measures, Pearson's correlations were run for gamma phase-locking values corresponding to simple visual stimuli in the right visual field (activating left occipital cortex) and diffusion measures extracted from manually masking left BA17. The results are summarized in Table 26. Additionally, correlations were run for gamma phase-locking values in left and right visual cortex and automated FA and MD values extracted from left and right BA17. These results are summarized in Table 27. One significant correlation was found between gamma phase-locking and FA. However, since this relationship was not found in both hemispheres, this relationship was not further explored.

	Left BA17 FA	Left BA17 MD	Left BA17 Θ_{rad} (manual masking)	Left BA17 $D_{\perp}$ (manual masking)

[6] Though Glu/Cr and GABA/Cr values are not reported in this thesis, correlations were also run for gamma phase-locking and metabolites corrected for Cr, since a previous paper used this method (Cousijn et al., 2014). No significant correlations were found.

	(manual masking)	(manual masking)		
Gamma Phase-Locking in Left Occipital Cortex	r = -0.080 **p = 0.760**	r = -0.025 **p = 0.923**	r = -0.260 **p = 0.314**	r = -0.239 **p = 0.356**

Table 26. Correlations between diffusion measures from manual masking of left BA17 and gamma phase-locking values in left occipital cortex.

	Left BA17 FA (automated masking)	Left BA17 MD (automated masking)		Right BA17 FA (automated masking)	Right BA17 MD (automated masking)
Gamma Phase-Locking in Left Occipital Cortex	r = -0.504 **p = 0.024***	r = 0.074 **p = 0.758**	Gamma Phase-Locking in Right Occipital Cortex	r = -0.282 **p = 0.228**	r = 0.264 **p = 0.260**

Table 27. Correlations between diffusion measures from automated masking and phase-locking values in V1.

Glu & Perceptual Capacity

It was hypothesized that some relationships may exist between performance on the Complex Visual Task and hyperexcitability. Pearson's bivariate correlations were run between CS Detection at set size 6 and Glu (absolute) in MPFC for the following reasons: 1) significant differences were found in CS detection at set size 6 between ASD and TD individuals, 2) CS detection at set size 6 correlated with ADOS scores (at the unadjusted alpha level), and 3) Glu levels (absolute) in MPFC correlated with ADOS scores. The results are shown in Figure 41 and in Table 28.

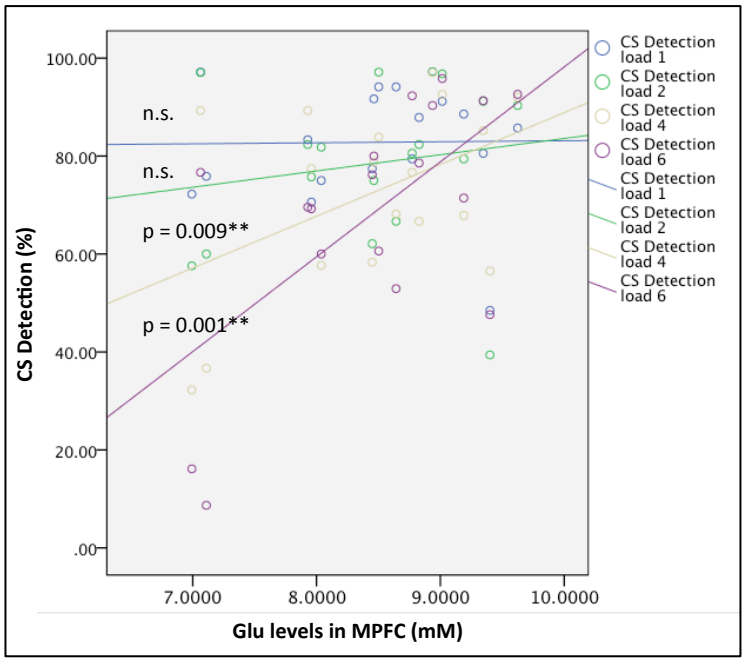

Figure 41. Correlations between Complex Visual Task Performance and Glu concentration in the MPFC voxel. Correlation between these two measurements became stronger with increasing set size (or perceptual load).

	CS Detection (set size 1)	CS Detection (set size 2)	CS Detection (set size 4)	CS Detection (set size 6)
Glu MPFC	r = 0.175 **p = 0.517**	r = 0.334 **p = 0.207**	r = 0.632 **p = 0.009****	r = 0.752 **p = 0.001****

Table 28. Summary of correlation between Glu (absolute) in MPFC and CS Detection.

Discussion

Modality 1: MEG

Simple Visual Task

The Simple Visual Task was used to determine if there were any abnormalities in gamma oscillations elicited by Gabor patches between ASD and TD individuals. Interestingly, no apparent differences were found between diagnostic groups in occipital areas of the brain within 300ms of stimulus onset or offset. Despite this, on average, TD individuals did show increased phase-locking in these occipital regions. Negative correlations were found between gamma phase-locking in occipital cortex and ADOS scores, driven by the ADOS Communication Subscore. Some significant differences in gamma phase-locking were observed between TD and ASD individuals, but these were not observed in occipital regions, but rather in frontal and parietal regions (corresponding to plots A2, B2, C1, and C2). Extracting the mean gamma phase-locking values for TD and ASD individuals in these frontal and parietal regions revealed that the TD group consistently had higher phase-locking values. However, the gamma phase-locking values from one of these frontal regions (A2) showed a positive correlation with ADOS scores, particularly the Social Interaction Subscore, revealing the complexity of the mechanism that might be at work. These results imply that significant impairments in occipital gamma phase-locking may not be apparent between high-functioning ASD and TD individuals, and that rather frontal responses to these simple visual stimuli may actually differentiate the groups. This type of relationship has previously been reported (Menassa, 2013; Rojas & Wilson, 2014; Wright et al., 2012) and adds value to the study of gamma oscillations as a potential ASD biomarker.

It is likely that fronto-parietal regions are recruited in addition to occipital brain areas during a simple visual task, and that altered frontal gamma phase-locking in ASD individuals may be the result of alterations in long-range, cortico-cortical connections, and in executive control (Just, Keller, Malave, Kana, & Varma, 2012). Also, since the stimuli are presented in a predictable pattern and do not contain an element of surprise, memory processes controlled by frontal regions may be involved (Busch et al., 2005). Overall, these results support the excitation/inhibition imbalance hypothesis of ASD (Rubenstein & Merzenich, 2003). Gamma oscillations have repeatedly shown to be linked to perisomatic inhibitory activity (Buzsáki & Wang, 2012; Buzsáki, 2004; Sohal et al., 2009), and alterations in these oscillations have been reported in several ASD studies investigating the excitation/inhibition balance (Cornew, Roberts, Blaskey, & Edgar, 2012; Rojas & Wilson, 2014; Snijders et al., 2013).

It is important to note that all ASD and TD individuals recruited for this study had normal or corrected-to-normal vision. Several participants who initially expressed interest in the study were excluded due to visual impairments, including strabismus, impaired binocular vision, and colour blindness. Many MEG studies in the literature do not specify the level of visual impairments in their participants. Given that light sensitivity and visual processing abnormalities are common in ASD (Leekam, Nieto, Libby, Wing, & Gould, 2007), outlining these details in studies may determine whether any differences found in occipital gamma activity should be attributed strictly to ASD or not.

One may argue that performing separate analyses for left and right visual fields complicated the results. However, studies have reported on atypical gamma oscillations lateralized to one hemisphere in ASD (Maxwell et al., 2013). Additionally, several electrophysiological studies have reported on atypical laterality in ASD (Burnette et al., 2011; Cantor, Thatcher, Hrybyk, & Kaye, 1986). Therefore, it was decided to keep the analysis separate for the two visual fields. Future work involves running statistical tests between epochs where stimuli were presented in the left visual field and right visual field, stratified by diagnostic group.

One of the limitations of this study is that eye tracking was not used to determine where participants were looking at a given time. While the button press task was incorporated to ensure participants kept their attention to the middle of the screen, epochs where participants did not correctly identify the target were not removed from the analysis, and may lead to confounding results. Moreover, the behavioural results from this task showed a great deal of variation for the ASD group, whereas the TD group performed quite consistently. However, all participants were monitored during the scan through video to ensure they were awake and focused. Moreover, no significant differences were found in behavioural performance between diagnostic groups. Additionally, no relationships were seen between gamma phase-locking values and behavioural responses, and no relationships were seen with ADOS (total scores) and behavioural responses from this task. These relationships were not formally reported, but are shown in the Appendix of this Chapter in Figure 42.

Lastly, it is worth mentioning that previous studies involving Gabor Patches used contextual modulation during the task, either by increasing the grating size of the Gabor Patch (Milne et al., 2009), or the orientation of the Gabor Patch (Snijders et al., 2013), and measured the change in gamma response as the stimuli changed. Both of these changes are supposed to increase gamma power in striate and extrastriate cortex. ASD groups in both papers were reported to show a smaller increase in gamma power with the change in stimuli, and not merely with stimuli presentation. The task used in the current study did not modulate the visual stimuli – the Gabor Patches were either present or absent. This may be one of the reasons no differences in occipital cortex were seen.

Complex Visual Task

The main findings from the Complex Visual Task are supported by the previous publication on heightened perceptual capacity in ASD individuals (Remington et al., 2012). ASD participants in this study were significantly better at detecting the CS when the perceptual load condition was

high, but showed no differences from TD individuals in performance when the perceptual load condition was low. Similar results were found when looking at the detection sensitivity, which accounts for both CS detection and the number of false alarms. ASD individuals demonstrated higher detection sensitivity in high load conditions, but showed no differences in low load conditions. It is important to note that the two groups performed very similarly on the letter search task across set sizes, and the superior performance by ASD individuals on detecting the CS was not affected by reduced accuracy of letter detection or by increased reaction time to the visual stimuli (see Figure 43 in the Appendix). These findings together strengthen the notion that high-functioning ASD individuals may have better ability to perceive details in visual space (O'Riordan et al., 2001).

As hypothesized in the previous publication (Remington et al., 2012), superior performance on this task may paradoxically be linked to core ASD severity that is related to object scrutiny and preoccupation, as well as attention to details. This hypothesis is partially supported by the positive correlation trending on significance between ADOS total scores and CS detection only at the high perceptual load condition (set size 6). It remains unclear whether this superior performance is "intrinsic" to the disorder, or whether core features of the disorder drive ASD individuals to take up interests and hobbies that help with visual tasks like the one described here.

A caveat with the Complex Visual Task is that one of the ASD individuals with valid behavioural results was left-handed. Since all individuals were asked to hold the buttons for letter identification in the right hand, and the buttons controlling for CS presence in the left hand, this may have contributed to this individual's success on the task. However, this discrepancy would not be able to explain why he also performed better than the ASD and TD group mean for the letter task accuracy. Another limitation of the study is that the number of individuals in both groups with valid behavioural results was lower than the number of individuals recruited in the study. This may have been due to miscomprehension of the task, despite all individuals receiving the same instructions and opportunities to practice before performing the task. The small cohort

size limited the ability to perform more stratified statistical analyses that controlled for factors like age and gender.

All ASD participants in this study were matched for chronological age, gender and non-verbal IQ. It was initially hypothesized that matching for IQ may play a role in reducing the effect of superior visual performance observed in ASD individuals. However, finding this result despite ASD individuals being matched on nonverbal IQ adds to the robustness of the perceptual load theory in ASD. Future work should involve larger cohorts with more variation in IQ, age and gender to determine the role these factors play on performance.

Modality 2: MRS

The MRS modality of this project had several advantages. Firstly, this is one of the very few ultra-high field MRS studies on ASD. The employment of 7T MRS helped increase the signal-to-noise ratio and measure Glu, and GABA. Quantifying these metabolites helped answer important questions specifically about the hyperexcitable state in ASD. Secondly, this is one of the few MRS ASD studies that solely included participants who were not on any medications affecting the brain (according to self-reports) within one year of the scan.

Though a significant region by diagnosis interaction was not found for Glu levels, the relationship trended on significance, and planned post-hoc tests revealed that Glu levels in the MPFC of ASD individuals were higher compared to controls, supporting the hyperexcitability hypothesis. However, no diagnostic differences were found in GABA levels, though these statistics were underpowered due to the quality of the GABA peaks for some participants. No differences in NAA were found between ASD and TD individuals, raising the question of whether neuronal differences exist in ASD, or whether NAA is the best marker to study neuronal differences. Lastly, Cr levels were elevated in the MPFC in individuals with ASD but unchanged in V1. These results taken together support the hyperexcitability hypothesis in ASD, and also

suggest that Cr levels in ASD may reflect an excess of glial cells or neurons, or increased metabolic function. These findings are supported by other MRS studies (Murphy et al., 2002), as well as post-mortem work completed in the Neuroanatomy and Cognition Group (Menassa, 2013).

One of the challenges with MRS results is contextualizing it within the literature. Several MRS studies use different baseline values to compare metabolites, making it difficult to compare findings between studies. Some researchers report metabolite values in reference to Cr (Cousijn et al., 2014), while others use NAA, which is thought to be a marker of neuronal integrity (Draper et al., 2014), or absolute values (Muthukumaraswamy et al., 2009). This thesis examined absolute values, as well as metabolites standardized to NAA. While diagnostic differences were found for absolute values of Glu, no diagnostic differences were found when evaluating GABA/NAA and Glu/NAA levels. However, NAA may not be the best marker for neurons. While studies have demonstrated that NAA levels are significantly lower in white matter compared to grey matter (Inglese et al., 2008), this reflects a global average, signifying that it is unclear whether this is across all brain regions. Cr levels were not used to standardize metabolites in this study because diagnostic differences were found in the MPFC. Moreover, researchers have reported that standardizing to Cr may introduce rather than reduce confounding results, suggesting that it may be more appropriate to report absolute metabolite values (Jansen, Backes, Nicolay, & Kooi, 2006; Li, Wang, & Gonen, 2003). Since there is currently not one established method to report MRS results, the current study gives most weight to the absolute metabolite differences found between groups.

Though reporting the absolute values of metabolites seem to reflect the most accurate picture, the main disadvantage is that the "absolute" quantification depends on how the water peak is measured. If the water peak is not accurately measured due to limitations in the acquisition, then the reported metabolites may be erroneous. However, given that the water peak is much larger than that of Cr, it is likely to be less erroneous (Warntjes, Dahlqvist, & Lundberg, 2007). A study

looking at the inter-individual differences in metabolite values using internal (water) and external (like Cr and NAA) references supported the notion that there is less variation when an internal reference is used (Minati, Aquino, Bruzzone, & Erbetta, 2010), further supporting the conclusion in this thesis that the absolute quantification of metabolites is the best method.

Another caveat with interpreting MRS studies in the context of the literature is that the voxel placement may vary significantly between studies, despite their investigation of the same region of interest. For example, two previous ASD studies investigating metabolite values in the frontal and occipital cortex used a technique called Magnetic Resonance Spectroscopic Imaging, which uses slices through the brain to choose the voxel of interest (DeVito et al., 2007; Levitt et al., 2003). In the Levitt et al. (2003) study, a voxel within the slice was chosen for acquisition of metabolites for occipital and frontal cortex with the criteria that 75% of the voxel should contain grey matter. The anatomical boundaries of where these voxels were placed in that study is unclear. However, it is worth noting that the average grey matter volume in the V1 and MPFC voxel used in this thesis were 56% and 78% respectively, suggesting that at least the percentage of grey matter in the MPFC voxel in this study is similar to the previous spectroscopy study on ASD. The V1 anatomical location of the current study is similar to other non-ASD MRS studies, which have used the medial occipital pole with the voxel centred around the calcarine sulcus as the main landmark (Goddard et al., 2001; Muthukumaraswamy et al., 2009). Other ASD studies which have looked at the MPFC specifically have used slightly different anatomical landmarks, with one study using a similar position in the anteroposterior axis, but with the voxel position on the right hemisphere rather than the midline, as was used in this current study (Endo et al., 2007; Murphy et al., 2002). Given the literature on atypical laterality in ASD, it was decided that the MRS voxel in the current study should be placed at the midline rather than in either hemisphere. These conclusions together suggest that there is some variation in the voxel positions used in this study compared to studies in the literature, especially for MPFC, which has less defined anatomical boundaries compared to V1.

One study looked at occipital, frontal and temporal grey matter, and found widespread reduction of a marker of glutamate (Glu) (DeVito et al., 2007), suggesting altered glutamatergic neurotransmission. Other studies have reported on reduced markers of Glu in the anterior cingulate cortex (Bernardi et al., 2011), as well as reduced GABA in an area of the frontal lobe (Harada et al., 2011).

Lastly, correlations between diagnostic scores and a few of the metabolites that showed significant differences between ASD and TD individuals revealed that only Glu levels (absolute) in the MPFC correlated with total ADOS scores. These findings are encouraging and suggest that elevated Glu levels in frontal regions like the MPFC may be characteristic of the disorder.

One caveat in the results of this modality is that there was one left-handed participant. However, there should have been no lateralization effects because both the V1 and the MPFC voxel included both hemispheres. Another limitation may be that the ASD sample was not representative of the ASD population. For example, contrary to the sample used in this study, a large number of ASD individuals present with psychiatric comorbidity, take medication for the brain, and show intellectual disabilities. While the sample used in this study may not wholly reflect the ASD population, the group was homogeneous, and most individuals were able to successfully participate in all the imaging modalities of the study, which was a great strength.

Modality 3: DTI

Similar to the DTI method used in Chapter 2, two analysis methods were used in the DTI data for this cohort. Automated masking techniques outputted FA and MD values in the three ROIs – BA17, FG, and BA9 – for both hemispheres. The manual masking technique was used in conjunction with CHIPS. Four main measures were outputted – FA and MD values that reflected radial organization of the cortex, as well as two novel measures of diffusion called Θ_{rad} and $D_{\perp}$.

From the automated masking, MD values across regions were reduced in ASD individuals. A significant hemisphere by diagnosis interaction was found, where TD individuals showed more leftward asymmetry. ASD individuals also showed a leftward asymmetry across the three brain regions but this was less pronounced, as shown in . Interestingly, the hemisphere by diagnosis interaction was most apparent for FG and BA9. BA17 showed reduced MD asymmetry and the values were very similar for both groups. Lastly, the diagnosis by gender interaction for MD values showed that the females in both groups were driving the diagnostic differences. The main findings from the DTI part of this multimodal study are in line with the idea that MD (rather than FA) values in cortex are likely to reflect changes with age and pathology (Jeon et al., 2012; McKavanagh, 2015).

A global reduction in MD was observed in ASD individuals; however, the biological significance of these findings is difficult to interpret. Studies that have looked at diffusion measures in cortex during development suggest that a reduction in MD may reflect increased cellular density and reduced water content (Gupta et al., 2005; McKinstry et al., 2002). If reduced MD is a reflection of increased cellular density, the results in this study may strengthen previous neuropathological findings in ASD, which suggest increased cell-packing density in the cortex (Bailey et al., 1998) as well as in subcortical regions (Kemper & Bauman, 1993; Palmen, van Engeland, Hof, & Schmitz, 2004). Differences in asymmetry reported here are in accordance with the hypothesis that ASD individuals show atypical brain structure and laterality (Chance, 2014; Maxwell et al., 2013). Lastly, the gender by diagnosis interaction in MD values demonstrated that the females were driving the overall diagnostic differences. These results, taken together with the MRS findings and the conclusions from Chapter 2 strengthen the importance of examining differences in ASD with consideration to gender.

Contrary to the results in Chapter 2, the automated rather than the manual masking technique showed more group differences, perhaps questioning which method may be more useful at

probing the cortical structure. This may be because the observed effects with the automated masking were mainly related to atypical laterality, which could not be observed with the manually masked data since only left ROIs were masked. Future work may involve manually masking the right hemisphere ROIs for this cohort to determine whether the interesting asymmetry trends seen with the automated masking also come up with the extra diffusion measures.

One caveat in the results presented here is that significant differences were found in total grey matter volume between ASD and TD individuals, with ASD individuals having higher grey matter volume. Therefore grey matter volume was not used as a covariate[7]. There is a possibility that grey matter volume affected the diagnostic differences seen in MD values. Future work may benefit from a voxel-based morphometric analysis in this dataset to further investigate volume differences between groups.

Bringing the Modalities Together

No correlations were found between gamma oscillations and GABA or gamma oscillations and Glu, supporting recent work completed in Oxford (Cousijn et al., 2014). This does not undermine either gamma or GABA/Glu as factors in determining the balance in the brain, and several papers do discuss a link between gamma and GABAergic activity (Buzsáki & Wang, 2012; Lodge, Behrens, & Grace, 2009; Sohal et al., 2009). It may be that these relationships are driven by a subset of GABAergic cells, like PV+ cells, suggesting that overall GABA and Glu levels measured by MRS may not be the best marker for gamma oscillations. It is perhaps worth noting that MEG analyses were performed in signal space, and phase-locking rather than power values were examined here. The relationship between gamma and GABA/Glu may appear if source

[7] Though head circumference was not investigated in this study, perhaps it is worth anecdotally mentioning that of the 13 recruited ASD individuals, four males had noticeably large head sizes. Two of them were unable to fit inside the MRI scanner. It is likely that head size was driving the difference seen in grey matter volume.

localization was performed, and if power instead of phase-locking was investigated. Moreover, previous studies

MEG and DTI may be a promising combination of techniques for future studies. However, no correlations were seen with gamma oscillations in left occipital cortex, and the four diffusion measures outputted from manually masking left BA17. The hypothesis motivating this correlation analysis was that minicolumn spacing and distribution are partly controlled by surrounding GABAergic cells (Raghanti, Spocter, Butti, Hof, & Sherwood, 2010). Despite the relationship of both minicolumns and gamma oscillations to inhibitory activity, no apparent correlations were seen. There are very few studies that have explored the relationship between microstructure and gamma oscillations. This may be because gamma oscillations result from the synchronous activity of 50,000-100,000 neurons, whereas a minicolumn refers to a group of 60-80 neurons. Understanding how cortical organization at the microscopic level affects electrophysiological activity at the macroscopic level may be central to further understanding brain dynamics in ASD. Given the hypothesis of underconnectivity in ASD between primary visual and more frontal regions in the brain, future work for the DTI data may involve performing tractography for the two diagnostic groups with a seed voxel placed in V1, and exploring the relationship between the tracts and gamma oscillations.

Previous reports have suggested that the superior perceptual functioning in ASD may be linked to hyperactivity of V1 (Mottron, Dawson, Soulières, Hubert, & Burack, 2006). However, findings in this study may indicate the opposite. The positive correlation found between CS detection at set size 6 in the Complex Visual Task and Glu levels in MPFC suggest that more executive areas of the brain are linked to enhanced perceptual capacity in ASD. What is interesting about this correlation is that it was only significant at the higher perceptual load conditions (set size 4 and 6). This provides some evidence for the role of Glu in MPFC specifically in processing distractor stimuli in high perceptual load conditions, and not simply in overall task responsiveness. Future

work involves recruiting more participants to participate in the Complex Visual Task and the MRI scans to increase the sample size.

One caveat in this study may be that the statistical tests used here were not sufficient for this multimodal dataset. An alternative way of analysing this dataset may be the use of a principal component analysis, which combines all the variables into components and investigates the components that show the largest variance between groups, or using tools like "Brain-CODE", which was formed by the Ontario Brain Institute in Canada in order to help integrate and analyse large amounts of brain data[8].

Conclusions

The results from this Chapter provide evidence that hyperexcitability (measured by elevated Glu) in the frontal rather than primary visual regions in ASD individuals characterize their behavioural differences. Though no apparent differences were observed in occipital phase-locking between the two groups, the significant differences in frontal gamma phase-locking imply an altered state of executive function in ASD. Moreover, ASD individuals showed reduced hemispheric asymmetry in MD values across all regions, but this pattern was much less pronounced in V1 than in FG and in BA9. These findings taken together support the idea that high-functioning ASD individuals show more pronounced differences in markers of hyperexcitability and atypical cortical structure in higher-order areas of the brain, leaving primary sensory regions largely unaffected.

[8] More information can be found at https://www.braincode.ca/content/about-brain-code.

Chapter 3 Appendix

Reasons why certain modalities lack data from participants:
ASD01 – performed poorly on control block of Complex Visual Task
ASD06 – diffusion MRI sequence failed to run
ASD09 – performed poorly on control block (of Complex Visual Task)
ASD10 – performed poorly on control block, head was too large for MRI scanner
ASD12 – was hypersensitive to visual and auditory stimuli
TD03 – fell asleep during Complex Visual Task
TD04 – was ineligible for MRI due to undisclosed appendectomy procedure
TD05 – felt uncomfortable in the MRI scanner towards the end of the second diffusion scan
TD07 – was part of the MRI pilot scan and was not recruited for MEG
TD09 – was not recruited for MRI due to repeated scanner malfunction
TD10 – was part of the MRI/MRS pilot scan and was not recruited for MEG, only V1 MRS data acquired
TD13 – performed poorly on control block
TD14 – performed poorly on control block
TD15 – performed poorly on control block

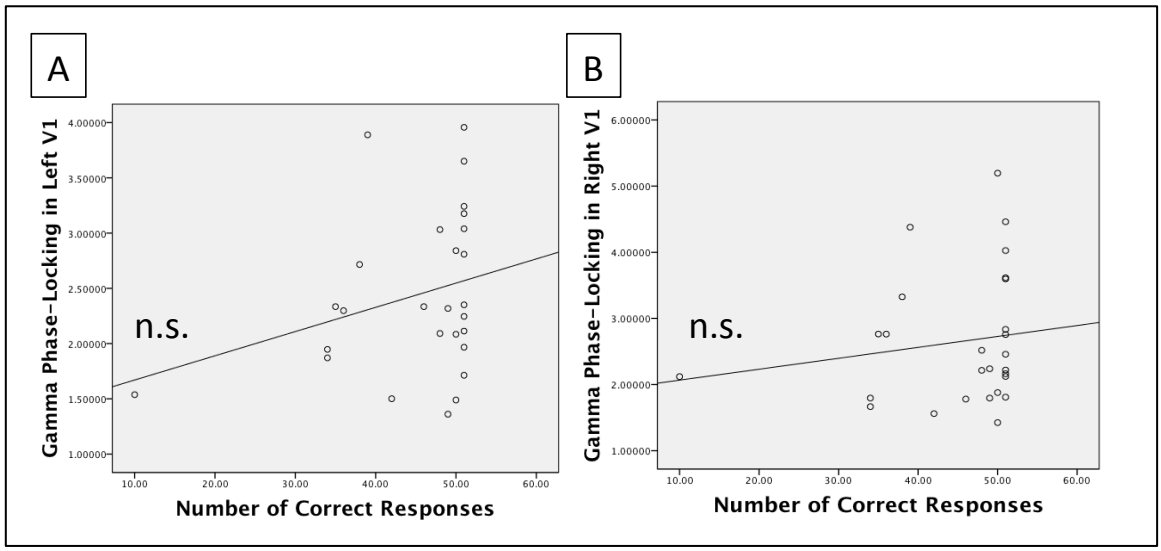

Figure 42. Correlations between behavioural responses and gamma phase-locking in occipital regions.

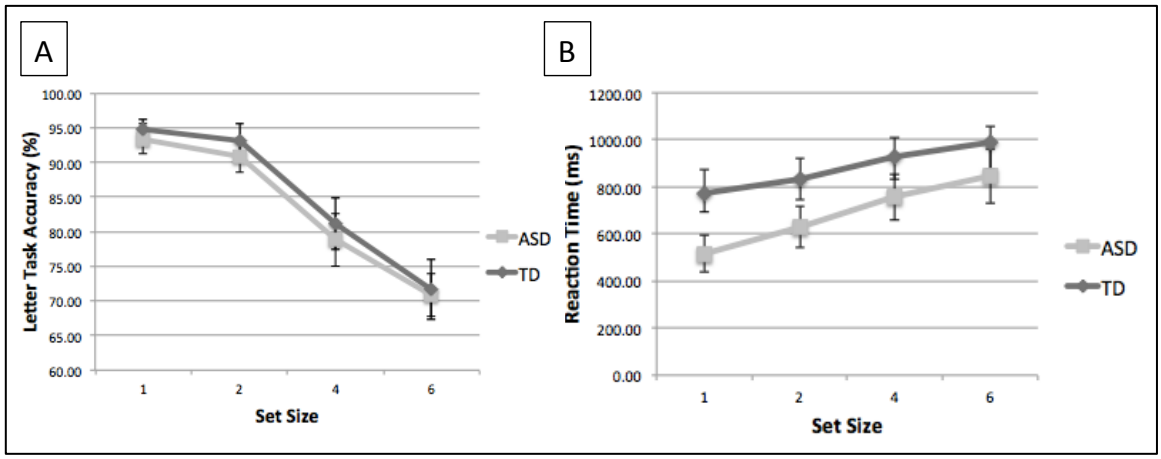

Figure 43. Letter task accuracy and reaction time results for TD and ASD individuals. No significant differences were found in either of these measurements between groups.

Chapter 4: Immunohistochemistry

Introduction

Neuroimaging provides excellent tools to study the macrostructure and function of the brain in vivo. However, techniques in histology involving post-mortem brain tissue are currently much better in probing the underlying structure at the cellular level. As outlined in Chapter 1, excitation and inhibition in the cortex can be measured through a number of different techniques, including quantifying GABAergic interneurons through immunohistochemistry. Among the different types of GABAergic interneurons, the three that involve calcium-binding proteins are 1) calretinin, 2) calbindin, and 3) parvalbumin. PV+ interneurons seem most relevant in the study of ASD, given their fast-spiking properties, and their involvement in gamma oscillations (Sohal et al., 2009). Moreover, many mouse models have directly implicated a reduction of PV+ cells in ASD (Gogolla et al., 2009).

PV+ interneurons are produced from the medial ganglionic eminence and represent approximately 40% of all neocortical interneurons (Miyoshi et al., 2010). They are mainly multipolar, and are predominantly found in layer three and four of the neocortex (Condé, Lund, Jacobowitz, Baimbridge, & Lewis, 1994). The two main subtypes of PV+ cells are basket and chandelier cells. The former can be identified by different morphological patterns, like diameter of the soma, the manner in which the cell fires, as well as the amount of arborisation (both in dendrites and axons) (Markram et al., 2004), whereas the latter are identified by their vertically oriented axonal arbors, which form a candlestick-like appearance (Fairén & Valverde, 1980).

PV+ basket cells are fast-spiking because of their fast action potential properties and spiking rates. These cells function through the P and Q subtype of presynaptic Ca^{2+} channels, which help with quick neurotransmitter release and action potential propagation (Zaitsev, Povysheva, Lewis, & Krimer, 2007). PV+ basket cells make direct contact with the soma of pyramidal cells – this allows for quick and efficient communication to inhibit pyramidal cell activity and promotes

precise cellular responses by limiting the time in which these pyramidal cells can fire (Pinto, Brumberg, & Simons, 2000). Moreover, PV+ basket cells are connected through electrical gap junctions as well as chemical synapses, which facilitate rapid cell synchrony. A previous study found that loss of connexin32, which is a protein that helps form gap junctions between PV+ cells, reduced task-oriented gamma oscillations (Buhl, Harris, Hormuzdi, Monyer, & Buzsáki, 2003). This provides further evidence that rapid communication between interneurons plays a role in neural synchrony.

PV+ chandelier cells are also fast-spiking, but are less abundant than basket cells, and may even show excitatory activity (Szabadics et al., 2006), though this seems dependent on region and experimental condition (Glickfeld, Roberts, Somogyi, & Scanziani, 2009; Woodruff, Anderson, & Yuste, 2010). Chandelier cells form synapses with the axon initial segment of pyramidal cells and show different morphological characteristics from basket cells. Limited work has been done in studying the subsets of PV+ cells in ASD. However, given the late development of these subset of interneurons as well as the concentration of these cells in the cortex, hippocampus, and the amygdala – all brain regions implicated in ASD – they provide an interesting target for research in this field.

In this Chapter, all PV+ cells were stained using immunohistochemistry in the three ROIs: V1, the FG, and BA9. Similar to the other Chapters, the aim was to determine diagnostic differences as well as regional differences. The following research questions were investigated in this Chapter.

Research Questions

1. Are there diagnostic differences in the distribution of PV+ cells?
2. Are there regional differences in PV+ cells, or a region by diagnosis interaction in PV+ cells?

Methods

Antibodies of Interest

Two antibodies were initially purchased for this project: 1) the Sigma-Aldrich P3088 parvalbumin antibody, which stains for PV+ cells, as well as 2) Millipore's MAB5284 Cat-301 antibody, which stains for the core protein in CSPGs. However, given the difficulty to quantify the amount of extracellular matrix proteoglycans with automated software, it was decided to focus on parvalbumin.

Frozen versus Paraffin Embedded Tissue

The parvalbumin antibody was initially optimized for frozen tissue, since this tissue was used previously in the Neuroanatomy and Cognition Group to study minicolumn structure in ASD (McKavanagh et al., 2015). The purpose of using the same tissue was to be able to make comparisons between the number of PV+ cells and minicolumn spacing. The optimized immunohistochemistry protocol for the P3088 antibody on frozen tissue is outlined in the Appendix of this Chapter. Despite the antibody working well on frozen tissue, there were several freeze artefacts that could potentially lead to confounding results, as shown in Figure 44. Therefore it was decided to change to paraffin-embedded tissue.

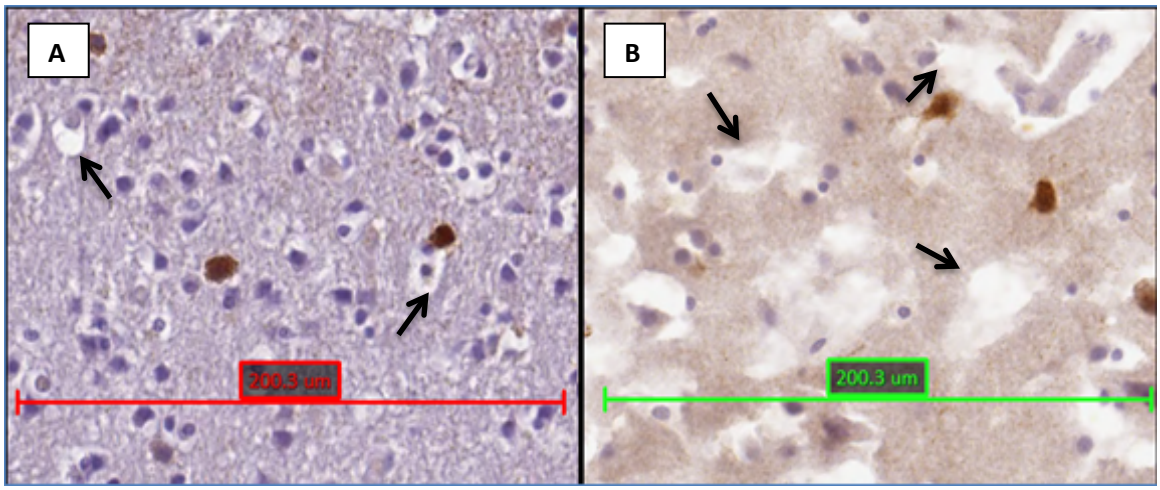

Figure 44. PV+ staining for A) paraffin-embedded and B) frozen tissue from the same TD case. The width of both images is 200 µm. Arrows point to areas of tissue shrinkage/erosion, which seems more evident for the frozen tissue.

Case Selection

After deciding to switch to paraffin-embedded tissue, ASD and TD cases were chosen from the Thomas Willis Oxford Brain Collection (TWOBC). All ASD individuals were carefully matched as best as possible with TD individuals in chronological age and gender. The demographic information, as well as the post-mortem interval (the time between death and fixation, known as the PMI) and the time spent in formalin for all cases in this study are outlined in Table 29. The three regions were sampled from 14 ASD cases and 15 TD cases. ADI-R (all three subscores) and SCQ scores were available for nine ASD cases, and SRS scores were available for seven ASD cases. The diagnostic data is summarized in Table 30.

Sampling Tissue

BA17, FG and BA9 were sampled from each of the 29 cases, which were stored in formalin for varying lengths of time. For BA17, wherever possible, the anterior limit of the block was determined by the intersection of the parieto-occipital fissure with the calcarine sulcus at the midline. Care was taken to ensure that all blocks sampled from this region included the stria of Gennari, which is the cytoarchitectural landmark of V1. For FG, the inferior temporal gyrus was used as the lateral limit and the PHG as the medial limit. Wherever possible, the anterior limit of the FG was determined by the posterior limit of the hippocampus. Also where possible, the PHG was sampled together with FG, for the interest of future studies. Lastly, BA9 was sampled using the anterior boundary of the cingulate gyrus as the posterior limit of the region, where possible. Care was taken to ensure that BA9 was always sampled anterior to the genu of the corpus callosum. All blocks were roughly 1cm in thickness. The anterior side of all blocks were marked with black ink in order to help with the paraffin-embedding process. Four blocks (one BA17, one FG, and two BA9) were embedded in the posterior to anterior direction because the anterior surface was damaged.

Tissue Processing

Since paraffin wax is immiscible with water, water content was removed from all blocks using ethanol and then washed in xylene, which is a wax soluble substance. After these steps, all blocks were washed with wax. For 21/29 cases, these steps were performed by Leica Biosystem's automated tissue processor over three nights. Eight of the 29 cases were previously placed in fomblin oil, a substance that is incompatible with the automated tissue processor, and therefore had to be hand-processed. The hand processing steps are outlined in the Appendix of this Chapter. After processing was completed for all blocks, they were embedded in paraffin wax. Further details of this are also provided in the Appendix.

Cutting Sections of Tissue Blocks

Once all blocks were embedded in paraffin wax, they were ready to be sectioned. 6-micron thick sections were cut on a microtome using Feather Microtome blades (S35, Surgipath Medical Industries) and placed onto Fisher's SuperFrost Plus slides. Approximately 10 sections were cut for each ROI and case. The sections were dried onto the slide overnight and were then ready to be stained.

Immunohistochemistry

The following immunohistochemistry protocol was used.

1. Paraffin-embedded tissue slides were placed in the oven at 70° C for 20 minutes to melt the wax.
2. Slides were rehydrated, placed in H_2O_2 for 30 minutes, and washed in tap water.
3. For antigen retrieval, slides were placed in citrate buffer and microwaved for 5 minutes at power 800, followed by a 5 minute cool-down in room temperature (two times).
4. Slides were cooled in running tap water.
5. Slides were placed onto the Thermo Fisher Coverplates and were loaded onto the Shandon Sequenza slide racks.

6. Slides were washed with Phosphate Buffered Saline with Triton-X (PBST) for 3 minutes (3 times).
7. The P3088 antibody was added onto the slides using a 1:4,000 dilution in PBST.
8. Slides were left at room temperature for 30 minutes, and then incubated overnight at 4° C.
9. The next morning, slides were washed with PBST for 3 minutes (3 times).
10. The HRP-conjugated secondary antibody (part of the Dako EnVision+ kit) was added onto the slides for 45 minutes.
11. Slides were washed with PBST for 3 minutes (3 times).
12. 3,3'-Diaminobenzidine (DAB) solution was made by mixing 1,000 µL of DAB substrate buffer with 20 µL of DAB chromogen, and subsequently was applied on the slides for 7 minutes. DAB bound to the antibody, and stained the PV+ cells in brown.
13. DAB was washed off the slides with distilled water and PBST.
14. Slides were counterstained with haematoxylin and eosin for 40 seconds, and then washed with distilled water.
15. Slides were placed in tap water, and then dehydrated.
16. Slides were cover slipped using Thermo Scientific DPX Mounting Media, and left to dry under the fume hood overnight.

Data and Statistical Analysis

All slides were looked at using a BX40 microscope (Olympus, Japan) in order to determine the overall staining quality. Afterwards, slides were scanned using the Aperio ScanScope slide scanner system in order to have a digital image that could later be used for data analysis. The contrast between tissue and white space was manually determined for each slide in order to attain the best scan quality. After slides were scanned, they were looked at using ImageScope (one of Aperio's built-in software) at x200 magnification.

In order to validate the automated cell counting program in ImageScope, manual cell counts were

done on 17 different frames, which were chosen semi-randomly. Cases and brain regions were not chosen randomly for the validation step because it was important to ensure a variety of staining qualities, brain regions and cases. However, the area within the slide was. Each slide was divided into several areas of roughly 8mm^2 each. Afterwards, a random number generator was used to determine which area to manually count cells from. In the validation step, 17 different areas were used, including 13 different cases and all three brain regions. Care was taken to include areas that were considered to have strong, medium, and weak-intensity staining in order to ensure that the algorithm worked well for varying levels of staining intensity.

The algorithm in the automated counting software incorporated parameters like cell size, cell roundedness, and RGB values for the DAB stain. Three different algorithms were used to test ImageScope's automated cell counting program. The algorithm was chosen based on which results most strongly correlated with the manual cell counts from the same area.

Demarcating the ROIs for Automated Cell Counts

After the algorithm was chosen, ImageScope's pen tool was used to demarcate the section of the tissue that would be analysed for each brain region. The negative pen tool was used to exclude areas of tissue damage/inadequate staining. For BA17, the gyrus around the calcarine sulcus was delineated. For the FG, the gyrus adjacent to the PHG was analysed. If this gyrus was damaged, then the best-preserved gyrus was used. Lastly, for BA9, the most dorsolateral gyrus of each slide was analysed. If this was damaged, then the best-preserved gyrus on the slide was analysed. Photos taken during the sampling process helped guide these demarcations. The analysis and demarcation process is depicted in Figure 45.

The algorithm of choice was run for all the ROIs across cases. For the statistical analysis, a 3x2 rmANCOVA was used, with ROI as a within-subject factor and diagnostic group as the between-subject factor. Age and time in formalin were used as covariates.

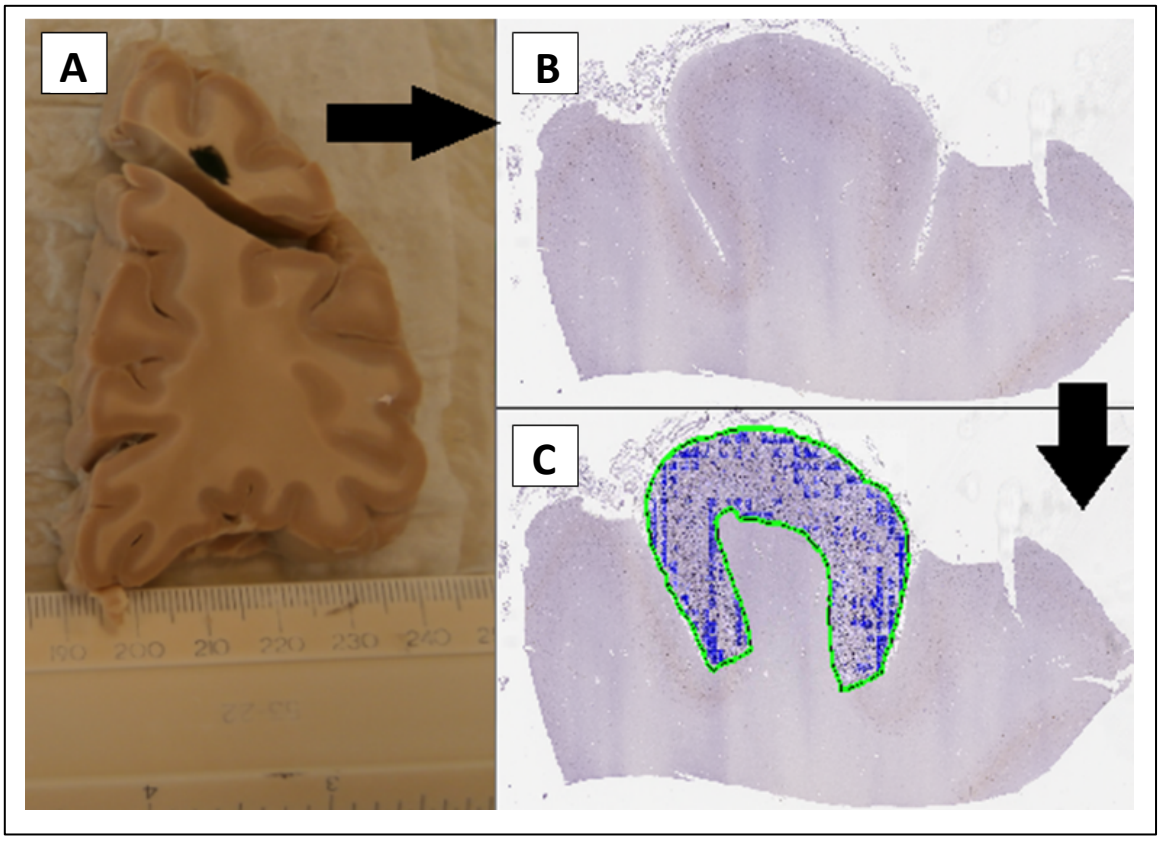

Figure 45. Sampling and staining of BA9. A) shows the sampling of BA9 from the left hemisphere, B) shows the digitalized slide of the same sampled region stained for PV+ cells, and C) shows the automated counting results from the gyrus of interest in BA9.

Results

Initially, it was thought that the brain regions had great variability in background staining with the same protocol. However upon closer analysis it was discovered that what seemed like background was actually the staining of dendritic processes, especially in layer four of cortex. This was most pronounced in BA17, depicted in Figure 47. The different cortical layers were more difficult to decipher in FG and BA9. Due to variations in clarity of the layer boundaries in each region, statistical analysis was performed without regard to layer differences.

Case – TWOBC Number	Group	Time in Formalin (months)*, PMI (hours)**	Age (years)	Sex	Hemisphere used for 3 ROIs	Case – TWOBC Number	Group	Time in Formalin (months)*, PMI (hours)**	Age (years)	Sex	Hemisphere used for 3 ROIs
ASD01 – 27/12	ASD	120, not known	13	M	R	TD01 – 98/1105	TD	198, not known	13	M	R
ASD02 – 27/11	ASD	47, not known	15	M	L	TD02 – 05/137	TD	111, not known	16	M	L
ASD03 – 72/11	ASD	42, 24	16	M	R	TD03 – C3569	TD	295, not known	18	M	L
ASD04 – 92/1014	ASD	289, 72	17	M	R	TD04 – 93/1351	TD	290, not known	18	M	R
ASD05 – 151/08	ASD	74, 144	19	M	L	TD05 – 91/1033	TD	290, 144	18	M	R
ASD06 – 07/09	ASD	71, 48	22	M	R	TD06 – 91/1134	TD	294, not known	21	F	L
ASD07 – 99/1071	ASD	191, not known	32	F	L	TD07 – C1384	TD	324, not known	25	M	R
ASD08 – 28/12	ASD	36, not known	35	M	R	TD08 – 94/1342	TD	254, not known	27	M	R
ASD09 – 98/1174	ASD + epilepsy	193, 72	35	M	R	TD09 – B8959	TD	362, not known	30	M	R
ASD10 – 10/56	ASD	55, 48	44	F	L	TD10 – 95/1348	TD	229, not known	35	F	L
ASD11 – 167/08	ASD	74, 48	44	F	R	TD11 – 93/1086	TD	260, not known	39	F	L
ASD12 – 05/162	ASD	110, not known	48	F	L	TD12 – C1754	TD	320, not known	45	M	R
ASD13 – 90/09	ASD	64, 72	50	50	R	TD13 – 103/13	TD	16, 48	48	M	R BA9, R BA17, L FG***

ASD14 – 29/12	ASD	97, not known	60	60	R	TD14 – B1277	TD	501, not known	49	M	L
						TD15 – 10/71	TD	53, 48	68	M	R
		Mean: 104.50, 66.00 **SD**: 72.67, 33.41	**Mean**: 32.21 **SD**: 14.99	**Total:** 9 M, 5 F	**Total:** 9 R, 5 L			**Mean**: 253.13, 80.00 **SD**: 122.21, 55.43	**Mean:** 31.33 **SD:** 15.73	**Total:** 10 M, 5 F	**Total:** 9 R, 6 L for BA9 and BA17 8 R, 7 L for FG

Table 29. Summary of demographic information for cases included in this study. ASD cases highlighted in bold had diagnostic scores available.

*This information was approximated – some cases did not contain information of the exact date when they were placed in formalin. For the cases where only the year of death was provided, January 1st of that year and the date of sampling were used to calculate the time in formalin. All cases are from the TWOBC.
**PMI information was not available for a number of cases.
***The right FG was not available from this case.

	ADI-R (Social Interaction)	ADI-R (Verbal Communication)	ADI-R (Non-verbal Communication)	ADI-R (Restricted Repetitive Behaviour)	SCQ	SRS
Mean	22.33	16.33	6.00	3.55	25.13	83.00
SD	5.92	4.69	2.92	1.59	6.38	10.69

Table 30. Summary of diagnostic scores for ASD individuals. SCQ scores were available for 8 cases, and SRS scores were available for 7 cases.

Overall Staining Quality

For all cases and brain regions, a qualitative assessment was done to determine the overall staining quality of the case. Each region for each case was scored on a 5-point scale, with a score of 1 corresponding with a very poor stain, and a score of 5 with an excellent stain. Level of background/unspecific staining, and intensity of the DAB staining were taken into consideration when assigning a score. The scores across regions were then averaged together for each case. Cases that received an average score below 3 were excluded from the study. 5 cases (1 ASD, 4 TD) were excluded from further analysis due to poor staining quality. For 2/5 cases, this was likely due to the time the tissue spent in formalin before being sampled. The relationship of staining quality and time tissue spent in formalin is depicted in Figure 46.

Automated versus Manual Cell Counting

Algorithm 1, 2, and 3 correlated with the manual cell counts with Pearson's r-values of 0.857, 0.887, and 0.790 respectively. Algorithm 2 was used for the automated cell counts for all the regions since it best represented the manual cell counts. An intra-class correlation was run for Algorithm 2 to determine the reliability of the manual and automated measurements and returned with an intraclass correlation coefficient of 0.898.

PV+ Cells

The mean PV+ cells in the different cortical regions are shown in Figure 48. Before running statistical tests, the assumptions were checked and summarized below.

Normality – The Shapiro-Wilk test confirmed the normality of mean PV+ cells across all 3 regions for both groups ($p > 0.05$).

Homogeneity of Variance – Levene's test failed to reject the null hypothesis, and therefore equal variances for all three regions were assumed.

Sphericity – The null hypothesis for Mauchly's test of sphericity was rejected ($p < 0.05$) and therefore Greenhouse-Geisser adjustments were used ($\epsilon < 0.75$).

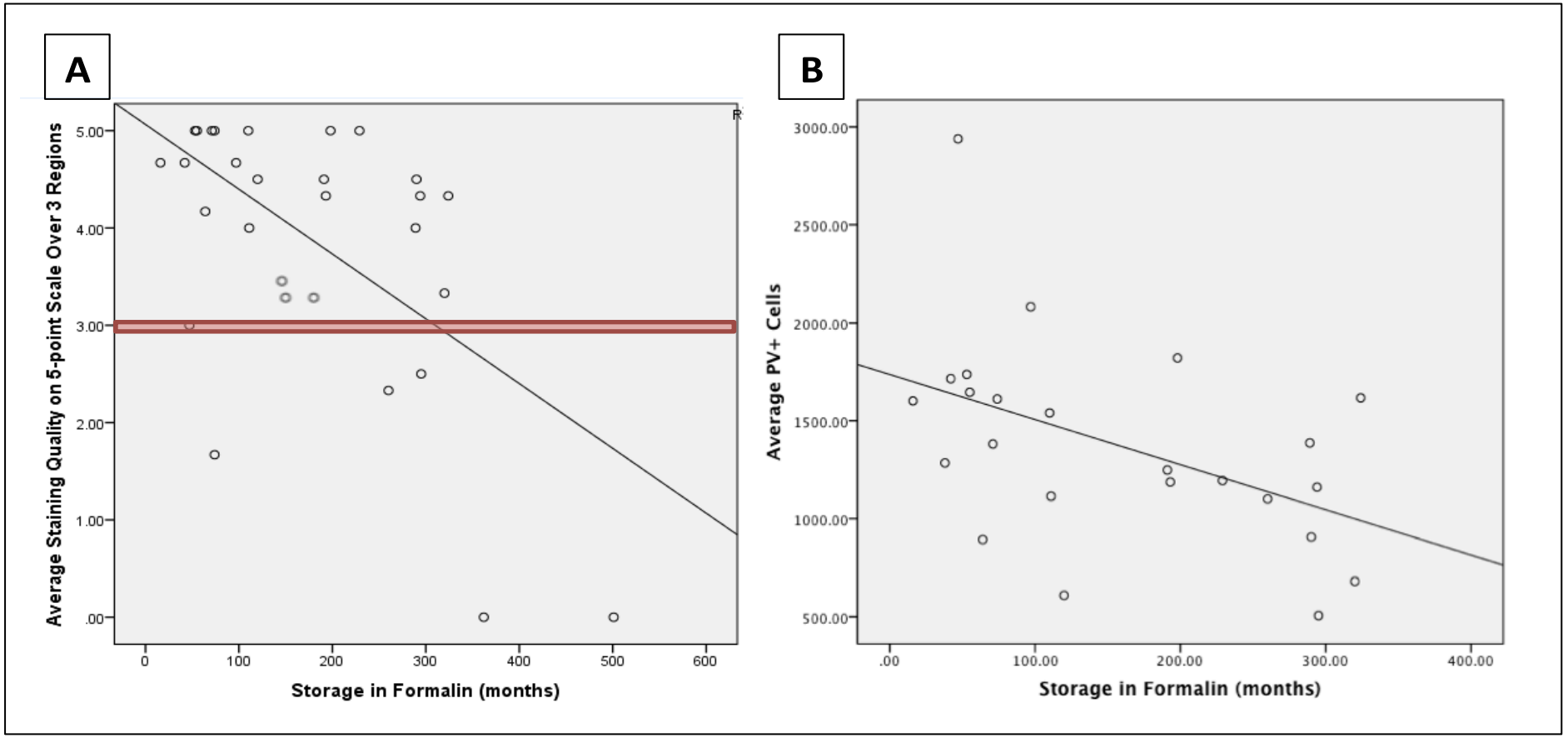

Figure 46. Staining as a function of time in formalin. A) shows the average staining quality (on a 5-point scale) plotted as a function of time in formalin. The five cases under the red bar were excluded due to poor staining quality. Despite this exclusion of 5 cases, B) shows the correlation that remained between time in formalin and average PV+ cells across all regions counted by the automated software for the 24 cases.

Figure 47. PV+ cells and an outline of the different layers in BA17. As suggested in the literature, PV+ cells are present in all layers of the cortex except layer 1.

Homogeneity of the Regression Slopes – The tests for the homogeneity of the regression slopes suggested no significant interaction between age and diagnosis group at all levels of the dependent variable. Similarly, no significant interaction was found between time in formalin and diagnostic group for both BA17 and FG. There was a significant interaction found for PV+ cells in BA9. However, since this interaction was not significant for the other two regions, time in formalin was still used as a covariate.

The results for the rmANCOVA are summarized in Table 31. The only main effect was brain region. Post-hoc tests revealed that the estimated marginal means of PV+ cells was greatest in BA17, followed by BA9, and lastly in the FG.

	PV+ cells
n-values	ASD = 10 TD = 10
Effect of brain region	F(2,32) = 4.963 **p = 0.013*** η^2 = 0.237
Effect of age	F(1,16) = 0.001 **p = 0.973** η^2 < 0.001
Effect of time in formalin	F(1,20) = 0.018 **p = 0.895** η^2 = 0.001
Effect of diagnosis	F(1,20) = 0.018 **p = 0.895** η^2 = 0.001
Region by time in formalin interaction	F(2,40) = 0.161 **p = 0.852** η^2 = 0.010
Region by age interaction	F(2,40) = 0.094 **p = 0.911** η^2 = 0.006
Region by diagnosis interaction	F(2,40) = 0.499 **p = 0.612** η^2 = 0.030

Table 31. Summary of rmANCOVA statistics for PV+ cells in the three cortical regions for 10 ASD and 10 TD cases.

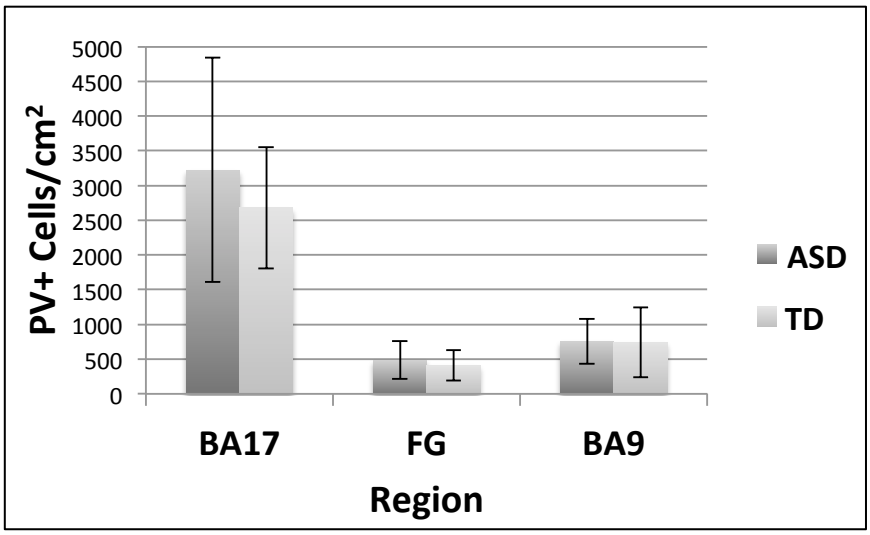

Figure 48. Mean PV+ cells in the three different cortical regions. Error bars represent SD.

Correlations with Diagnostic Scores

Pearson's bivariate correlations were run for each of the subscores of the ADI-R and the average of PV+ cells for each case. The results are summarized in Table 32. The only significant correlation found was for the restricted repetitive behaviour subscore – this relationship is demonstrated in Figure 49.

	ADI-R (Social Interaction)	ADI-R (Verbal Communication)	ADI-R (Non-verbal Communication)	ADI-R (Restricted Repetitive Behaviour)
PV+ cells/cm^2	r = -0.209 **p = 0.589**	r = -0.015 **p = 0.970**	r = 0.242 **p = 0.530**	r = -0.685 **p = 0.042***

Table 32. Pearson's bivariate correlations between diagnostic scores and mean PV+ cells across regions.

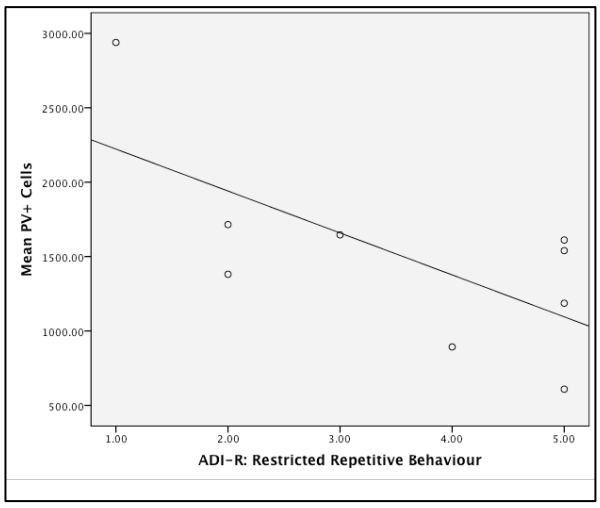

Figure 49. Correlation between ADI-R subscore and mean PV+ cells.

Discussion

The purpose of this Chapter was to explore differences in PV+ cell distribution in the three different ROIs (BA17, FG, and BA9) between ASD and TD individuals. Based off the theory of hyperexcitability in ASD, the hypothesis was that PV+ cells would be reduced in one or more of the ROIs. However, the results generated from automatic cell counting demonstrated no significant group differences. These results are in line with other studies that showed no differences in the distribution of PV+ cells in the cerebellum, prefrontal cortex, posterior cingulate cortex, and the fusiform gyrus in ASD (Edmonson et al., 2014; Oblak et al., 2011; Whitney et al., 2008). Perhaps reduced number of PV+ cells would have been observed if the ASD cases used in this study had a more severe presentation of the disorder. This explanation is supported by the negative correlation seen between the ADI-R restricted repetitive behaviour subscore and the mean number of PV+ cells. This correlation also suggests that a deficit in GABAergic signalling may affect ASD individuals with the most severe symptoms.

Interestingly, there was a strong main effect of region – the number of PV+ cells was greatest in BA17 and fewest in FG. This effect probes the question of why fast-spiking GABAergic interneurons may be more abundant in certain regions and not others. Previous studies have found that manipulation of PV+ cells affect the gain of primary sensations (Atallah, Bruns, Carandini, & Scanziani, 2012; Lee et al., 2012). For example, a previous optogenetic study found that modulating PV+ cells in V1 of mice increased these animals' perceptual discrimination (Lee et al., 2012). Another study also demonstrated the importance of PV+ interneurons (and not somatostatin-expressing interneurons) in visual perception, where suppressing PV+ cells impaired the ability of mice to effectively detect natural stimuli. These results suggest that PV+ cells in V1 play a pivotal role in visual perception, and may explain the regional differences observed here. Another interpretation is that PV+ cells are thought to play a critical role both in feedforward and feedback inhibition (Hu, Gan, & Jonas, 2014), and in reducing the time allotted for temporal summation of pyramidal cell action potentials (Pouille & Scanziani, 2001). These

mechanisms may be more important in primary sensory and prefrontal regions, involved in bottom-up and top-down modulatory activity, respectively, and less important in regions like FG, and therefore may explain why the number of cells in BA17 and BA9 were greater than in FG.

Immunohistochemistry studies often add PMI as a covariate as opposed to time in formalin. Thus, omitting PMI as a covariate in this study may be a confounding factor in the results. However, a previously published study showed that there was no correlation found between PMI and number of neurons in a certain area of the brain, but the number of neurons did negatively correlate with the time tissue had spent in formalin (Craven, Priddle, Cooper, Crow, & Esiri, 2005). Though the relationship between PMI and the number of PV+ cells was not explored here[9], time in formalin negatively correlated with the number of cells identified as PV+. Hence, it was important to add this factor as a covariate into the analysis.

Differences in paraffin-embedded and frozen tissue were indirectly explored in this Chapter. From the preliminary findings in this Chapter, frozen tissue required less antigen retrieval, and as a result may be a better reflection of the true structure. However, the frozen tissue was more prone to storage artefacts and was less robust. These findings are in line with what other researchers have concluded on the differences between frozen and paraffin-embedded tissue – for long-term use and storage, paraffin-embedded rather than frozen tissue may be better for immunohistochemistry (Hofman, 2002).

Future work involves studying the distribution of GABAergic interneurons positive for the other calcium-binding proteins, as well as other markers of GABAergic activity, like the different isoforms of glutamate decarboxylase, which is the enzyme responsible for decarboxylating Glu into GABA (and CO_2). Unlike PV+ cells, these markers of inhibition have not shown the same relationship with gamma oscillations. However, their distribution patterns have shown to be

[9] PMI data was not available for all cases, and time in formalin was easier to estimate for all cases.

altered in different regions of the ASD brain and may be worthwhile exploring in the context of the results reported here (Lawrence et al., 2010; Pizzarelli & Cherubini, 2011; Yip, Soghomonian, & Blatt, 2008, 2009).

Conclusion

In this Chapter, the distribution of PV+ cells was explored in ASD and TD individuals. No significant diagnostic differences were found. However, the number of PV+ cells negatively correlated with a symptom severity subscore, where more severely affected cases showed a reduction of mean PV+ cells. This finding is in line with the theory of hyperexcitability in ASD. The strong region effect revealed that the fast-spiking properties of PV+ cells may be more important in primary sensory processing than in other types of brain function. Future studies should focus on characterizing the distribution of other GABAergic markers, as well as further understanding how PV+ cells relate to ASD symptom severity.

Chapter 4 Appendix

Hand-Processing Tissue

Day 1

1. Drain formalin from cassettes under the fume hood.
2. Rinse cassettes with 70% Industrial Methylated Spirits (IMS).
3. Leave cassettes immersed in 70% IMS overnight under the fume hood.

Day 2

4. Discard 70% IMS solution, and rinse cassettes with 100% IMS.
5. Replace 100% IMS solution once every 90 minutes (four times).
6. Discard 100% IMS solution and rinse cassettes in Xylene twice.
7. Leave cassettes immersed in Xylene overnight.

Day 3

8. Discard and replace solution with fresh Xylene every two hours (three times).
9. Discard the Xylene solution, and immerse cassettes in molten wax in the oven at 63° C.
10. Leave cassettes overnight in wax in the oven.

Day 4

11. Discard wax and replace with fresh molten wax, every two hours (three times).
12. Follow steps for paraffin-embedding tissue, outlined below.

Paraffin-Embedding Tissue

1. Pour molten wax (63° C) into a plastic cassette holder.
2. Place cassette with tissue into the plastic cassette holder, and top up the holder with warm wax.
3. After wax cools, remove plastic cassette holder.

Parvalbumin Staining Optimization Protocol for Frozen Tissue

1. Place frozen tissue slides in the oven at 70° C for 20 minutes (this is the antigen retrieval step – no microwave needed).
2. Place tissue in H_2O_2 for 30 minutes, and wash in tap water.
3. Follow step 5 onwards from the paraffin-embedded tissue protocol, outlined in the Methods of this Chapter.

Generally, frozen tissue required a lower concentration of antibody for the same quality of staining.

Chapter 5: Conclusions

This thesis used a multidisciplinary approach to study the neuroanatomical and pathophysiological differences in ASD individuals, with a specific focus on the contrast between primary sensory and higher-order processing brain regions. The main research questions were centred on the theory of hyperexcitability and atypical connectivity in ASD. Specifically, MEG, MRS, and immunohistochemistry were used to study the excitation/inhibition imbalance theorized in ASD, and DTI was used to study atypical structure.

The novelty of the work stemmed from different aspects. In Chapter 2 and in Chapter 3, diffusion imaging was used in a new way to study microstructural differences in cortical grey matter. Specifically, diffusion measures that are hypothesized to reflect the orientation and spacing of minicolumns were extracted from BA17, FG, and BA9. The multimodal approach used in Chapter 3 was useful in answering whether ASD individuals showed differences across a range of measures, but also whether any relationships existed between modalities. Moreover, the employment of a 7T MRI machine was helpful in MRS to resolve peaks that have historically been reported as one. Lastly, the immunohistochemistry experiment in Chapter 4 was the first to investigate the distribution of PV+ cells in such diverse areas of the ASD brain.

Regional Differences

Several studies have suggested that ASD may be characterized by a dysfunction of prefrontal brain regions, while other works show evidence that primary sensory areas are affected as well, and point to the sensory abnormalities often reported in ASD individuals. As a result, the research questions in this thesis were guided by an interest on regional differences in ASD. Interesting regional effects were found in different parts of this thesis, including the automated masking results of the DTI modality in Chapter 3, as well as in the distribution of PV+ cells in Chapter 4. In Chapter 3, the diffusion data from the automated masking results revealed that MD was much higher in BA9 compared to the other regions, suggesting that the neuronal density here may be

relatively less across all individuals. Additionally in Chapter 3, ASD individuals showed a global reduction in left hemisphere MD values, and showed less hemispheric asymmetry compared to their TD counterparts. This type of pattern is in line with other studies looking at hemispheric laterality in ASD, and may be an interesting future avenue of research. The main effect of region found in Chapter 4 demonstrated that the number of PV+ cells was much greater in BA17, likely due to this region requiring rapid inhibition of pyramidal cells to neurally encode visual information.

In Chapter 3, no significant differences between diagnostic groups were found in occipital gamma phase-locking in response to simple visual stimuli, but some differences were seen in frontal gamma phase-locking, where TD individuals demonstrated more phase-locked activity in these frontal regions. These results suggest that there may be a top-down modulatory effect in response to simple visual stimuli in TD individuals, but not in ASD individuals. MRS results showed that there were increased Cr levels in MPFC specifically, suggesting an altered state of glial function and/or metabolic state of neurons in this region. Additionally, a global increase in Glu was found in ASD, and post-hoc tests revealed that these differences were driven by the MPFC. These results interpreted together suggest that, in high-functioning ASD individuals with normal or corrected-to-normal vision, it may be more frontal rather than primary sensory regions that show differences.

Relationships Between Modalities

It was difficult to make direct comparisons between the diffusion data presented in Chapter 2 and in Chapter 3 because the dataset collected in Oxford was acquired using a higher magnetic field, the MRI acquisition parameters were different, and the demographic information of the two groups were not homogeneous. Interestingly, in both datasets ASD individuals showed reduced MD values across brain regions compared to TD individuals, but this reduction effect was only statistically significant for the Oxford data. This may be due to the fact that the resolution of the

7T diffusion data was higher, giving rise to more sensitivity in any diagnostic differences, or may be due to the age groups being different across both Chapters. While the literature on diffusion values in cortical grey matter are limited, grey and white matter diffusion studies suggest that MD values in the brain change over the lifespan (Giorgio et al., 2010; Pfefferbaum et al., 2010). Interpreted broadly, the results of MD in the two datasets may suggest that ASD individuals show increased cell density, which is often associated with reduced MD, as a function of age. This research topic has not been directly studied before, but studies have suggested cellular reorganization in different brain regions for ASD individuals as they age (Courchesne et al., 2001; McKavanagh, 2015).

The hypothesis of frontal rather than primary sensory regions being more affected is partly supported by the relationship found between performance on the Complex Visual Task and levels of Glu in MPFC. Interestingly, no relationships were found between MEG measures and MRS measures of the excitation/inhibition balance, which have previously shown to correlate. While this lack of correlation does not undermine the role that GABA, Glu, and gamma oscillations play in helping set the balance in the brain, it does suggest that there may be other factors involved. Lastly, no relationships were found between cortical diffusion measures and gamma oscillations, questioning whether diffusion measures can provide the link between hyperexcitability and atypical connectivity.

Relationships with Severity Scores

Relationships between severity scores and the different measures of hyperexcitability were seen throughout this thesis, including a positive correlation between gamma phase-locking in an area of frontal cortex and ADOS scores from the MEG results in Chapter 3, a positive correlation between Glu values in MPFC and ADOS scores from the MRS results in Chapter 3, as well as a negative correlation between an ADI-R subscore and mean PV+ cells from the immunohistochemistry results in Chapter 4. All of these findings interpreted together support the

theory of hyperexcitability in ASD, but also suggest that this imbalance favouring excitation may only be apparent in the most severely affected individuals. No relationships were found for any of the diffusion measures and severity scores, suggesting that hyperexcitability rather than atypical connectivity may be a better way to generally characterize the disorder.

Future Work

The main limitation across the Chapters is a low subject size, especially in the neuroimaging studies. However, studies that incorporate more than one imaging modality often use similar sample sizes to the one used in this study. Despite the limited sample size, significant differences between ASD and TD individuals have been found across the Chapters, as well as significant effects of both age and gender. Future work should involve using a more diverse cohort to fully understand these other factors on the different measures studied in this thesis. In addition, it may be worth employing more sophisticated analysis tools to fully understand the multidimensional data presented here. Lastly, future work should focus on further developing the DTI measures for minicolumn structure, so that the relationship between gamma oscillations, GABA, Glu, and minicolumn structure can be reinvestigated, as well as on using the DTI data to explore the white matter connectivity differences in ASD and TD individuals, which may be altered based on the results presented here.

Final Remarks

It is well established that ASD is a complex developmental disorder with multiple aetiologies and phenotypes. Many researchers have referred to ASD as the “autisms”, due to the diversity and complexity of the condition. It is exactly for these reasons that a multidisciplinary approach was taken in this thesis to answer the neural and behavioural underpinnings of ASD. As expected, there was not one main but several findings throughout the thesis, reflecting the diversity and complexity. Moreover, relationships between different modalities demonstrate why it may be interesting to study ASD with a broad and multi-dimensional perspective.

References

Amaral, D. G., Schumann, C. M., & Nordahl, C. W. (2008). Neuroanatomy of autism. *Trends in Neurosciences*, *31,* 137-145.

American Psychiatric Association. (2000). *DSM-IV. Diagnostic and Statistical Manual of Mental Disorders 4th edition TR.*

Andersson, J. L. R., Skare, S., & Ashburner, J. (2003). How to correct susceptibility distortions in spin-echo echo-planar images: Application to diffusion tensor imaging. *NeuroImage*, *20*, 870–888.

Atallah, B. V., Bruns, W., Carandini, M., & Scanziani, M. (2012). Parvalbumin-expressing interneurons linearly transform cortical responses to visual stimuli. *Neuron*, *73*, 159–170.

Bailey, A., Luthert, P., Dean, A., Harding, B., Janota, I., Montgomery, M., … Lantos, P. (1998). A clinicopathological study of autism. *Brain*, *121*, 889–905.

Baron-Cohen. (2002). The extreme male brain theory of autism. *Trends in Cognitive Sciences*, *6*, 248–254.

Baron-Cohen, S. (1989). The autistic child's theory of mind: a case of specific developmental delay. *Journal of Child Psychology and Psychiatry, and Allied Disciplines*, *30*, 285–297.

Baron-Cohen, S., Knickmeyer, R. C., & Belmonte, M. K. (2005). Sex differences in the brain: implications for explaining autism. *Science*, *310*, 819–823.

Baron-Cohen, S., Richler, J., Bisarya, D., Gurunathan, N., & Wheelwright, S. (2003). The systemizing quotient: an investigation of adults with Asperger syndrome or high-functioning autsm, and normal sex differences. *Philosophical Transactions: Biological Sciences*, *358*, 361–374.

Baron-Cohen, S., & Wheelwright, S. (2004). The empathy quotient: an investigation of adults with asperger syndrome or high functioning autism, and normal sex differences. *Journal of Autism and Developmental Disorders*, *34,* 163-175.

Baruth, J. M., Wall, C. a, Patterson, M. C., & Port, J. D. (2013). Proton magnetic resonance spectroscopy as a probe into the pathophysiology of autism spectrum disorders (ASD): a review. *Autism Research, 6*, 119–133.

Beacher, F. D., Minati, L., Baron-Cohen, S., Lombardo, M. V., Lai, M.-C., Gray, M. A., … Critchley, H. D. (2012). Autism attenuates sex differences in brain structure: a combined voxel-based morphometry and diffusion tensor imaging study. *American Journal of Neuroradiology*, *33,* 83-89.

Belmonte, M. K., Allen, G., Beckel-Mitchener, A., Boulanger, L. M., Carper, R. A., & Webb, S. J. (2004). Autism and abnormal development of brain connectivity. *The Journal of Neuroscience, 24*, 9228–9231.

Bernardi, S., Anagnostou, E., Shen, J., Kolevzon, A., Buxbaum, J. D., Hollander, E., … Fan, J. (2011). In vivo 1H-magnetic resonance spectroscopy study of the attentional networks in autism. *Brain Research*, *1380*, 198–205.

Bertrand, O., & Tallon-Baudry, C. (2000). Oscillatory gamma activity in humans: a possible role for object representation. *International Journal of Psychophysiology, 38*, 211–223.

Bishop, D. V. M., Jacobs, P. A., Lachlan, K., Wellesley, D., Barnicoat, A., Boyd, P. A., … Scerif, G. (2011). Autism, language and communication in children with sex chromosome trisomies. *Archives of Disease in Childhood*, *96*, 954–959.

Blakemore, S. J., Tavassoli, T., Calo, S., Thomas, R. M., Catmur, C., Frith, U., & Haggard, P. (2006). Tactile sensitivity in Asperger syndrome. *Brain and Cognition*, *61*, 5–13.

Braeutigam, S. (2013). Magnetoencephalography: fundamentals and established and emerging clinical applications in radiology. *ISRN Radiology*, *18*.

Braeutigam, S., Rose, S. P. R., Swithenby, S. J., & Ambler, T. (2004). The distributed neuronal systems supporting choice-making in real-life situations: Differences between men and women when choosing groceries detected using magnetoencephalography. *European Journal of Neuroscience*, *20*, 293–302.

Brannen, J. H., Badie, B., Moritz, C. H., Quigley, M., Meyerand, M. E., & Haughton, V. M. (2001). Reliability of functional MR imaging with word-generation tasks for mapping Broca's area. *American Journal of Neuroradiology*, *22*, 1711–1718.

Buhl, D. L., Harris, K. D., Hormuzdi, S. G., Monyer, H., & Buzsáki, G. (2003). Selective impairment of hippocampal gamma oscillations in connexin-36 knock-out mouse in vivo. *The Journal of Neuroscience, 23*, 1013–1018.

Burack, J. A. (1994). Selective attention deficits in persons with autism: preliminary evidence of an inefficient attentional lens. *Journal of Abnormal Psychology*, *103*, 535–543.

Burnette, C. P., Henderson, H. A., Inge, A. P., Zahka, N. E., Schwartz, C. B., & Mundy, P. C. (2011). Anterior EEG asymmetry and the modifier model of autism. *Journal of Autism and Developmental Disorders*, *41*, 1113–1124.

Burnette, C. P., Mundy, P. C., Meyer, J. A., Sutton, S. K., Vaughan, A. E., & Charak, D. (2005). Weak central coherence and its relations to theory of mind and anxiety in autism. *Journal of Autism and Developmental Disorders*, *35*, 63–73.

Busch, R. M., Booth, J. E., McBride, A., Vanderploeg, R. D., Curtiss, G., & Duchnick, J. J. (2005). Role of executive functioning in verbal and visual memory. *Neuropsychology*, *19*, 171–180.

Buxhoeveden, D. P., Semendeferi, K., Buckwalter, J., Schenker, N., Switzer, R., & Courchesne, E. (2006). Reduced minicolumns in the frontal cortex of patients with autism. *Neuropathology and Applied Neurobiology*, *32*, 483–491.

Buxhoeveden, D. P., Switala, A. E., Litaker, M., Roy, E., & Casanova, M. F. (2001). Lateralization of minicolumns in human planum temporale is absent in nonhuman primate cortex. *Brain, Behavior and Evolution*, *57*, 349–358.

Buzsáki, G. (2004). Neuronal oscillations in cortical networks. *Science*, *304*, 1926–1929.

Buzsáki, G., & Wang, X.-J. (2012). Mechanisms of gamma oscillations. *Annual Review of Neuroscience*, *35,* 203.

Cantor, D. S., Thatcher, R. W., Hrybyk, M., & Kaye, H. (1986). Computerized EEG analyses of autistic children. *Journal of Autism and Developmental Disorders*, *16*, 169–187.

Casanova, M., Buxhoeveden, D., Switala, A., & Roy, E. (2002). Minicolumnar pathology in autism. *Neurology*, *58*, 428–32.

Chance, S. A. (2014). The cortical microstructural basis of lateralized cognition: a review. *Frontiers in Psychology*, *5*, 820.

Chance, S. A., Casanova, M. F., Switala, A. E., & Crow, T. J. (2008). Auditory cortex asymmetry, altered minicolumn spacing and absence of ageing effects in schizophrenia. *Brain*, *131*, 3178-3192.

Chance, S. A., Sawyer, E. K., Clover, L. M., Wicinski, B., Hof, P. R., & Crow, T. J. (2013). Hemispheric asymmetry in the fusiform gyrus distinguishes Homo sapiens from chimpanzees. *Brain Structure and Function*, *218*, 1391–1405.

Chang, E. F., & Merzenich, M. M. (2003). Environmental noise retards auditory cortical development. *Science*, *300*, 498–502.

Chapman, E., Baron-Cohen, S., Auyeung, B., Knickmeyer, R., Taylor, K., & Hackett, G. (2006). Fetal testosterone and empathy: evidence from the empathy quotient (EQ) and the "reading the mind in the eyes" test. *Social Neuroscience*, *1*, 135–148.

Chaumon, M., Schwartz, D., & Tallon-Baudry, C. (2009). Unconscious learning versus visual perception: dissociable roles for gamma oscillations revealed in MEG. *Journal of Cognitive Neuroscience*, *21*, 2287–2299.

Condé, F., Lund, J. S., Jacobowitz, D. M., Baimbridge, K. G., & Lewis, D. A. (1994). Local circuit neurons immunoreactive for calretinin, calbindin D-28k or parvalbumin in monkey prefrontal cortex: distribution and morphology. *The Journal of Comparative Neurology*, *341*, 95–116.

Cornew, L., Roberts, T. P. L., Blaskey, L., & Edgar, J. C. (2012). Resting-state oscillatory activity in autism spectrum disorders. *Journal of Autism and Developmental Disorders*, *42*, 1884–1894.

Courchesne, E. (1997). Brainstem, cerebellar and limbic neuroanatomical abnormalities in autism. *Current Opinion in Neurobiology*, *7,* 269-278.

Courchesne, E., Carper, R., & Akshoomoff, N. (2003). Evidence of brain overgrowth in the first year of life in autism. *JAMA : The Journal of the American Medical Association*, *290*, 337–344.

Courchesne, E., Karns, C. M., Davis, H. R., Ziccardi, R., Carper, R. A., Tigue, Z. D., … Courchesne, R. Y. (2001). Unusual brain growth patterns in early life in patients with autistic disorder: an MRI study. *Neurology*, *57*, 245–254.

Cousijn, H., Haegens, S., Wallis, G., Near, J., Stokes, M. G., Harrison, P. J., & Nobre, A. C. (2014). Resting GABA and glutamate concentrations do not predict visual gamma frequency or amplitude. *Proceedings of the National Academy of Sciences of the United States of America*, *111*, 9301–9306.

Craven, R. M., Priddle, T. H., Cooper, S. J., Crow, T. J., & Esiri, M. M. (2005). The dorsal raphe nucleus in schizophrenia: A post mortem study of 5-hydroxytryptamine neurones. *Neuropathology and Applied Neurobiology*, *31*, 258–269.

Davies, W., Isles, A. R., & Wilkinson, L. S. (2001). Imprinted genes and mental dysfunction. *Annals of Medicine*, *33*, 428–436.

Dawson, G., Munson, J., Webb, S. J., Nalty, T., Abbott, R., & Toth, K. (2007). Rate of head growth decelerates and symptoms worsen in the second tear of life in autism. *Biological Psychiatry*, *61*, 458–464.

DeVito, T. J., Drost, D. J., Neufeld, R. W. J., Rajakumar, N., Pavlosky, W., Williamson, P., & Nicolson, R. (2007). Evidence for cortical dysfunction in autism: a proton magnetic resonance spectroscopic imaging study. *Biological Psychiatry*, *61*, 465–473.

Doherty, B. (2013). Investigating the relationship between the cortical inhibition/excitation ratio and enhanced perceptual capacity in autism spectrum disorders: a MEG/MRS/DTI study. *University of Oxford*.

Donnelly, S. L., Wolpert, C. M., Menold, M. M., Bass, M. P., Gilbert, J. R., Cuccaro, M. L., … Pericak-Vance, M. A. (2000). Female with autistic disorder and monosomy X (Turner syndrome): Parent- of-origin effect of the X chromosome. *American Journal of Medical Genetics - Neuropsychiatric Genetics*, *96*, 312–316.

Draper, A., Stephenson, M. C., Jackson, G. M., Pepes, S., Morgan, P. S., Morris, P. G., & Jackson, S. R. (2014). Increased GABA contributes to enhanced control over motor excitability in Tourette Syndrome. *Current Biology*, *24*, 2343–2347.

Dufour-Rainfray, D., Vourc'h, P., Tourlet, S., Guilloteau, D., Chalon, S., & Andres, C. R. (2011). Fetal exposure to teratogens: Evidence of genes involved in autism. *Neuroscience and Biobehavioral Reviews, 35,* 1254-1265.

Edmonson, C., Ziats, M. N., & Rennert, O. M. (2014). Altered glial marker expression in autistic post-mortem prefrontal cortex and cerebellum. *Molecular Autism*, *5*, 1.

Endo, T., Shioiri, T., Kitamura, H., Kimura, T., Endo, S., Masuzawa, N., & Someya, T. (2007). Altered Chemical Metabolites in the Amygdala-Hippocampus Region Contribute to Autistic Symptoms of Autism Spectrum Disorders. *Biological Psychiatry*, *62*, 1030–1037.

Fairén, A., & Valverde, F. (1980). A specialized type of neuron in the visual cortex of cat: a Golgi and electron microscope study of chandelier cells. *The Journal of Comparative Neurology*, *194*, 761–779.

Fischl, B., & Dale, a M. (2000). Measuring the thickness of the human cerebral cortex from magnetic resonance images. *Proceedings of the National Academy of Sciences of the United States of America*, *97*, 11050–11055.

Folstein, S. E., & Rosen-Sheidley, B. (2001). Genetics of autism: complex aetiology for a heterogeneous disorder. *Nature Reviews. Genetics*, *2*, 943–955.

Folstein, S., & Rutter, M. (1977). Infantile autism: a genetic study of 21 twin pairs. *Journal of Child Psychology and Psychiatry*, *18*, 297–321.

Fombonne, E. (2005). The changing epidemiology of autism. In *Journal of Applied Research in Intellectual Disabilities*, *18*, 281–294.

Fontolan, L., Krupa, M., Hyafil, A., & Gutkin, B. (2013). Analytical insights on theta-gamma coupled neural oscillators. *Journal of Mathematical Neuroscience*, *3*, 16.

Frazier, T. W., Youngstrom, E. A., Speer, L., Embacher, R., Law, P., Constantino, J., … Eng, C. (2012). Validation of proposed DSM-5 criteria for autism spectrum disorder. *Journal of the American Academy of Child and Adolescent Psychiatry*, *51*, 28-40.

Freeman, W. J. (2007). Definitions of state variables and state space for brain-computer interface: Part 1. Multiple hierarchical levels of brain function. *Cognitive Neurodynamics*, *1*, 3–14.

Frith, U. (1989). Autism: explaining the enigma (cognitive development).

Gazdzinski, S., Millin, R., Kaiser, L. G., Durazzo, T. C., Mueller, S. G., Weiner, M. W., & Meyerhoff, D. J. (2010). BMI and neuronal integrity in healthy, cognitively normal elderly: a proton magnetic resonance spectroscopy study. *Obesity*, *18*, 743–748.

Gazzaley, A., Rissman, J., Cooney, J., Rutman, A., Seibert, T., Clapp, W., & D'Esposito, M. (2007). Functional interactions between prefrontal and visual association cortex contribute to top-down modulation of visual processing. *Cerebral Cortex*, *17*, 125-135.

Giorgio, A., Santelli, L., Tomassini, V., Bosnell, R., Smith, S., De Stefano, N., & Johansen-Berg, H. (2010). Age-related changes in grey and white matter structure throughout adulthood. *NeuroImage*, *51*, 943–951.

Glickfeld, L. L., Roberts, J. D., Somogyi, P., & Scanziani, M. (2009). Interneurons hyperpolarize pyramidal cells along their entire somatodendritic axis. *Nature Neuroscience*, *12*, 21–23.

Goddard, A. W., Mason, G. F., Almai, A., Rothman, D. L., Behar, K. L., Petroff, O. A., … Krystal, J. H. (2001). Reductions in occipital cortex GABA levels in panic disorder detected with 1h-magnetic resonance spectroscopy. *Archives of General Psychiatry*, *58*, 556–561.

Gogolla, N., LeBlanc, J. J., Quast, K. B., Südhof, T. C., Fagiolini, M., & Hensch, T. K. (2009). Common circuit defect of excitatory-inhibitory balance in mouse models of autism. *Journal of Neurodevelopmental Disorders*, *1*, 172–181.

Good, C. D., Johnsrude, I., Ashburner, J., Henson, R. N., Friston, K. J., & Frackowiak, R. S. (2001). Cerebral asymmetry and the effects of sex and handedness on brain structure: a voxel-based morphometric analysis of 465 normal adult human brains. *NeuroImage*, *14*, 685–700.

Grill-Spector, K., Knouf, N., & Kanwisher, N. (2004). The fusiform face area subserves face perception, not generic within-category identification. *Nature Neuroscience*, *7*, 555–562.

Grzadzinski, R., Huerta, M., & Lord, C. (2013). DSM-5 and autism spectrum disorders (ASDs): an opportunity for identifying ASD subtypes. *Molecular Autism*, *4*, 12.

Gupta, R. K., Hasan, K. M., Trivedi, R., Pradhan, M., Das, V., Parikh, N. A., & Narayana, P. A. (2005). Diffusion tensor imaging of the developing human cerebrum. *Journal of Neuroscience Research*, *81*, 172–178.

Hadjikhani, N., Chabris, C. F., Joseph, R. M., Clark, J., McGrath, L., Aharon, I., … Harris, G. J. (2004). Early visual cortex organization in autism: an fMRI study. *Neuroreport*, *15*, 267–270.

Hallmayer, J., Cleveland, S., Torres, A., Phillips, J., Cohen, B., Torigoe, T., … Risch, N. (2011). Genetic heritability and shared environmental factors among twin pairs with autism. *Archives of General Psychiatry*, *68,* 1095-1102.

Happé, F., & Frith, U. (2006). The weak coherence account: Detail-focused cognitive style in autism spectrum disorders. *Journal of Autism and Developmental Disorders*, *36,* 5-25.

Happé, F. G. E. (1997). Central coherence and theory of mind in autism: reading homographs in context. *British Journal of Developmental Psychology*, *15*, 1–12.

Harada, M., Taki, M. M., Nose, A., Kubo, H., Mori, K., Nishitani, H., & Matsuda, T. (2011). Non-invasive evaluation of the GABAergic/glutamatergic system in autistic patients observed by MEGA-editing proton MR spectroscopy using a clinical 3 Tesla instrument. *Journal of Autism and Developmental Disorders*, *41*, 447–454.

Headley, D. B., & Paré, D. (2013). In sync: gamma oscillations and emotional memory. *Frontiers in Behavioral Neuroscience*, 30.

Heekeren, H. R., Marrett, S., Bandettini, P. A., & Ungerleider, L. G. (2004). A general mechanism for perceptual decision-making in the human brain. *Nature*, *431*, 859–862.

Hendry, S. H., Schwark, H. D., Jones, E. G., & Yan, J. (1987). Numbers and proportions of GABA-immunoreactive neurons in different areas of monkey cerebral cortex. *The Journal of Neuroscience, 7*, 1503–1519.

Hill, E. L. (2004). Evaluating the theory of executive dysfunction in autism. *Developmental Review*, *24,* 189-233.

Hofman, F. (2002). Immunohistochemistry. *Current Protocols in Immunology.*

Honkanen, R., Rouhinen, S., Wang, S., Palva, J., & Palva, S. (2014). Gamma oscillations underlie the maintenance of feature-specific information and the contents of visual working memory. *Cerebral Cortex*, *263.*

Hu, H., Gan, J., & Jonas, P. (2014). Interneurons. Fast-spiking, parvalbumin^{+} GABAergic interneurons: from cellular design to microcircuit function. *Science*, *345*, 1255263.

Hu, V., Sarachana, T., Sherrard, R. M., & Kocher, K. M. (2015). Investigation of sex differences in the expression of RORA and its transcriptional targets in the brain as a potential contributor to the sex bias in autism. *Molecular Autism*, *6*, 1.

Hubel, D. H., & Wiesel, T. N. (1962). Receptive fields, binocular interaction and functional architecture in the cat's visual cortex. *Journal of Physiology*, *160*, 106–154.

Iaria, G., Robbins, S., & Petrides, M. (2008). Three-dimensional probabilistic maps of the occipital sulci of the human brain in standardized stereotaxic space. *Neuroscience*, *151*, 174–185.

Inglese, M., Rusinek, H., George, I. C., Babb, J. S., Grossman, R. I., & Gonen, O. (2008). Global average gray and white matter N-acetylaspartate concentration in the human brain. *NeuroImage*, *41*, 270–276.

Jansen, J. F. A., Backes, W. H., Nicolay, K., & Kooi, M. E. (2006). 1H MR spectroscopy of the brain: absolute quantification of metabolites. *Radiology*, *240*, 318–332.

Jeon, T., Mishra, V., Uh, J., Weiner, M., Hatanpaa, K. J., White, C. L., … Huang, H. (2012). Regional changes of cortical mean diffusivities with aging after correction of partial volume effects. *NeuroImage*, *62*, 1705–1716.

Johnson, W. G. (2003). Teratogenic alleles and neurodevelopmental disorders. *BioEssays*, *25,* 464-477.

Jones, E. G. (2000). Microcolumns in the cerebral cortex. *Proceedings of the National Academy of Sciences of the United States of America*, *97*, 5019–5021.

Jones, E. G. (2009). The origins of cortical interneurons: Mouse versus monkey and human. *Cerebral Cortex*, *19,* 1953-1956.

Just, M. A., Keller, T. A., Malave, V. L., Kana, R. K., & Varma, S. (2012). Autism as a neural systems disorder: A theory of frontal-posterior underconnectivity. *Neuroscience and Biobehavioral Reviews*, *36,* 1292-1313.

Kanner, L. (1968). Autistic disturbances of affective contact. *Acta Paedopsychiatrica*, *35*, 100–136.

Kelada, S. N., Eaton, D. L., Wang, S. S., Rothman, N. R., & Khoury, M. J. (2003). The role of genetic polymorphisms in environmental health. *Environmental Health Perspectives*, *111,* 1055.

Kemper, T. L., & Bauman, M. L. (1993). The contribution of neuropathologic studies to the understanding of autism. *Neurologic Clinics*, *11*, 175–187.

Klin, A. (2008). Three things to remember if you are a functional magnetic resonance imaging researcher of face processing in autism spectrum disorders. *Biological Psychiatry*, *64*, 549–551.

Kopp, S., & Gillberg, C. (2011). The Autism Spectrum Screening Questionnaire (ASSQ)-Revised Extended Version (ASSQ-REV): an instrument for better capturing the autism phenotype in girls? A preliminary study involving 191 clinical cases and community controls. *Research in Developmental Disabilities*, *32*, 2875–2888.

Kopp, S., Kelly, B., & Gillberg, C. (2010). Girls with social and/or attention deficits: a descriptive study of 100 clinic attenders. *Journal of Attention Disorders*, *14*, 167–181.

Koshino, H., Kana, R. K., Keller, T. A., Cherkassky, V. L., Minshew, N. J., & Just, M. A. (2008). fMRI investigation of working memory for faces in autism: visual coding and underconnectivity with frontal areas. *Cerebral Cortex*, *18*, 289–300.

Lai, M.-C., Lombardo, M. V, & Baron-Cohen, S. (2014). Autism. *Lancet*, *383*, 896–910.

Lavie, N. (1995). Perceptual load as a necessary condition for selective attention. *Journal of Experimental Psychology. Human Perception and Performance*, *21*, 451–468.

Lavie, N., Hirst, A., de Fockert, J. W., & Viding, E. (2004). Load theory of selective attention and cognitive control. *Journal of Experimental Psychology, 133,* 339-354.

Lawler, C. P., Croen, L. A., Grether, J. K., & Van De Water, J. (2004). Identifying environmental contributions to autism: provocative clues and false leads. *Mental Retardation and Developmental Disabilities Research Reviews*, *10,* 292-302.

Lawrence, Y. A., Kemper, T. L., Bauman, M. L., & Blatt, G. J. (2010). Parvalbumin-, calbindin-, and calretinin-immunoreactive hippocampal interneuron density in autism. *Acta Neurologica Scandinavica*, *121*, 99–108.

Lee, S.-H., Kwan, A. C., Zhang, S., Phoumthipphavong, V., Flannery, J. G., Masmanidis, S. C., … Dan, Y. (2012). Activation of specific interneurons improves V1 feature selectivity and visual perception. *Nature*. doi:10.1038/nature11312

Leekam, S. R., Nieto, C., Libby, S. J., Wing, L., & Gould, J. (2007). Describing the sensory abnormalities of children and adults with autism. *Journal of Autism and Developmental Disorders*, *37*, 894–910.

Leslie, A. M. (1987). Pretense and representation: The origins of "theory of mind." *Psychological Review*, *94,* 412.

Leuze, C. W. U., Anwander, A., Bazin, P. L., Dhital, B., Stüber, C., Reimann, K., … Turner, R. (2014). Layer-specific intracortical connectivity revealed with diffusion MRI. *Cerebral Cortex*, *24*, 328–339.

Levitt, J. G., O'Neill, J., Blanton, R. E., Smalley, S., Fadale, D., McCracken, J. T., … Alger, J. R. (2003). Proton magnetic resonance spectroscopic imaging of the brain in childhood autism. *Biol Psychiatry*, *54*, 1355–1366.

Li, B. S. Y., Wang, H., & Gonen, O. (2003). Metabolite ratios to assumed stable creatine level may confound the quantification of proton brain MR spectroscopy. *Magnetic Resonance Imaging*, *21*, 923–928.

Li, Y., Xu, D., Chen, A., Vigneron, D., & Nelson, S. (2008). Proton spectroscopy of human brain at 3T and 7T: signal-to-noise ratio, spectral linewidth and relaxation times. *Proceedings 16th Scientific Meeting, International Society for Magnetic Resonance in Medicine*, 1592.

Lo, Y. C., Soong, W. T., Gau, S. S. F., Wu, Y. Y., Lai, M. C., Yeh, F. C., … Tseng, W. Y. I. (2011). The loss of asymmetry and reduced interhemispheric connectivity in adolescents with autism: A study using diffusion spectrum imaging tractography. *Psychiatry Research - Neuroimaging*, *192*, 60–66.

Lodge, D. J., Behrens, M. M., & Grace, A. A. (2009). A loss of parvalbumin-containing interneurons is associated with diminished oscillatory activity in an animal model of schizophrenia. *The Journal of Neuroscience, 29*, 2344–2354.

Lotter, V. (1967). Epidemiology of autistic conditions in young children - II. Some characteristics of the parents and children. *Social Psychiatry*, *1*, 163–173.

Macdonald, J. S. P., & Lavie, N. (2008). Load induced blindness. *Journal of Experimental Psychology. Human Perception and Performance*, *34*, 1078–1091.

Maffei, L. (2002). Plasticity in the visual system: Role of neurotrophins and electrical activity. *Archives Italiennes de Biologie*, *140*, 341–346.

Mannion, A., & Leader, G. (2013). Comorbidity in autism spectrum disorder: A literature review. *Research in Autism Spectrum Disorders*, *7,* 1595-1616.

Marco, E. J., Hinkley, L. B. N., Hill, S. S., & Nagarajan, S. S. (2011). Sensory processing in autism: A review of neurophysiologic findings. *Pediatric Research*, *69*.

Markram, H., Toledo-Rodriguez, M., Wang, Y., Gupta, A., Silberberg, G., & Wu, C. (2004). Interneurons of the neocortical inhibitory system. *Nature Reviews. Neuroscience*, *5*, 793–807.

Martin, I., & McDonald, S. (2003). Weak coherence, no theory of mind, or executive dysfunction? Solving the puzzle of pragmatic language disorders. *Brain and Language*, *85*, 451–466.

Matson, J. L., & Nebel-Schwalm, M. S. (2007). Comorbid psychopathology with autism spectrum disorder in children: An overview. *Research in Developmental Disabilities*, *28*, 341–352.

Maxwell, C. R., Villalobos, M. E., Schultz, R. T., Herpertz-Dahlmann, B., Konrad, K., & Kohls, G. (2013). Atypical laterality of resting gamma oscillations in Autism Spectrum Disorders. *Journal of Autism and Developmental Disorders*, *45,* 292-297.

Maylor, E. A., & Lavie, N. (1998). The influence of perceptual load on age differences in selective attention. *Psychology and aging*, *13,* 563–573.

McKavanagh, R. (2015). The Neuropathology of the Social Cognitive Network in Autism. *University of Oxford*.

McKavanagh, R., Buckley, E., & Chance, S. (2015). Wider minicolumns in autism: a neural basis for altered processing? *Brain*, *138,* 2034-2045.

McKinstry, R. C., Mathur, A., Miller, J. H., Ozcan, A., Snyder, A. Z., Schefft, G. L., … Neil, J. J. (2002). Radial organization of developing preterm human cerebral cortex revealed by non-invasive water diffusion anisotropy MRI. *Cerebral Cortex*, *12*, 1237–1243.

Mekle, R., Gambarota, G., Mlynarik, V., & Gruetter, R. (2008). Improved spectral quality through enhanced shimming on a clinical platform at 3T and 7T. In *Proceedings 16th Scientific Meeting, International Society for Magnetic Resonance in Medicine,* 3243.

Menassa, D. A. (2013). Magnetoencephalography and neuropathological studies of autism spectrum disorders and the comorbidity with epilepsy. *University of Oxford*.

Milne, E., Scope, A., Pascalis, O., Buckley, D., & Makeig, S. (2009). Independent component analysis reveals atypical electroencephalographic activity during visual perception in individuals with autism. *Biological Psychiatry*, *65*, 22–30.

Minati, L., Aquino, D., Bruzzone, M. G., & Erbetta, A. (2010). Quantitation of normal metabolite concentrations in six brain regions by in-vivo H-MR spectroscopy. *Journal of Medical Physics / Association of Medical Physicists of India*, *35*, 154–163.

Miyoshi, G., Hjerling-Leffler, J., Karayannis, T., Sousa, V. H., Butt, S. J. B., Battiste, J., … Fishell, G. (2010). Genetic fate mapping reveals that the caudal ganglionic eminence produces a large and diverse population of superficial cortical interneurons. *The Journal of Neuroscience, 30*, 1582–1594.

Mottron, L., Dawson, M., Soulières, I., Hubert, B., & Burack, J. (2006). Enhanced perceptual functioning in autism: An update, and eight principles of autistic perception. *Journal of Autism and Developmental Disorders*.

Mountcastle, V. B. (1997). The columnar organization of the neocortex. *Brain*. doi:10.1093/brain/120.4.701

Movshon, J. A., Thompson, I. D., & Tolhurst, D. J. (1978). Spatial summation in the receptive fields of simple cells in the cat's striate cortex. *The Journal of Physiology*, *283*, 53–77.

Muhle, R., Trentacoste, S. V., & Rapin, I. (2004). The genetics of autism. *Pediatrics*, *113*, 472–486.

Murphy, D. G., Critchley, H. D., Schmitz, N., McAlonan, G., Van Amelsvoort, T., Robertson, D., … Howlin, P. (2002). Asperger syndrome: a proton magnetic resonance spectroscopy study of brain. *Arch Gen Psychiatry*, *59*, 885–891.

Muthukumaraswamy, S. D., Edden, R. A. E., Jones, D. K., Swettenham, J. B., & Singh, K. D. (2009). Resting GABA concentration predicts peak gamma frequency and fMRI amplitude in response to visual stimulation in humans. *Proceedings of the National Academy of Sciences of the United States of America*, *106*, 8356–8361.

Near, J. (2010). Magnetic Resonance Spectroscopy. *Vanderbilt University*.

Nomi, J. S., & Uddin, L. Q. (2015). Developmental changes in large-scale network connectivity in autism. *NeuroImage: Clinical*, *6*(7), 732–741.

O'Riordan, M. A., Plaisted, K. C., Driver, J., & Baron-Cohen, S. (2001). Superior visual search in autism. *Journal of Experimental Psychology. Human Perception and Performance*, *27*, 719–730.

Oblak, A., Gibbs, T. T., & Blatt, G. J. (2009). Decreased GABAA receptors and benzodiazepine binding sites in the anterior cingulate cortex in autism. *Autism Research*, *2*, 205–219.

Oblak, A. L., Gibbs, T. T., & Blatt, G. J. (2010). Decreased GABAB receptors in the cingulate cortex and fusiform gyrus in Autism. *Journal of Neurochemistry*, *114*, 1414–1423.

Oblak, A. L., Rosene, D. L., Kemper, T. L., Bauman, M. L., & Blatt, G. J. (2011). Altered posterior cingulate cortical cyctoarchitecture, but normal density of neurons and interneurons in the posterior cingulate cortex and fusiform gyrus in autism. *Autism Research*, *4*, 200–211.

World Health Organization. (2011). International Classification of Diseases (ICD).

Ozonoff, S., Pennington, B. F., & Rogers, S. J. (1991). Executive function deficits in high-functioning autistic individuals: relationship to theory of mind. *Journal of Child Psychology and Psychiatry, and Allied Disciplines*, *32*, 1081–1105.

Pal, D., Trivedi, R., Saksena, S., Yadav, A., Kumar, M., Pandey, C. M., … Gupta, R. K. (2011). Quantification of age- and gender-related changes in diffusion tensor imaging indices in deep grey matter of the normal human brain. *Journal of Clinical Neuroscience*, *18*, 193–196.

Palmen, S. J. M. C., Hulshoff Pol, H. E., Kemner, C., Schnack, H. G., Durston, S., Lahuis, B. E., … Van Engeland, H. (2005). Increased gray-matter volume in medication-naive high-functioning children with autism spectrum disorder. *Psychological Medicine*, *35*, 561–570.

Palmen, S. J. M. C., van Engeland, H., Hof, P. R., & Schmitz, C. (2004). Neuropathological findings in autism. *Brain : A Journal of Neurology*, *127*, 2572–83.

Parvizi, J., Jacques, C., Foster, B. L., Withoft, N., Rangarajan, V., Weiner, K. S., & Grill-Spector, K. (2012). Electrical stimulation of human fusiform face-selective regions distorts face perception. *Journal of Neuroscience*, *32,* 14915-14920.

Pfefferbaum, A., Adalsteinsson, E., Rohlfing, T., & Sullivan, E. V. (2010). Diffusion tensor imaging of deep gray matter brain structures: Effects of age and iron concentration. *Neurobiology of Aging*, *31*, 482–493.

Pierce, K., & Redcay, E. (2008). Fusiform function in children with an autism spectrum disorder is a matter of "who." *Biological Psychiatry*, *64*, 552–560.

Pinto, D. J., Brumberg, J. C., & Simons, D. J. (2000). Circuit dynamics and coding strategies in rodent somatosensory cortex. *Journal of Neurophysiology*, *83,* 1158-1166.

Pizzarelli, R., & Cherubini, E. (2011). Alterations of GABAergic signaling in autism spectrum disorders. *Neural Plasticity*, *2011.*

Pizzorusso, T., Medini, P., Berardi, N., Chierzi, S., Fawcett, J. W., & Maffei, L. (2002). Reactivation of ocular dominance plasticity in the adult visual cortex. *Science*, *298*, 1248–1251.

Polleux, F., & Lauder, J. M. (2004). Toward a developmental neurobiology of autism. *Mental Retardation and Developmental Disabilities Research Reviews*, *10,* 303-317.

Pouille, F., & Scanziani, M. (2001). Enforcement of temporal fidelity in pyramidal cells by somatic feed-forward inhibition. *Science*, *293*, 1159–1163.

Premack, D., & Woodruff, G. (1978). Does the chimpanzee have a theory of mind? *Behavioral and Brain Sciences*, *1,* 515-526.

Prior, M., & Hoffmann, W. (1990). Brief report: Neuropsychological testing of autistic children through an exploration with frontal lobe tests. *Journal of Autism and Developmental Disorders*, *20*, 581–590.

Provencher, S. (2014). LCModel & LCMgui User's Manual.

Provencher, S. W. (2001). Automatic quantitation of localized in vivo 1H spectra with LCModel. *NMR in Biomedicine*, *14*, 260–264.

Raghanti, M. A., Spocter, M. A., Butti, C., Hof, P. R., & Sherwood, C. C. (2010). A comparative perspective on minicolumns and inhibitory GABAergic interneurons in the neocortex. *Frontiers in Neuroanatomy*, *4*, 3.

Remington, A., Swettenham, J., Campbell, R., & Coleman, M. (2009). Selective attention and perceptual load in autism spectrum disorder. *Psychological Science*, *20*, 1388–1393.

Remington, A., Swettenham, J. G., & Lavie, N. (2012). Lightening the load - perceptual load impairs visual detection in typical adults but not in autism. *Journal of Abnormal Pscyhology*, *121*, 544–551.

Rieger, M., & Rabbitt, P. (1999). Methodology of frontal and executive function. *Zeitschrift Für Neuropsychologie*, *41,* 49-100.

Rojas, D. C., & Wilson, L. B. (2014). Gamma-band abnormalities as markers of autism spectrum disorders. *Biomarkers in Medicine*, *8*, 353–368.

Rubenstein, J. L. R., & Merzenich, M. M. (2003). Model of autism: increased ratio of excitation/inhibition in key neural systems. *Genes, Brain, and Behavior*, *2*, 255–267.

Rumsey, J. M., & Hamburger, S. D. (1988). Neuropsychological findings in high-functioning men with infantile autism, residual state. *Journal of Clinical and Experimental Neuropsychology*, *10*, 201–221.

Schumann, C. M., Hamstra, J., Goodlin-Jones, B. L., Lotspeich, L. J., Kwon, H., Buonocore, M. H., … Amaral, D. G. (2004). The amygdala is enlarged in children but not adolescents with autism; the hippocampus is enlarged at all ages. *The Journal of Neuroscience*, *24*, 6392–6401.

Serre, T. (2014). Hierarchical models of the visual system. *Encycopledia of Computational Neuroscience*, 1–12.

Shih, P., Keehn, B., Oram, J. K., Leyden, K. M., Keown, C. L., & Müller, R. A. (2011). Functional differentiation of posterior superior temporal sulcus in autism: A functional connectivity magnetic resonance imaging study. *Biological Psychiatry*, *70*, 270–277.

Shimony, J. S., McKinstry, R. C., Akbudak, E., Aronovitz, J. A., Snyder, A. Z., Lori, N. F., … Conturo, T. E. (1999). Quantitative diffusion-tensor anisotropy brain MR imaging: normative human data and anatomic analysis. *Radiology*, *212*, 770–784.

Slotnick, S. D., & Moo, L. R. (2006). Prefrontal cortex hemispheric specialization for categorical and coordinate visual spatial memory. *Neuropsychologia*, *44*, 1560–1568.

Smith, S. M. (2002). Fast robust automated brain extraction. *Human Brain Mapping*, *17*, 143–155.

Snijders, T. M., Milivojevic, B., & Kemner, C. (2013). Atypical excitation-inhibition balance in autism captured by the gamma response to contextual modulation. *NeuroImage: Clinical*, *3*, 65–72.

Sohal, V. S., Zhang, F., Yizhar, O., & Deisseroth, K. (2009). Parvalbumin neurons and gamma rhythms enhance cortical circuit performance. *Nature*, *459*, 698–702.

Solomon, M., Ozonoff, S. J., Ursu, S., Ravizza, S., Cummings, N., Ly, S., & Carter, C. S. (2009). The neural substrates of cognitive control deficits in autism spectrum disorders. *Neuropsychologia*, *47*, 2515–2526.

Srinivasan, R., Sailasuta, N., Hurd, R., Nelson, S., & Pelletier, D. (2005). Evidence of elevated glutamate in multiple sclerosis using magnetic resonance spectroscopy at 3 T. *Brain : A Journal of Neurology*, *128*, 1016–1025.

Stokstad, E. (2001). Development. New hints into the biological basis of autism. *Science*. *294,* 34-37.

Stroganova, T. A., Orekhova, E. V., Prokofyev, A. O., Tsetlin, M. M., Gratchev, V. V., Morozov, A. A., & Obukhov, Y. V. (2012). High-frequency oscillatory response to illusory contour in typically developing boys and boys with autism spectrum disorders. *Cortex*, *48*, 701–717.

Szabadics, J., Varga, C., Molnár, G., Oláh, S., Barzó, P., & Tamas, G. (2006). Excitatory effect of GABAergic axo-axonic cells in cortical microcircuits. *Science*, *311*, 233–235.

Tamamaki, N., Yanagawa, Y., Tomioka, R., Miyazaki, J. I., Obata, K., & Kaneko, T. (2003). Green fluorescent protein expression and colocalization with calretinin, parvalbumin, and somatostatin in the GAD67-GFP knock-in mouse. *Journal of Comparative Neurology*, *467*, 60–79.

Uddin, L. Q., Supekar, K., & Menon, V. (2013). Reconceptualizing functional brain connectivity in autism from a developmental perspective. *Frontiers in Human Neuroscience*, *7*, 458.

Uludağ, K., & Roebroeck, A. (2014). General overview on the merits of multimodal neuroimaging data fusion. *NeuroImage*, *102,* 3-10.

Van Kooten, I. A. J., Palmen, S. J. M. C., Von Cappeln, P., Steinbusch, H. W. M., Korr, H., Heinsen, H., … Schmitz, C. (2008). Neurons in the fusiform gyrus are fewer and smaller in autism. *Brain*, *131*, 987–999.

Van Rijn, S., Bierman, M., Bruining, H., & Swaab, H. (2012). Vulnerability for autism traits in boys and men with an extra X chromosome (47,XXY): The mediating role of cognitive flexibility. *Journal of Psychiatric Research*, *46*, 1300–1306.

Walsh, V., & Cowey, A. (2000). Transcranial magnetic stimulation and cognitive neuroscience. *Nature Reviews Neuroscience*, *1*, 73–79.

Warntjes, J. B. M., Dahlqvist, O., & Lundberg, P. (2007). Novel method for rapid, simultaneous T1, T2*, and proton density quantification. *Magnetic Resonance in Medicine*, *57*, 528–537.

Werling, D. M., & Geschwind, D. H. (2013). Sex differences in autism spectrum disorders. *Current Opinion in Neurology*, *26*, 146–153.

White, S., & Saldana, D. (2011). Performance of children with autism on the Embedded Figures Test: a closer look at a popular task. *Journal of Autism and Developmental Disorders*, *41*, 1565–1572.

Whitney, E. R., Kemper, T. L., Bauman, M. L., Rosene, D. L., & Blatt, G. J. (2008). Cerebellar Purkinje cells are reduced in a subpopulation of autistic brains: A stereological experiment using calbindin-D28k. *Cerebellum*, *7*, 406–416.

Whittington, M. A., Traub, R. D., & Jefferys, J. G. (1995). Synchronized oscillations in interneuron networks driven by metabotropic glutamate receptor activation. *Nature*, *373*, 612–615.

Wing, L. (1997). The history of ideas on autism: legends, myths and reality. *Autism*. *1,* 13-23.

Wing, L. (2004). The spectrum of autistic disorders. *Hospital Medicine (London, England : 1998)*, *65*, 542–545.

Woodruff, A. R., Anderson, S. A., & Yuste, R. (2010). The enigmatic function of chandelier cells. *Frontiers in Neuroscience*. *4,* 201.

Wright, B., Alderson-Day, B., Prendergast, G., Bennett, S., Jordan, J., Whitton, C., … Green, G. (2012). Gamma activation in young people with autism spectrum disorders and typically-developing controls when viewing emotions on faces. *PLoS ONE*, *7*.

Yip, J., Soghomonian, J. J., & Blatt, G. J. (2008). Increased GAD67 mRNA expression in cerebellar interneurons in autism: Implications for Purkinje cell dysfunction. *Journal of Neuroscience Research*, *86*, 525–530.

Yip, J., Soghomonian, J. J., & Blatt, G. J. (2009). Decreased GAD65 mRNA levels in select subpopulations of neurons in the cerebellar dentate nuclei in autism: An in situ hybridization study. *Autism Research*, *2*, 50–59.

Yizhar, O., Fenno, L. E., Prigge, M., Schneider, F., Davidson, T. J., O'Shea, D. J., … Deisseroth, K. (2011). Neocortical excitation/inhibition balance in information processing and social dysfunction. *Nature*, *477*, 171–178.

Zaitsev, A. V, Povysheva, N. V, Lewis, D. A., & Krimer, L. S. (2007). P/Q-type, but not N-type, calcium channels mediate GABA release from fast-spiking interneurons to pyramidal cells in rat prefrontal cortex. *Journal of Neurophysiology*, *97*, 3567–3573.

Zaitsev, A. V., Gonzalez-Burgos, G., Povysheva, N. V., Kröner, S., Lewis, D. A., & Krimer, L. S. (2005). Localization of calcium-binding proteins in physiologically and morphologically characterized interneurons of monkey dorsolateral prefrontal cortex. *Cerebral Cortex*, *15*, 1178–1186.

Zhang, L. I., Bao, S., & Merzenich, M. M. (2001). Persistent and specific influences of early acoustic environments on primary auditory cortex. *Nature Neuroscience*, *4*, 1123–1130.

Zhu, H., & Barker, P. B. (2011). MR spectroscopy and spectroscopic imaging of the brain. *Methods in Molecular Biology, 711*, 203–226.